Design of modified metal-organic frameworks for the catalytic application in liquid phase fine chemistry

Zur Erlangung des akademischen Grades eines
DOKTORS DER NATURWISSENSCHAFTEN
(Dr. rer. nat.)

von der KIT-Fakultät für Chemie und Biowissenschaften
des Karlsruher Instituts für Technologie (KIT)

genehmigte
DISSERTATION
von

Dipl.-Chem. Meike Antonia Gotthardt

aus
Speyer

KIT-Dekan:	Prof. Dr. Willem M. Klopper
Referent:	Priv.-Doz. Dr. Wolfgang Kleist
Korreferent:	Prof. Dr. Peter W. Roesky
Tag der mündlichen Prüfung:	23.10.2015

Abstract

In the late 1990s, metal-organic frameworks (MOFs) emerged as an interesting new class of materials. Due to their remarkable chemical and physical properties the research interest rapidly increased focusing on the development of new structures and improved synthetic methods as well as potential applications. Due to the highly versatile design, the defined metal sites and the high porosity, metal-organic frameworks are an interesting class of materials for a multitude of different uses, *e.g.* catalytic applications in fine chemistry. In addition, MOF-based catalysts should combine the beneficial characteristics of both homogeneous and heterogeneous catalysts. The frameworks contain a high concentration of well-defined single-sites, which should result in high catalytic activity, while at the same time easy separation and reuse should be feasible for the solid MOF materials.

In the present thesis, novel concepts for the synthesis and modification of metal-organic frameworks were developed to obtain innovative heterogeneous catalysts. To achieve this aim, two different approaches were realized utilizing free functional groups at the organic linker molecules as well as unsaturated framework metal centers.

In the first approach, defined Pd^{2+} complexes were immobilized on free amine groups at the linker molecules of MIL-53-NH_2(Al), which is constructed from Al^{3+} ions connected by 2-aminobenzene-1,4-dicarboxylate linkers, *via* a two-step post-synthetic modification (PSM) reaction (Chapter 2). A novel synthetic strategy at ambient pressure was applied for the preparation of the framework resulting in a phase-pure material without any additional purification steps, which are typically required for the solvothermally synthesized material. This preparation route also facilitates an easy scale-up, which is relevant for potential applications where large amounts of the material are needed. The framework is chemically and thermally stable and, therefore, its structure was retained throughout the two-step modification process. The immobilization of defined Pd^{2+} complexes and the absence of additional undesired palladium nanoparticles and clusters were corroborated by X-ray absorption spectroscopy. The resulting material MIL-53-NH_2(Al)-Mal-Pd was highly active in Heck-type C-C coupling reactions of bromo- or chlorobenzene with styrene (TON = 8240 and 1740, respectively) and hot filtration tests confirmed contributions of a truly heterogeneous pathway. In contrast, a “quasi-homogeneous” reaction pathway of dissolved palladium species is widely accepted in literature for conventional heterogeneous catalysts. This led to the conclusion that *via* the immobilization of defined complexes in a MOF, alternative reaction pathways may be accessible and the leaching of active species might be

reduced. However, blocking of the pores was observed throughout the modification process, which indicated that the active complexes were mainly incorporated on the surface of the framework.

To guarantee a homogeneous distribution of the complexes in the porous structure, mixed-linker metal-organic frameworks (MIXMOFs) MIL-53-NH_2(x) (x = 40, 60, 80; percentage of amine linker) were synthesized and modified under comparable reaction conditions (Chapter 3). Although the modification degree of the amine groups (^{1}H NMR) and the palladium content (AAS) were higher for the MIXMOFs, the immobilized complexes were well distributed in the material resulting in high specific surface areas even after modification. The modified frameworks were again tested in Heck-type C-C coupling reactions and the results were compared to the previous study. Since all catalysts achieved comparable conversion, the Pd^{2+} complexes inside the pores were obviously accessible and active. A higher selectivity could be achieved in the coupling of chlorobenzene and styrene with the modified mixed-linker frameworks compared to pure MIL-53-NH_2(Al)-Mal-Pd. The catalytic results and the increased porosity of the mixed-linker frameworks prove the advantages of combining the MIXMOF and the PSM concepts.

To broaden the scope of possible substrates for modification reactions and ultimately also catalysis, functionalized single- and mixed-linker frameworks based on DUT-5 with larger pore dimensions were prepared at ambient pressure (Chapter 4). DUT-5 is isoreticular to MIL-53-NH_2(Al) and is built from Al^{3+} ions interconnected by biphenyl-4,4'-dicarboxylate linkers. Linker molecules bearing an additional amine, alkyne, nitro or azide group were synthesized by the Bräse group (Institute of Organic Chemistry, KIT). The introduction of defined ratios of functionalized and unfunctionalized linker molecules could be proven by thermogravimetric analysis coupled with FT-IR or by ^{1}H NMR spectroscopy. The thermal stability and specific surface area could be tuned depending on the number of functional groups in the resulting framework, again illustrating the benefits of the MIXMOF concept. MIXDUT-5-amine(50) was applied in a number of post-synthetic modification reactions and the resulting frameworks proved to be highly porous even after the modification, hence, confirming the advantages of applying metal-organic frameworks with larger pore dimensions for PSM. In future studies the functionalized metal-organic frameworks based on DUT-5 could be utilized for the immobilization of larger and more sophisticated complexes and, additionally, they might also be interesting materials for size- and shape-selective catalysis. Due to the modular design of the framework-based catalysts obtained by post-synthetic modification, the catalysts can be tailored for a specific catalytic transformation.

In another approach, a synthetic protocol for the direct preparation of a bimetallic framework based on HKUST-1 was developed (Chapter 5). HKUST-1, also known as Cu-BTC, is constructed from dimeric Cu^{2+} units, which are connected by benzene-1,3,5-tricarboxylate linkers. Cu^{2+} was partially replaced by Ru^{3+} in the framework synthesis, which was again performed at ambient pressure *via* a non-solvothermal strategy. The resulting MOF with the chemical formula $Cu_{2.75}Ru_{0.25}(BTC)_2*xH_2O$ was isoreticular to HKUST-1. X-ray absorption spectroscopy confirmed the successful incorporation of Ru^{3+} into the paddlewheel structure of HKUST-1 and, furthermore, could also be utilized to exclude the undesired formation of additional phases (*e.g.* clusters or nanoparticles). In future studies, Cu-Ru-BTC might be applied as bimetallic catalyst featuring accessible unsaturated Cu^{2+} and Ru^{3+} sites.

The MOF-based systems presented in this thesis clearly illustrate the potential of metal-organic frameworks for the design of highly versatile heterogeneous single-site catalyst systems. The high activity, selectivity and the reduced leaching of the palladium-containing frameworks based on MIL-53 in Heck-type C-C coupling reactions nicely demonstrate the advantages of the novel catalyst systems compared to conventional materials. Therefore, attractive results can also be expected in future studies employing immobilized transition metal complexes in DUT-5 and the bimetallic framework Cu-Ru-BTC.

Kurzfassung

Metallorganische Gerüstverbindungen (*metal-organic frameworks*, MOFs) sind seit Ende der 90er Jahre als interessante neue Materialklasse bekannt und zogen aufgrund ihrer bemerkenswerten chemischen und physikalischen Eigenschaften schnell das Forschungsinteresse auf sich. Der Fokus lag dabei auf der Entwicklung neuer Strukturen und verbesserter Synthesestrategien sowie auf möglichen Anwendungsbereichen. Die hohe Variabilität im Aufbau, die definierte chemische Umgebung der Metallzentren und hohe spezifische Oberflächen machen metallorganische Gerüstverbindungen zu interessanten Materialien für diverse Einsatzgebiete, z.B. für katalytische Anwendungen, insbesondere in der Herstellung von Feinchemikalien. Zusätzlich vereinen MOF-basierte Katalysatoren vorteilhafte Eigenschaften heterogener (einfache Abtrennung und Wiederverwendbarkeit) und homogener (definierte Zentren und hohe Aktivität) Katalysatorsysteme.

In der vorliegenden Arbeit wurden neuartige Konzepte für die Synthese und Modifizierung metallorganischer Gerüstverbindungen entwickelt, um innovative Heterogenkatalysatoren zu erhalten. Um dieses Ziel zu erreichen, wurden zwei unterschiedliche Herangehensweisen realisiert. Zum einen wurden freie funktionelle Gruppen der organischen Linkermoleküle genutzt und zum anderen Gerüstverbindungen mit ungesättigten Metallzentren eingesetzt.

Im ersten Fall wurden definierte Pd^{2+}-Komplexe an den freien Amingruppen der Linkermoleküle in MIL-53-NH_2(Al) immobilisiert, wobei eine zweistufige postsynthetische Modifizierungsreaktion (PSM) angewandt wurde (Kapitel 2). MIL-53-NH_2(Al) ist aus oktaedrisch koordinierten Al^{3+}-Ionen aufgebaut, die über 2-Aminobenzol-1,4-dicarboxylate verbunden sind. Zur Herstellung der Gerüstverbindung wurde zunächst eine neue Synthesestrategie unter Normaldruck entwickelt. Dabei entstand eine phasenreine Verbindung, die im Gegensatz zu dem Material, das in der Literatur über die solvothermale Synthese hergestellt wurde, keiner weiteren Aufarbeitung bedurfte. Diese Syntheseroute ermöglicht außerdem die Vergrößerung des Ansatzes, was im Hinblick auf potentielle Anwendungen von Bedeutung ist, für die größere Mengen der Verbindung benötigt werden. MIL-53-NH_2(Al) ist chemisch und thermisch sehr stabil, weshalb die Struktur im Verlauf der zweistufigen Modifizierungsreaktion erhalten blieb. Mittels Röntgenabsorptionsspektroskopie konnte die Immobilisierung definierter Pd^{2+}-Komplexe bewiesen und gleichzeitig die Bildung unerwünschter Palladium Nanopartikel ausgeschlossen werden. Der erhaltene Katalysator MIL-53-NH_2(Al)-Mal-Pd war in der Heck-Reaktion von Brom- oder Chlorbenzol mit Styrol sehr aktiv (TON = 8240 bzw. 1740) und Filtrationstests bestätigten die

tatsächliche Beteiligung eines heterogenen Reaktionspfades. Im Gegensatz dazu ist in der Literatur für konventionelle heterogene Katalysatoren ein „quasi-homogener“ Mechanismus belegt, nach dem die Reaktion ausschließlich von gelösten Palladiumkomplexen katalysiert wird. Folglich werden durch die Immobilisierung definierter Metallkomplexe im MOF alternative Reaktionsverläufe ermöglicht und zudem das Auswaschen aktiver Spezies deutlich reduziert. Allerdings wurde während der Modifizierung ein enormer Rückgang der spezifischen Oberfläche und des zugänglichen Porenvolumens beobachtet, was darauf hindeutet, dass die Modifizierung hauptsächlich an der Oberfläche der Gerüstverbindung stattfand, und dadurch die Poreneingänge blockiert wurden.

Um die homogene Verteilung der Komplexe im gesamten Material zu garantieren, wurden metallorganische Gerüstverbindungen mit gemischten Linkermolekülen (*mixed-linker metal-organic frameworks*, MIXMOFs) MIL-53-NH_2(x) (x = 40, 60, 80, prozentualer Anteil des Aminlinkers) unter vergleichbaren Bedingungen synthetisiert und modifiziert (Kapitel 3). Obwohl ^{1}H-NMR- und Atomabsorptionsspektroskopie der MIXMOFs einen höheren Modifizierungsgrad der Amingruppen und einen höheren Palladiumgehalt ergaben, konnten eine homogene Verteilung der Komplexe im Material und eine hohe spezifische Oberfläche, auch nach der Modifizierung, bestätigt werden. Die modifizierten Gerüstverbindungen wurden erneut in Heck-Reaktionen auf ihre katalytische Aktivität untersucht, um die Ergebnisse mit denen der vorangegangenen Studie zu vergleichen. Da mit allen Katalysatoren vergleichbare Umsätze erreicht wurden, waren folglich auch die im Innern der Poren immobilisierten Komplexe erreichbar und aktiv. In der Kupplungsreaktion von Chlorbenzol und Styrol konnte mit den modifizierten MIXMOFs eine bessere Selektivität erzielt werden als mit MIL-53-NH_2(Al)-Mal-Pd. Die Ergebnisse der katalytischen Untersuchungen und die deutlich höhere Porosität der Gerüstverbindungen mit gemischten Linkermolekülen belegen eindeutig die Vorteile, die aus der Kombination des MIXMOF- und des PSM-Konzepts resultieren.

Um eine größere Vielfalt möglicher Substrate für Modifizierungsreaktionen und letztendlich auch katalytische Umsetzungen zu realisieren, wurden MOFs mit einem oder mehreren Linkermolekülen basierend auf DUT-5 mit größerem Porendurchmesser unter Normaldruck synthetisiert (Kapitel 4). DUT-5 ist isoretikulär zu MIL-53-NH_2(Al) und aus Al^{3+}-Ionen aufgebaut, die über Biphenyl-4,4‘-dicarboxylate verknüpft sind. Die Linkermoleküle mit einer zusätzlichen Amin-, Alkin-, Nitro- oder Azidgruppe wurden in der Gruppe von Prof. Bräse (Institut für Organische Chemie, KIT) hergestellt. Die Einbindung definierter Linkerverhältnisse in die MOFs wurde über Thermogravimetrie gekoppelt mit

FT-IR-Spektroskopie oder mittels ^{1}H-NMR-Spektroskopie nachgewiesen. Die thermische Stabilität der Materialien sowie ihre spezifische Oberfläche konnten über den Einbau verschiedener Linkerverhältnisse gezielt variiert werden, was erneut die Vorteile des MIXMOF-Konzepts aufzeigt. MIXDUT-5-amine(50) wurde für eine Reihe postsynthetischer Modifizierungen verwendet. Die Materialien waren auch nach der Modifizierung noch hoch porös, was deutlich den Vorteil von Gerüstverbindungen mit großen Poren in Modifizierungsreaktionen darlegt. In weiterführenden Studien könnten die neuartigen Materialien basierend auf DUT-5 für die Immobilisierung sterisch anspruchsvoller und komplexer Substrate herangezogen werden. Außerdem könnten diese Gerüstverbindungen für größen- und formselektive katalytische Anwendungen interessant sein. Aufgrund der modularen Bauweise der postsynthetisch modifizierten MOFs können die Katalysatoren gezielt an die speziellen Anforderungen der jeweiligen katalytischen Reaktion angepasst werden.

Im zweiten Fall wurde eine Syntheseroute entwickelt, die den direkten Einbau zweier unterschiedlicher Metallzentren in eine metallorganische Gerüstverbindung basierend auf HKUST-1 ermöglicht (Kapitel 5). HKUST-1, auch bekannt als Cu-BTC, ist aus dimeren Cu^{2+}-Einheiten aufgebaut, die über Benzol-1,3,5-tricarboxylate verknüpft sind. Das Cu^{2+}-Salz wurde in der Synthese, die ebenfalls unter Normaldruck durchgeführt wurde, partiell durch ein Ru^{3+}-Salz ersetzt. Die resultierende Gerüstverbindung Cu-Ru-BTC mit der Summenformel $Cu_{2.75}Ru_{0.25}(BTC)_2$*x$H_2O$ ist isoretikulär zu HKUST-1. Mittels Röntgen-absorptionsspektroskopie konnte der erfolgreiche Einbau der Ru^{3+}-Zentren in die HKUST-1-Struktur bestätigt und außerdem auch die zusätzliche Bildung unerwünschter Phasen (z.B. Cluster oder Nanopartikel) ausgeschlossen werden. In weiterführenden Arbeiten könnte Cu-Ru-BTC aufgrund seiner ungesättigten Metallzentren als bimetallischer Katalysator verwendet werden.

Die metallorganischen Gerüstverbindungen, die in dieser Arbeit vorgestellt werden, zeigen deutlich das Potential dieser Materialklasse für das Design äußerst vielseitiger Katalysatormaterialien. Die hohe Aktivität und Selektivität sowie die Reduzierung des Anteils gelöster Metallspezies in Heck-Kupplungen mit den palladiumhaltigen Gerüstverbindungen, die auf MIL-53 basieren, zeigen eindrucksvoll die Vorteile der neuartigen gegenüber herkömmlichen Katalysatormaterialien auf. Daher können in zukünftigen Studien auch vielversprechende Ergebnisse für das metallorganische Netzwerk DUT-5 mit immobilisierten Komplexen und die bimetallische Verbindung Cu-Ru-BTC erwartet werden.

Table of contents

1. Literature overview

1.1. General introduction

Metal-organic frameworks (MOFs) or porous coordination polymers (PCPs) are a relatively new class of materials (first reported in the late 1990s), which was pioneered by the groups of Férey[1-4], Kitagawa[5-8] and Yaghi[9-12]. MOFs are built of metal ions or clusters connected by organic linker molecules with at least two functional groups that can bind to the metal units. This architecture results in one-, two- or three-dimensional porous structures, whose topology is determined by the coordination sphere at the metal ions or clusters (so-called secondary building units, SBUs) and the geometry of the linker molecules. Since a multitude of diverse linker molecules (*e.g.* di- or tricarboxylates, diphosphonates) and different metal ions can be employed, the synthesis of metal-organic frameworks resulted in a multitude of different structures.[3, 6, 11-12] An important concept is the synthesis of isoreticular (also called isostructural) metal-organic frameworks, an approach which is highlighted in Chapter 1.2.1.

The framework structures can be highly porous with specific surface areas that are usually in the range of S_{BET} = 1000 m^2/g - 2000 m^2/g (BET: Brunauer-Emmett-Teller), but can also reach significantly higher values *e.g.* $S_{Langmuir}$ = 5900 m^2/g for MIL-101[13] (Matériaux de l'Institut Lavoisier), S_{BET} = 6240 m^2/g for MOF-210[14] and S_{BET} = 7140 m^2/g for NU-100[15] (Northwestern University). In addition to the high porosity and the thermal and chemical stability of the metal-organic frameworks, also the accessibility of the pores or the relevant sites is of great importance for potential applications. There are a number of promising reports for applications[16-18] of MOFs *e.g.* in gas adsorption and storage[19-26], gas separation[27-32], heterogeneous catalysis (Chapter 1.4 and Chapter 1.5.2), but also for the use as sensors[33-36], optical switches[37] or for drug release[38-40].

Another focus in the research area of metal-organic frameworks is on the development of improved synthetic routes to accomplish the preparation of new structures as well as phase-pure materials and to enable an easy scale-up, which is important for possible applications where large quantities of the framework are needed. Such novel methods include, *e.g.* high-throughput synthesis[41-43] for fast parameter screening, microwave assisted preparation routes[44-45] or the deposition of MOF thin films[46] on surfaces (*e.g.* SURMOFs[35, 47]).

1.2. Structure, properties and applications of important metal-organic frameworks

Although there have been earlier reports of one-dimensional coordination polymers[48-50], porous three-dimensional metal-organic framework structures were first reported in the late 1990s. Figure 1 depicts the number of "MOF" structures (1D, 2D and 3D) reported in the Cambridge Structural Database (CSD) each year. The number of different MOF structures is extremely high and is doubled approximately every four years. Therefore, only those MOFs that are relevant for this thesis are introduced in detail. The structure, properties and possible applications of the metal-organic frameworks MIL-53(Al)[51], DUT-5[52] (Dresden University of Technology) and HKUST-1[53] (Hong Kong University of Science and Technology, also known as Cu-BTC) are highlighted in the following sections (Chapter 1.2.2 to Chapter 1.2.4).

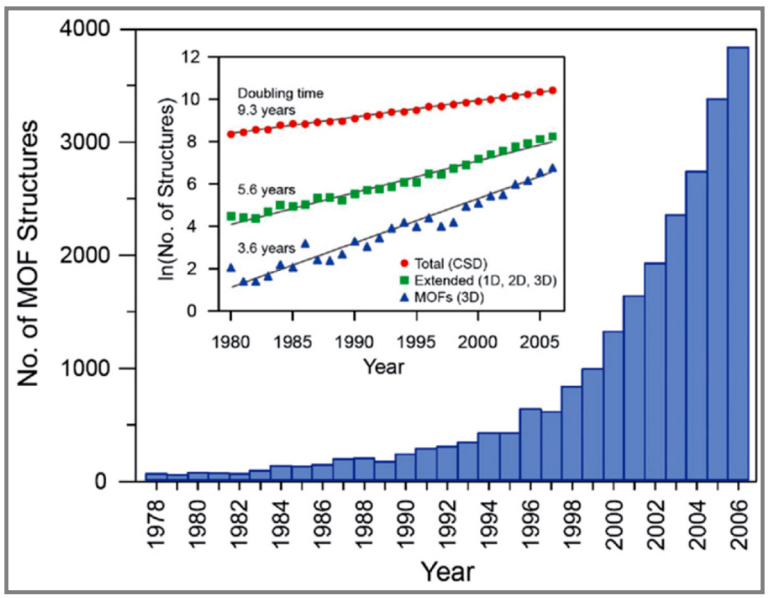

Figure 1: Number of MOF structures reported in the Cambridge Structural Database (CSD) until 2006; the inset shows the natural log of the number of structures as a function of time, indicating the doubling time of all structures in the database (red), of the MOF structures (green) and of the three-dimensional MOF structures (blue); reproduced from [54] with permission of The Royal Society of Chemistry.

1.2.1. Isoreticular framework synthesis

Isoreticular materials share the same framework topology, but either the linker molecules or the framework metal centers have been substituted. The concept of isoreticular synthesis was first developed by the Yaghi group based on MOF-5[10], which is, thus, also called IRMOF-1. MOF-5 is built of Zn_4O tetrahedra (Scheme 1, blue polyhedra) and all six edges are bridged

by a benzene-1,4-dicarboxylate (terephthalate, BDC) linker. This coordination results in octahedral SBUs, which form a cubic framework with space group $Fm\bar{3}m$ (Scheme 1, IRMOF-1). MOF-5 has a specific surface area of $S_{Langmuir}$ = 2900 m^2/g and is thermally stable to at least 300 °C in dry air.[10] The series of isoreticular metal-organic frameworks based on MOF-5 is the so-called IRMOF[11, 19-20, 55] series (Scheme 1). The isoreticular materials share the same framework topology but are constructed from different linker molecules, therefore, leading to functionalized frameworks with additional free organic groups (Scheme 1, IRMOF-2 to -7) or structures with a larger pore diameter due to elongated linker molecules (Scheme 1, IRMOF-8 to -16).

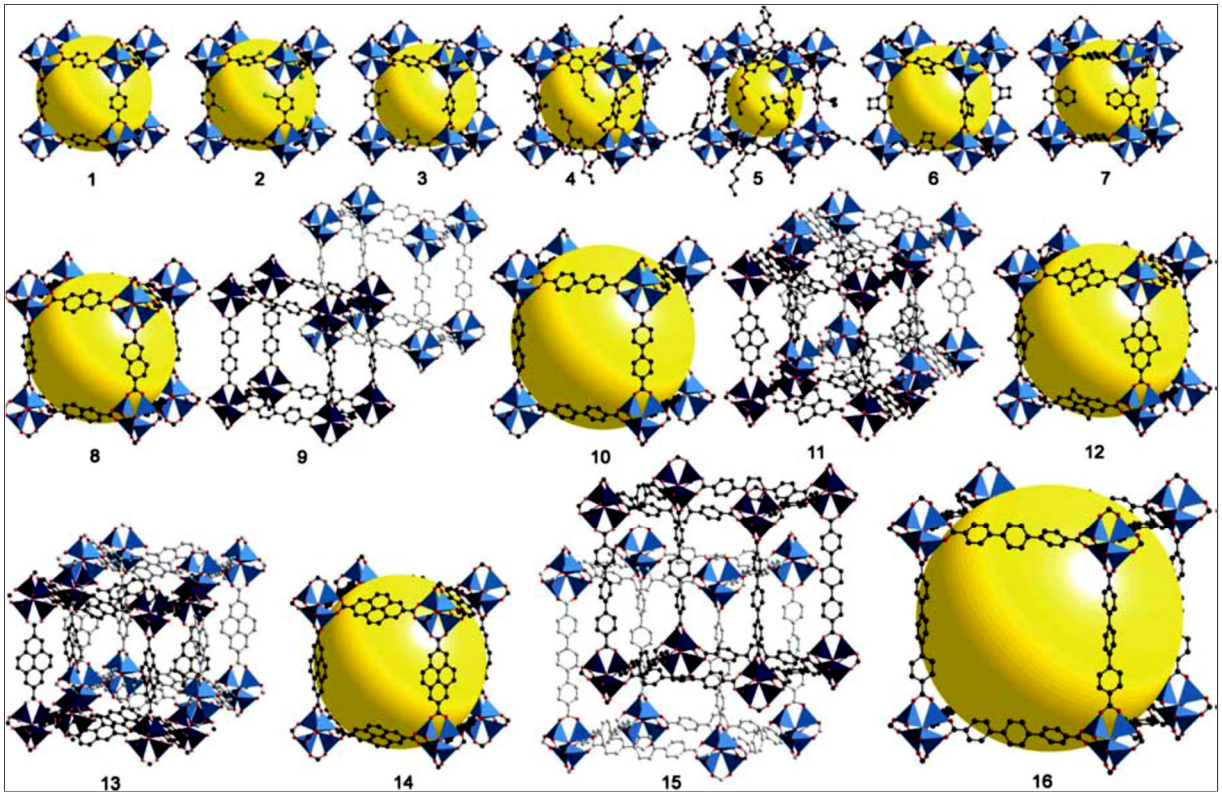

Scheme 1: Schematic representation of the IRMOF series based on MOF-5 (IRMOF-1); yellow spheres represent the internal void space; IRMOF-2 to -7: functionalized BDC linkers; IRMOF-8 to -16: elongated linkers; IRMOF-9, -11, -13, -15: interpenetrated structures; reprinted from [11] with permission from Elsevier.

There are a multitude of other examples for isoreticular frameworks to date based on, *e.g.* MIL-53[51, 56-57], MIL-140[58], STA-12[59-60] (University of St Andrews), UMCM-1[61] (University of Michigan Crystalline Material), UHM-2[62] (University of Hamburg Material) or HKUST-1[53, 63-65], which nicely illustrates the importance of this synthetic concept. However, the synthesis of isoreticular frameworks is not always straightforward, since

additional organic functionalities at the linker molecules could prevent the framework formation. This might be due to steric hindrance or coordination of the functional groups to the framework metal centers resulting in entirely different structures. A problem that might occur when longer linker molecules are applied during synthesis is the interpenetration or catenation of the structure. Due to the increased pore entrances a second framework, whose metal nodes are positioned in the pores of the first structure, might be formed (Scheme 1, structures 9, 11, 13 and 15). The interpenetration of a structure would reduce the accessible pore volume significantly contradicting the intended reason for applying elongated linkers.
Not only the linker molecules but also the metal nodes can be exchanged to achieve isoreticular framework structures. Prominent examples are the structures of MIL-53 (Chapter 1.2.2) and HKUST-1 (Chapter 1.2.4).

1.2.2. MIL-53(Al)

The metal-organic framework MIL-53 (Matériaux de l'Institut Lavoisier) was first synthesized by Serre *et al.* in 2002 under solvothermal conditions with Cr^{3+} ions as metal centers and benzene-1,4-dicarboxylate (terephthalate, BDC) as the linker molecules.[2, 66] In 2004, the synthesis of the aluminium-based analog MIL-53(Al) was achieved by the same group.[51] In the structure of MIL-53, the Al^{3+} ions are octahedrally coordinated by six oxygen atoms, four belonging to carboxylate groups and two to OH groups. The octahedra are linked by corner sharing -OH groups resulting in infinite Al-OH- chains, which are connected by the organic linker molecules to form a three-dimensional framework structure with one-dimensional channels (Scheme 2).
For MIL-53, a so-called "breathing effect" has been observed[2, 4, 51, 67-70], which describes the ability of the framework to adapt its pore geometry depending on the guest molecules incorporated in the channels. The three main geometries[51] are MIL-53(Al)_as (as-synthesized) with free residual acid molecules in the pores, MIL-53(Al)_ht (high temperature) without any guest molecules incorporated in the structure and MIL-53(Al)_lt (low temperature) with adsorbed water molecules in the channels (Scheme 2). Whereas the pores are wide open for MIL-53(Al)_as (7.3 Å x 7.7 Å, space group *Pnma*[51]) and MIL-53(Al)_ht (8.5 Å x 8.5 Å, space group *Imma*[51]), the strong interaction of the water molecules adsorbed in MIL-53(Al)_lt with the linker molecules results in a closed pore structure (2.6 Å x 13.6 Å, space group *Cc*[51]).

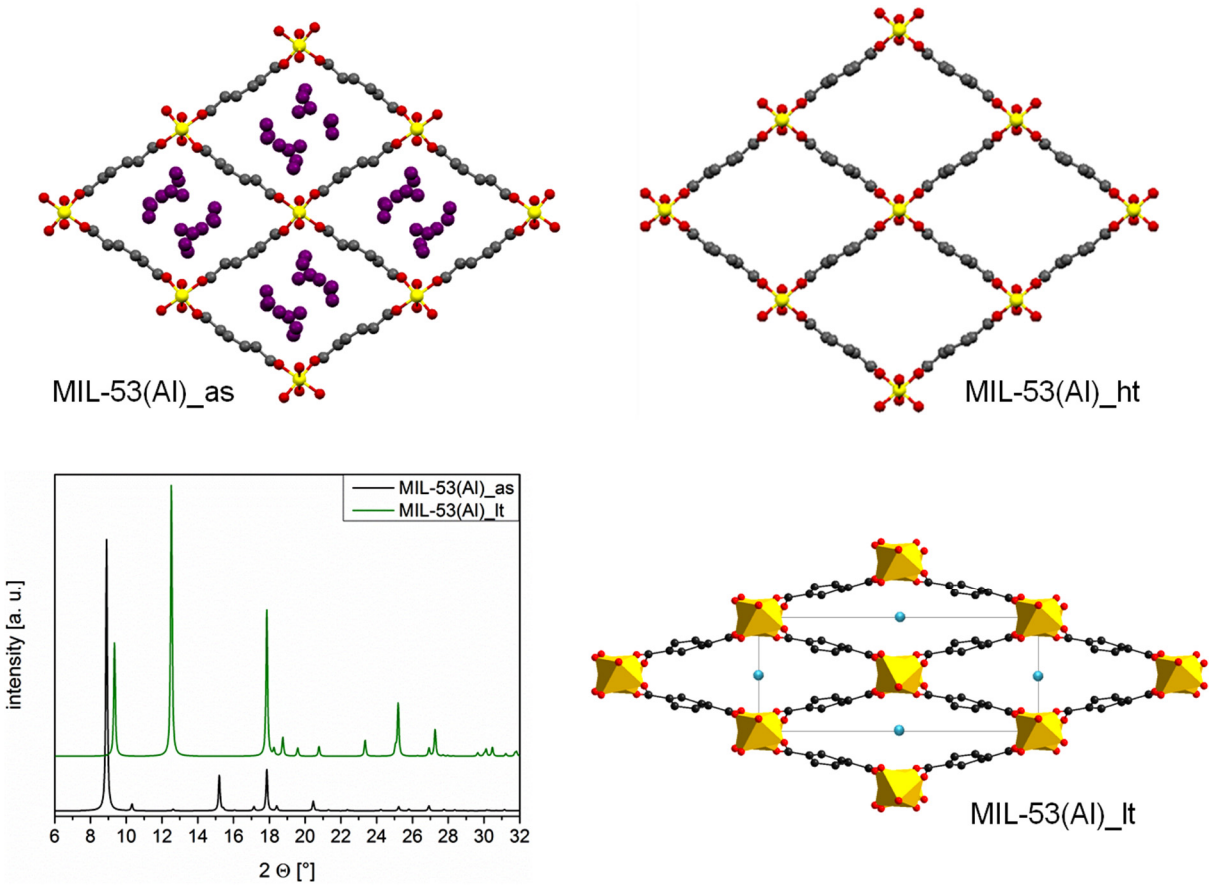

Scheme 2: Structures of the metal-organic framework MIL-53(Al); top left: MIL-53(Al)_as, space group *Pnma*; top right: MIL-53(Al)_ht, space group *Imma*; bottom right: MIL-53(Al)_lt, space group *Cc*; yellow: Al, grey: C, red: O, purple: free acid molecules, blue: H_2O; bottom left: simulated X-ray diffraction patterns of MIL-53(Al)_as (black) and MIL-53(Al)_lt (green).

The topological changes are clearly visible in the X-ray diffraction patterns of the samples (Scheme 2, bottom left). To remove the free acid molecules from the as-synthesized sample an activation step is necessary. For MIL-53(Al), empty pores were accomplished by heating to 275 °C[51], whereas for MIL-53-NH_2(Al) (*vide infra*) an exchange of the acid molecules with *N,N*-dimethylformamide (DMF) and subsequent removal of the solvent at 150 °C[56] had to be employed. The structure of MIL-53(Al) is retained up to 500 °C in air, and the framework is highly porous with a specific surface area of S_{BET} = 1140 m^2/g.[51]

There are a number of frameworks isoreticular to MIL-53(Al), which bear an additional functional group at the linker molecules that can influence the properties of the material or that can be used for further modification of the framework. The most prominent example is MIL-53-NH_2(Al)[56], which is synthesized using 2-aminobenzene-1,4-dicarboxylate (aminoterephthalate, ABDC) as linker molecule, but there are also frameworks with additional –Cl[57], -Br[57], -CH_3[57], -NO_2[57], –OH[57] or –COOH[71] groups. MIL-53-NH_2(Al) is thermally slightly less stable than MIL-53(Al), but the observed stability of approximately

400 °C in air[56] is still very high for a metal-organic framework compound. The specific surface area of MIL-53-NH_2(Al) is approximately S_{BET} = 1000 m^2/g[72] and the micropore volume is around 0.45 cm^3/g[57, 72]. Moreover, the synthesis of frameworks isoreticular to MIL-53 has also been achieved with a number of other metal ions besides Al, *e.g.* Sc[73], Cr[66], Fe[74] and Ga[75].

The high thermal and chemical stability as well as the high porosity and flexibility of the frameworks based on MIL-53(Al) resulted in a number of applications in *e.g.* gas adsorption[21, 24, 76-77], gas separation[25, 78-79], post-synthetic modification[80-81] and heterogeneous catalysis[80, 82].

1.2.3. DUT-5 and UiO-67

The metal-organic framework DUT-5 (Dresden University of Technology) was first synthesized by Senkovska *et al.* in 2009 under solvothermal conditions using biphenyl-4,4'-dicarboxylate (BPDC) as the linker molecule and Al^{3+} as metal nodes.[52] The structure of DUT-5 (space group *Imma*) is isoreticular to MIL-53_ht and is built of infinite Al-OH- chains connected by the linker molecules to form a three-dimensional framework structure with one-dimensional channels (Scheme 3). The pore entrances of DUT-5 are considerably larger (19.2 Å x 22.6 Å) compared to MIL-53_ht (8.5 Å x 8.5 Å) due to the longer linker molecules applied during synthesis. The structure is highly porous with a specific surface area of S_{BET} = 1610 m^2/g and thermally stable up to 430 °C.[52]

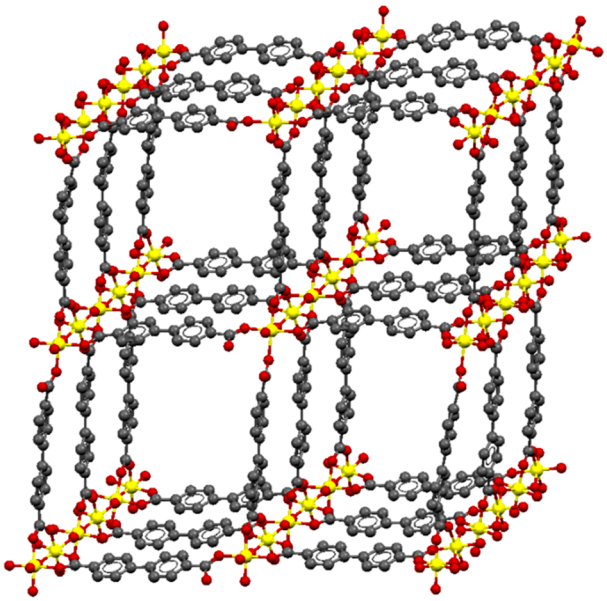

Scheme 3: Schematic representation of the structure of DUT-5; yellow: Al, grey: C, red: O.

Recently, the synthesis of functionalized frameworks isoreticular to DUT-5 was accomplished with linker molecules bearing additional sulfone groups[83-84], amine-[84] or nitro functionalities[84]. All materials were highly porous (S_{BET} = 1530 m^2/g – 1960 m^2/g) and stable to temperatures > 360 °C.[84] The larger pore dimensions and windows of DUT-5 might be beneficial for applications in gas storage and separation or for the immobilization of sophisticated metal complexes and their subsequent utilization in catalysis. To date the materials based on DUT-5 have been probed for their H_2 storage capacity[52], the adsorption of small molecules (CO_2, H_2, CH_4)[84] and the separation of alkanes and alkenes from aromatics[83].

Another metal-organic framework that could be synthesized with biphenyl-4,4'-dicarboxylate (BPDC) as the linker molecule is the zirconium-based material UiO-67 (Universitetet i Oslo, Scheme 4) from the Lillerud group.[85]

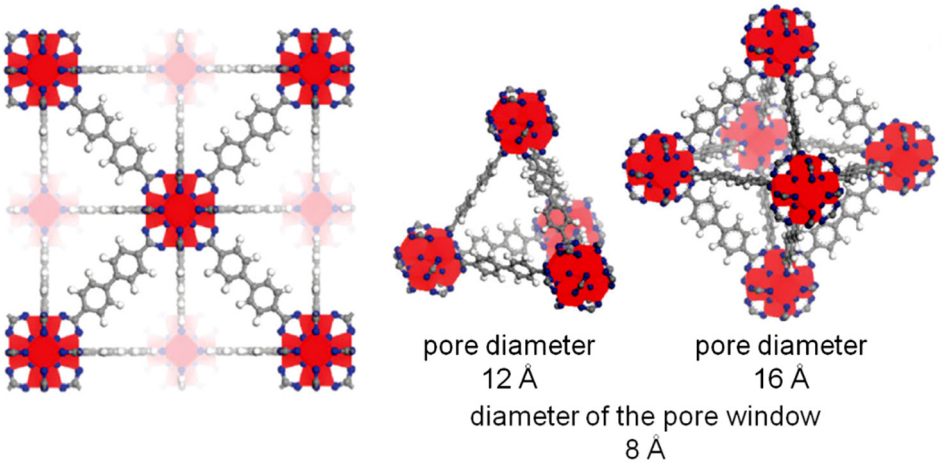

Scheme 4: Schematic representation of the structure of UiO-67 and the two types of pores present in the framework; adapted from [86] with permission of The Royal Society of Chemistry.

Although the framework has a high specific surface area of $S_{Langmuir}$ = 3000 m^2/g and two types of pores with a diameter of 12 Å and 16 Å, respectively, the pore windows only have a diameter of 8 Å. There are a multitude of reports on applications[86-92] of UiO-67 and its isoreticular analogs, however, the small windows might be a drawback regarding the accessibility of the pores for bigger substrates in post-synthetic modification reactions and catalysis.

Therefore, DUT-5 is an interesting alternative material built with the same linker molecules, but due to the framework topology with significantly larger pore windows of 19.2 Å x 22.6 Å. Nonetheless, the DUT-5 frameworks have only been utilized for a few studies so far.[52, 83-84]

1.2.4. HKUST-1

The metal-organic framework HKUST-1[53] (Hong Kong University of Science and Technology) was first synthesized by Chui *et al.* in 1999. This structure, which is also known as MOF-199[93-95], Cu-BTC[30, 96-99] or $Cu_2(BTC)_3$[45, 100-103] (benzene-1,3,5-tricarboxylate), is one of the best investigated metal-organic frameworks to date. The typical structural element in HKUST-1 is a Cu-Cu paddlewheel SBU (Scheme 5, right), which is constructed from a copper dimer bridged by four benzene-1,3,5-tricarboxylate linker molecules. In the equatorial position each Cu^{2+} ion is coordinated to four oxygen atoms of four different carboxylate groups, and the axial position is saturated by a solvent molecule, *e.g.* H_2O. Connecting those paddlewheel SBUs results in a three-dimensional cubic framework structure with channels of approximately 9.5 Å x 9.5 Å in diameter. Although a specific surface area of only S_{BET} = 692 m^2/g[53] was determined in the first report due to impurities (copper oxide species), the specific surface area could be increased since then up to S_{BET} = 1600 m^2/g by applying refined preparation methods[45, 98-100, 103-106], *e.g.* enhanced solvothermal or microwave assisted synthesis.

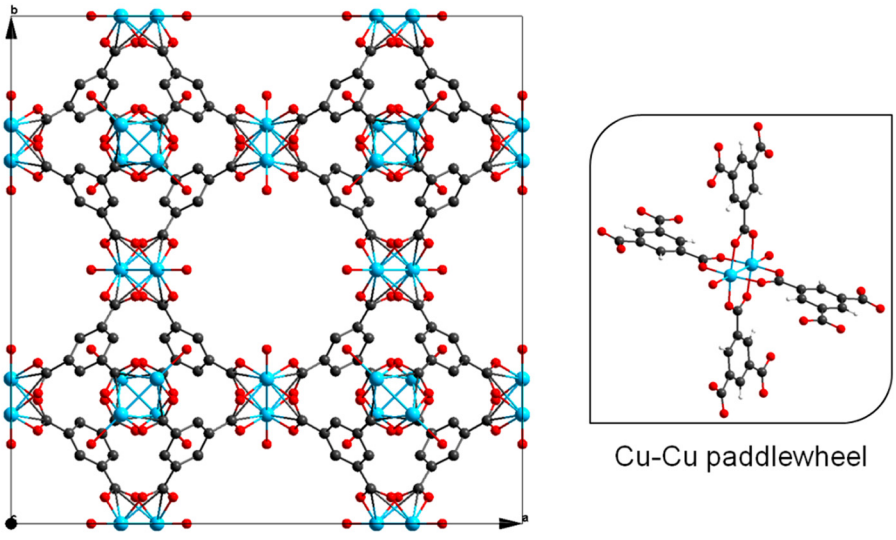

Scheme 5: Left: structure of HKUST-1; right: Cu-Cu paddlewheel SBU; blue: Cu, grey: C, red: O, white: H.

The solvent molecule at the Cu^{2+} centers can easily be removed upon heating (Scheme 6) without effecting the framework structure, thus, creating a free coordination site. Those Lewis acidic sites render Cu-BTC an interesting material for gas adsorption[26, 99, 107-108], gas separation[16, 28, 30, 96], catalysis[94-95, 97, 100-102, 109] and post-synthetic modification[110-111].

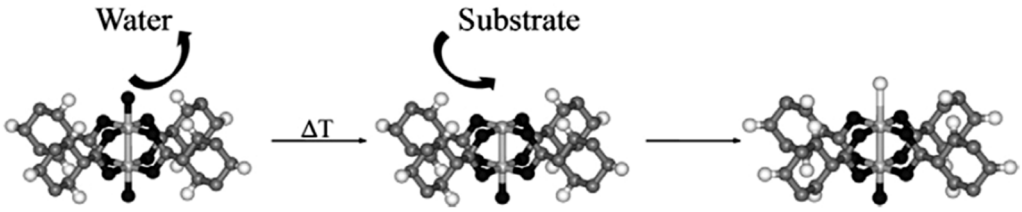

Scheme 6: Removal of water and subsequent coordination of a substrate molecule at a Cu-Cu paddlewheel unit of HKUST-1; adapted from [97] with permission from Elsevier.

Metal-organic frameworks isoreticular to HKUST-1 were also successfully synthesized with other metal ions[107] besides Cu, *e.g.* Cr[112], Fe[113], Ni[114], Zn[115-116], Mo[117] and Ru[46]. Additionally, the incorporation of functionalized linker molecules with an additional group, namely 2-aminobenzene-1,3,5-tricarboxylic acid[63] or 2-fluorobenzene-1,3,5-tricarboxylic acid[65], into Cu-BTC was achieved.[63-65]

1.2.5. Mixed-component metal-organic frameworks

Recently, the interest in mixed-component metal-organic frameworks (MC-MOFs) has increased significantly.[118-119] There are four different types of mixed-component frameworks, which can be distinguished (Scheme 7).

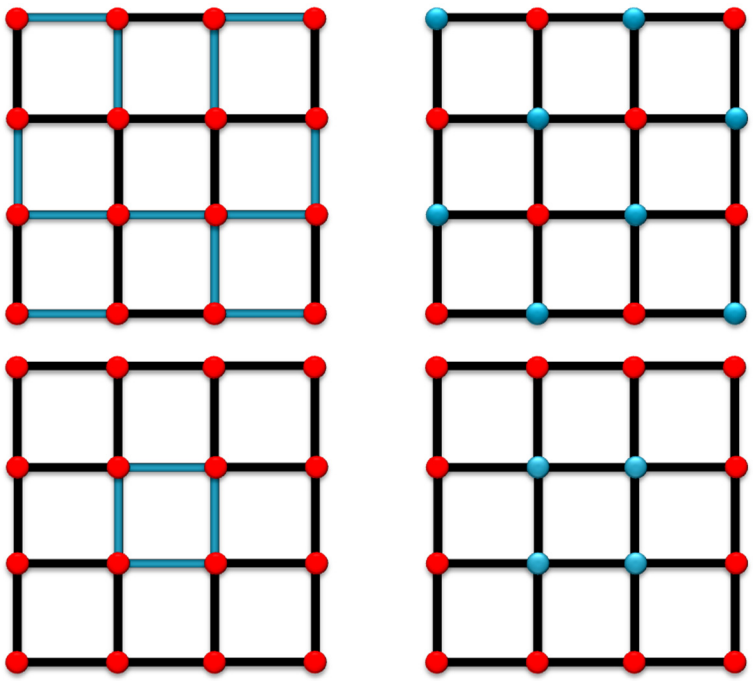

Scheme 7: Schematic representation of mixed-component MOFs (MC-MOFs); top left: mixed-linker MOF (MIXMOF); top right: mixed-metal or bimetallic MOF; bottom left: core-shell MOF with different linker molecules, bottom right: core-shell MOF with different metal centers.

One example are the so called mixed-linker metal-organic frameworks (MIXMOFs) containing more than one kind of linker molecules, which will be introduced in detail in Chapter 1.2.5.1 (Scheme 7, top left). Another possibility is the incorporation of different metal ions into the framework lattice resulting in mixed-metal or bimetallic metal-organic frameworks, which will be discussed in Chapter 1.2.5.2 (Scheme 7, top right). Both approaches aim at the homogeneous distribution of all components in the resulting framework structure. In contrast, the other two options are the formation of core-shell[120-125] structures (Scheme 7, bottom). In core-shell materials the composition on the inside and outside of the framework are different resulting in a phase change inside the particle. Since this approach is not relevant for this thesis, it is not discussed more detailed here.

1.2.5.1. Mixed-linker frameworks

The concept of mixed-linker metal organic-frameworks (MIXMOFs), which are sometimes also called multivariate metal-organic frameworks (MTV-MOFs[126]), was first established by Burrows *et al.*[127] and Kleist *et al.*[128] There are a number of different examples for MIXMOFs[118-119, 129] to date, but most reports focused on the substitution of a defined number of terephthalate linker molecules by functionalized terephthalate linkers (isostructural linker molecules), such as 2-aminobenzene-1,4-dicarboxylate. The best investigated MIXMOF series are based on MOF-5[126, 128, 130-131] and MIL-53(Al)[72, 132-133]. An important task in the synthesis of MIXMOFs is to quantify the ratio of the linker molecules incorporated in the framework and compare it to the initially applied ratio.[129] Moreover, confirming the homogeneous distribution of both linker molecules in the resulting materials instead of the formation of two separate phases or core-shell particles, is crucial.[129] The ratio of the incorporated linker molecules could be determined by, for example, solid state[134] and liquid phase[43] NMR or thermogravimetric analysis[128]. The homogeneity of the materials can be investigated using analytical techniques such as high-resolution X-ray diffraction[128, 132], thermogravimetric analysis[128, 132] and, in case of flexible MOFs, also physisorption measurements[72, 135].

The synthesis of MIXMOFs based on MOF-5 with up to 40 % of the 2-aminobenzene-1,4-dicarboxylate linkers was accomplished by Kleist *et al.*[128, 130] and thermogravimetric analysis revealed that the thermal stability steadily decreased with increasing amine ratio. The basicity and the catalytic activity of the materials could also be tuned depending on the number of incorporated amine functionalities.[128, 130] Mixed-linker frameworks based on MOF-5 could not only be synthesized with two linker molecules but

with up to eight different linkers.[126] In this study by the Yaghi group, the authors revealed that the properties of the MIXMOFs are not necessarily proportional to those of the single-linker composites, but that the combination of some linker molecules can have a beneficial influence on, *e.g.* the selectivity in the separation of CO_2 from CO.[126]

Mixed-linker metal-organic frameworks based on MIL-53 were successfully synthesized from defined mixtures of H_2BDC and H_2ABDC, and they have been extensively analyzed to establish trends in their thermal stability[132] and adsorption behavior[135] depending on the ratio of amine-functionalized linker molecules in the structure. Moreover, the effect of dehydration on the structure at the aluminium centers has been studied.[133] The quantification of the incorporated linker ratio was possible using solid state ^{1}H and ^{27}Al NMR[134], and the homogeneity could be proven by investigation of the breathing behavior[72, 135]. Kim *et al.*[136] prepared a mixed-linker MOF based on UiO-66 with a mixture of bromo- and amino-functionalized benzene-1,4-dicarboxylate linkers and applied it in an orthogonal post-synthetic modification reaction first modifying one functional group and then the other.

In the examples presented so far, the linkers were partly substituted by other linker molecules, which had an additional functional group, but the same coordinating groups for the formation of the framework. However, there are also examples where the coordinating groups are partially replaced. In the synthesis of Cu-BTC-PyDC[97] up to 50 % of the benzene-1,3,5-tricarboxylate (BTC) linker molecules could be substituted by pyridine-3,5-dicarboxylate linkers (PyDC) resulting in a defect coordination site, where the nitrogen atom of the pyridine occupies the coordination place of a carboxylate group. It was revealed that the introduction of such defect sites strongly influenced the catalytic selectivity of the Cu-BTC-PyDC frameworks compared to that of pure Cu-BTC.[97] A comparable MIXMOF could also be synthesized based on the ruthenium equivalent of HKUST-1.[137] In this study the incorporation of the PyDC linkers led to a partial reduction of the ruthenium centers and at the same time to an increased CO sorption capacity of the framework.[137]

Those examples clearly illustrate that the properties of MOFs can be tuned and, in some cases, even improved depending on the incorporated linker molecules. Therefore, the frameworks can be adjusted for targeted applications in gas adsorption or separation as well as in heterogeneous catalysis.

1.2.5.2. Bimetallic frameworks

The incorporation of two different metal centers into one material[118-119] might be interesting for applications in gas storage and separation or for catalysis. In catalysis, those materials could *e.g.* be utilized as bifunctional catalysts or in tandem reactions.

Botas *et al.*[138] achieved the substitution of up to 25 % of the Zn^{2+} centers in MOF-5 by Co^{2+} centers, which was confirmed by UV-vis spectroscopy, thermogravimetric analysis and the cell parameters derived from X-ray diffraction patterns. The incorporation of cobalt centers was limited to one fourth of all metal centers, *i.e.* one cobalt ion per SBU (see Chapter 1.2.1), even if a higher ratio was applied during synthesis. With increasing percentage of Co^{2+} incorporated in the frameworks, the adsorption capacity for H_2, CH_4 and CO_2 at high pressure was slightly increased.[138] Serre *et al.*[139] synthesized a bimetallic framework named MIL-78, which is built of benzene-1,3,5-tricarboxylate linkers and a mixture of yttrium and lanthanide ions (*e.g.* Eu, Tb, Dy). A high thermal stability up to 450 °C (for MIL-78(Y, Eu)) was determined and a strong fluorescence was observed under UV irradiation depending on the lanthanide ions incorporated in the structure (Eu: red, Tb: green, Dy: blue).[139]

A number of different bimetallic frameworks based on HKUST-1 have been reported. The first and also best investigated mixed-metal structure was Cu-Zn-BTC[140-143], in which up to 21 % of the Cu^{2+} centers could be replaced by Zn^{2+} ions[140]. The zinc ratio found in the framework structure was always lower than the ratio applied during synthesis and the specific surface area decreased significantly with increasing amount of Zn^{2+}, which was explained by coordination defects at the Zn^{2+} centers. The incorporation of the second metal into the framework structure was confirmed by a combination of ^{1}H and ^{13}C solid state NMR and EPR spectroscopy[140], and the resulting bimetallic framework was subject of further theoretical as well as spectroscopic studies[141-142]. Recently, the incorporation of manganese (6 %), iron (13.5 %) and cobalt (25.5 %) ions into Cu-BTC was accomplished *via* a post-synthetic metal exchange reaction.[143] In this approach, the MOF is first synthesized with Cu^{2+} ions and is then placed in a solution of the second metal to facilitate the ion exchange. The different substituted metal ions strongly influence the sorption properties of the framework towards nitrogen and oxygen, which was in good agreement with the binding energies to N_2 and O_2, respectively, calculated for the different metal ions.[143]

Although the bimetallic frameworks were mainly applied in sorption studies, the presented results exemplify the benefits of those materials. For future research applying bimetallic metal-organic frameworks as bifunctional catalysts or in tandem reactions might be interesting.

1.3. Post-synthetic modification (PSM)

For several potential applications (*e.g.* gas storage or separation, catalysis) additional free functionalities at the linker molecules, which are not coordinated to the framework metal centers, might be beneficial or even essential. However, not all groups can be introduced into the framework structure *via* direct synthesis, since the side group at the linker molecules might hinder the crystallization of the framework.[127, 144-147] This might be due to steric requirements of the additional groups or because the functionalities are also able to coordinate to the framework metal centers, therefore, preventing the formation of the targeted framework structure or resulting in a completely different topology. In those cases, post-synthetic modification[147-148] of the metal-organic frameworks – *i.e.* the formation of a bond between the linker molecules or unsaturated metal centers and a substrate after framework synthesis – is advantageous. This research area has been pioneered by the Cohen group[144, 147-151] but has since attracted a lot of interest from other groups[152-159]. Besides the presence of suitable free groups (*e.g.* amine or alkyne groups) or free coordination sites at the framework metal centers for the post-synthetic modification, there are also other important requirements for MOFs to be used in the PSM approach. First, the functional groups have to be accessible and, second, the framework structure has to be stable under the applied reaction conditions throughout the modification process.

1.3.1. Post-synthetic modification of amine groups

Metal-organic frameworks with additional free amine groups at the linker molecules have great potential for a number of simple post-synthetic modification reactions, *e.g.* with anhydrides[144-146, 157, 160-163], aldehydes[149, 152, 156, 158] or isocyanates[153-154, 164] (Scheme 8). In addition, the amine functionalities can be transformed into isocyanate[159, 165], isothiocyanate[165] or azide[155, 159] groups, which can then be used for further modification reactions. IRMOF-3 is the amine-functionalized framework that was most thoroughly studied in PSM investigations. This framework was applied in various "proof-of-principle" studies to demonstrate that covalent post-synthetic modification can be accomplished and that the approach enables the introduction of side chains, which are not accessible *via* direct synthesis.[144-145] The framework could also be modified in a two-step tandem PSM reaction facilitating the introduction of groups that cannot be incorporated in a single step[158, 160] or the introduction of more than one functionality[160] into one framework.

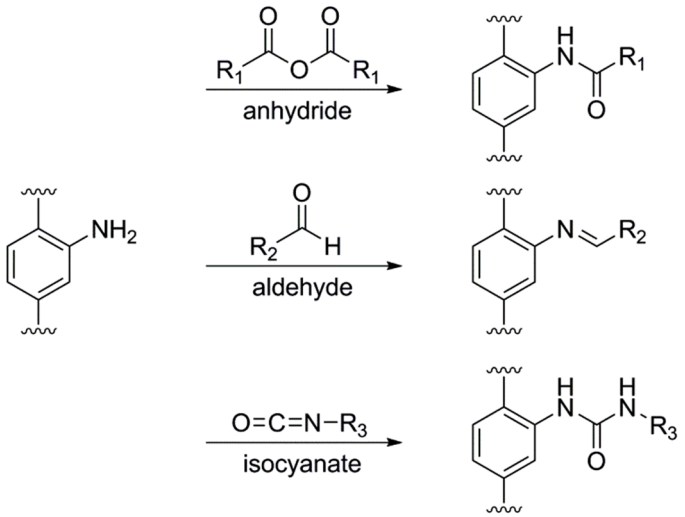

Scheme 8: Post-synthetic modification of amine groups with anhydrides (top), aldehydes (middle) and isocyanates (bottom).

Since IRMOF-3 is not stable in some protic solvents and acids[146], it might be beneficial to use a more robust framework for the modification reactions. MIL-53-NH_2(Al) is thermally and chemically very stable and has, therefore, been utilized for post-synthetic modification reactions of amine groups.[163, 165] Garibay *et al.*[163] modified MIL-53-NH_2(Al) with various anhydrides forming the corresponding amides. Whereas linear anhydrides, *e.g.* acetic anhydride, lead to the additional formation of the corresponding carboxylic acid in stoichiometric quantities, cyclic anhydrides, *e.g.* maleic anhydride, are incorporated altogether minimizing the purification process after PSM. It was shown that about 40 % of the amine functionalities were successfully modified when 60 eq of maleic anhydride were applied per amine group.[163] Utilizing maleic anhydride also results in the formation of a side chain, which can potentially be employed as chelating ligand for the immobilization of metal ions. Volkringer *et al.*[165] modified the amine groups to accomplish the formation of isocyanates and isothiocyanates, which can be transformed into urea, thiourea, carbamate and thiocarbamate derivatives in a second modification step. They observed that the breathing (pore opening) of the framework was only achieved with some solvents and revealed that the modification was only successful when those solvents were used during PSM.[165] Lescouet *et al.*[159] also successfully transformed the amine group into isocyanate functionalities, but these authors have chosen a reaction pathway *via* the azide. In the final step the isocyanates could again be converted into urea derivatives. Due to the highly reactive nitrene radicals formed during this reaction pathway, the formation of the urea derivatives was only possible with mixed-linker MIL-53-NH_2(20), in which only 20 % of the linker molecules bear amine

groups. The dilution of the radicals prevented side reactions and resulted in the targeted modification of the framework.[159]

1.3.2. Modification of alkyne groups

A relatively new modification approach for metal-organic frameworks is the Cu^+-catalyzed click reaction of an azide and an alkyne group (Scheme 9, top).[91, 166-167]

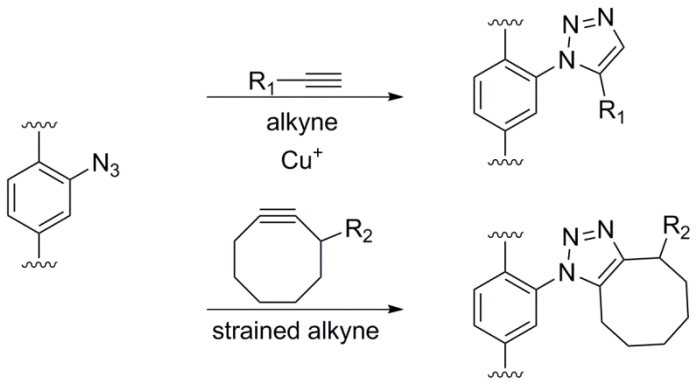

Scheme 9: Post-synthetic modification of azide groups *via* Cu^+-catalyzed click reaction with alkynes (top) and *via* copper-free click reaction with strained alkynes (bottom).

To realize this approach, an azide or alkyne group has to be available at the linker molecules for post-synthetic modification. For the incorporation of an azide functionality in the framework structure, mild reaction conditions are essential to prevent the transformation of the azide group, *e.g.* to the corresponding carbazole.[91] In most of the reports[91, 166-167], copper catalysts were employed to facilitate the click reaction, which most probably leads to undesired traces of the metal in the resulting modified MOF. Even traces of copper could prevent the application of the resulting MOFs, *e.g.* in catalysis or in life science. A possibility to avoid the use of Cu^+ catalysts in the click reaction is the application of strained alkynes, *e.g.* cyclooctyne (Scheme 9, bottom).[47, 168]

1.3.3. Introduction of defined metal complexes

Beside organic side chains, also defined metal centers can be introduced into the framework structure *via* the post-synthetic modification approach.[169] Various metal complexes were successfully incorporated in amine-functionalized UMCM-1-NH_2 (University of Michigan Crystalline Material) utilizing different modification routes.[152, 162] Doonan *et al.*[152] accomplished the immobilization of 2-pyridinecarboxaldehyde, which was then utilized as a

chelating ligand for Pd^{2+} ions (Scheme 10, left). The successful coordination of Pd^{2+} to the side chain of the linker molecules was confirmed by X-ray absorption spectroscopy (XAS).[152] Tanabe *et al.*[162] utilized the same framework for the immobilization of Fe^{3+} and Cu^{2+} complexes (Scheme 10, middle and right). The iron-containing framework could be applied as catalyst in a Mukaiyama-aldol reaction.[162]

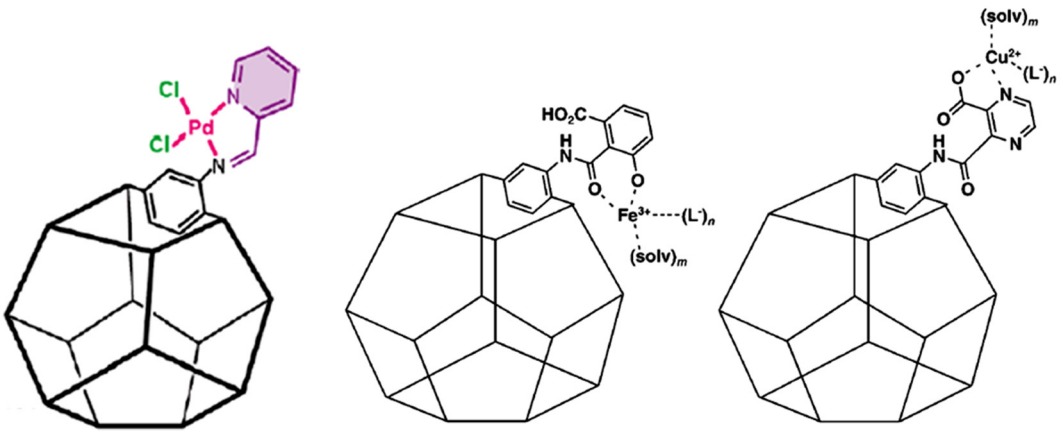

Scheme 10: Post-synthetic modification of UMCM-1-NH_2 by Doonan *et al.* (left, adapted with permission from [152]. Copyright 2009 American Chemical Society) and Tanabe *et al.* (middle and right, adapted from [162]. Copyright © 2009 Wiley-VCH Verlag GmbH & Co. KGaA, Weinheim).

The metal-organic framework IRMOF-3 has also been utilized for the immobilization of metal complexes. Bhattacharjee *et al.*[156] accomplished the immobilization of a manganese complex by covalently binding it to the amine groups in IRMOF-3 and applied the Mn-containing framework as catalyst in the aerobic epoxidation of alkenes. Liu *et al.*[170] successfully incorporated a chromium complex in IRMOF-3 using a two-step modification process. First, a chelating side chain was created by modification of the amine groups with salicylaldehyde, which were then used to immobilize Cr^{3+} ions. Although the structure was retained throughout the modification process, the specific surface area decreased due to the additional side chains in the porous structure.[170] Leus *et al.*[171] immobilized a titanium complex at the amine functionalities of MIL-47-NH_2(V), thus, creating a bimetallic catalyst system for aerobic oxidation reactions.

An interesting linker molecule that has been applied in the formation of a number of framework structures is 2,2'-bipyridine-5,5'-dicarboxylate (BPyDC). Due to the two nitrogen atoms of the pyridine rings and their respective positions, this linker is a perfect substrate for the direct immobilization of metal complexes into the framework structure. Bloch *et al.*[172] first applied the BPyDC linker in the synthesis of MOF-253 (Scheme 11), which is isoreticular to MIL-53 and DUT-5. They further accomplished the immobilization of Pd^{2+} and

Cu^{2+} complexes at the free bipyridine coordination sites of the linkers, which was proven for Pd^{2+} by X-ray absorption spectroscopy (XAS).[172] Carson *et al.*[173] loaded a Ru^{3+} complex into MOF-253 and applied the resulting framework as catalyst in the oxidation of alcohols.

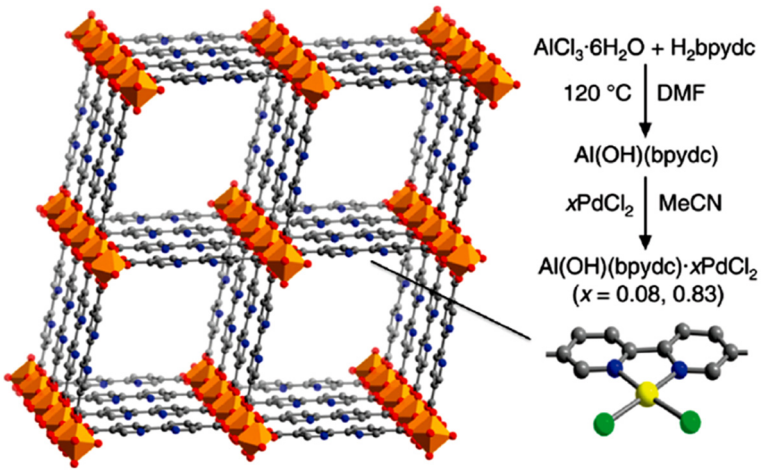

Scheme 11: Schematic representation of the structure of MOF-253 adapted with permission from [172], Copyright 2010 American Chemical Society; orange: AlO_6-octahedra, red: O, grey: C, blue: N, yellow: Pd, green: ligands.

Leus *et al.*[174] achieved the synthesis of the gallium-based framework COMOC-4 (Centre for Ordered Materials, Organometallics and Catalysis) and immobilized a Mo^{6+} complex on the bipyridine linkers. The resulting Mo-containing MOF was applied as catalyst in the epoxidation of alkenes.[174]

Defined metal complexes can not only be immobilized on free functional groups of the organic linker molecules but also on free coordination sites of framework metal ions. One example is the grafting of a Mo^{6+} complex on the free coordination sites of the Cu^{2+} centers in HKUST-1.[111] However, the porosity of the framework was lost completely throughout the modification process.[111] Kim *et al.*[175] immobilized diethylenetriamine at the free coordination sites of the Cr^{3+} centers in MIL-101(Cr) and subsequently incorporated Pd^{2+} ions. The immobilization of palladium was confirmed by ICP-OES (inductively coupled plasma optical emission spectrometry). However, the additional formation of small Pd^0 nanoparticles or clusters could not be excluded completely, since very small particles cannot be detected by XRD measurements owing to their lacking long-range order. The catalytic activity of the material was subsequently probed in a Heck reaction (see also Chapter 1.5.2).[175]

1.4. Metal-organic frameworks in catalysis

There are various reviews on metal-organic frameworks in catalysis, which give a profound overview of the topic.[176-186] Metal-organic frameworks, which are applied in catalysis, have to fulfill certain criteria most of which concern their stability. The framework structures have to be stable under the applied reaction conditions and, thus, a high thermal and chemical stability are required. The stability of the utilized frameworks is also important regarding the leaching of active species and the reusability of the catalyst material. In addition, the accessibility of the active centers in the framework structure has to be guaranteed. Therefore, the evaluation of the required properties of the catalyst and a careful selection of suitable metal-organic frameworks are essential.

1.4.1. Location of potentially active sites in metal-organic frameworks

Active centers can be introduced into a metal-organic framework structure in various forms and at several locations, which are schematically depicted as blue spheres in Scheme 12.

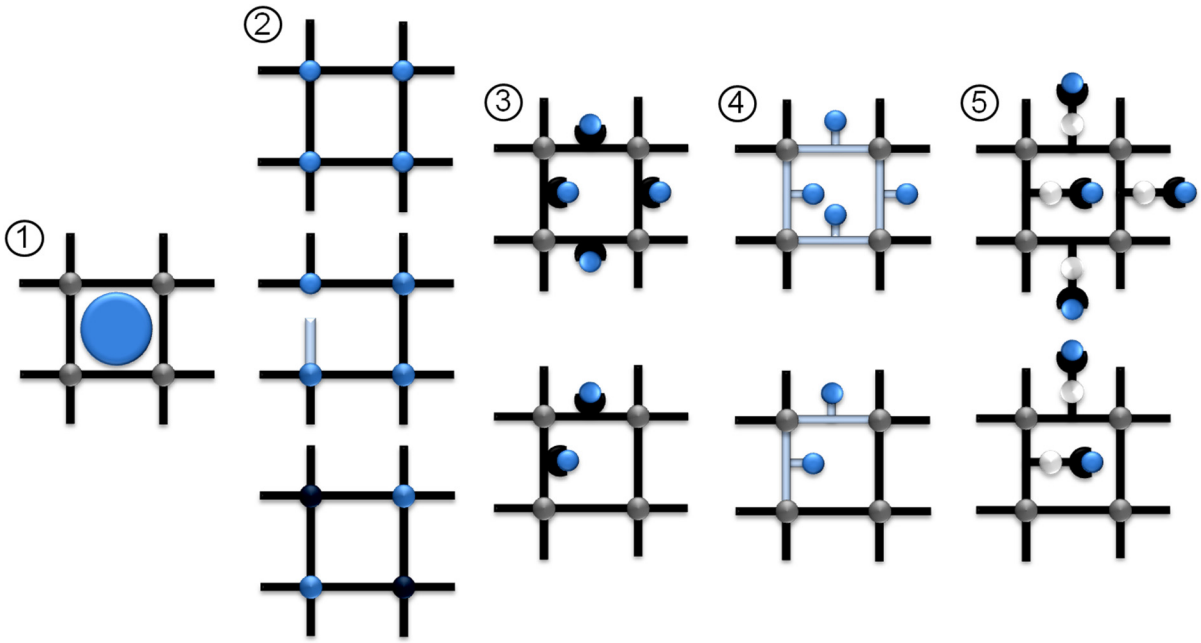

Scheme 12: Possible locations of potentially active sites (blue spheres) in MOFs; ① MOF as support for active species; ② unsaturated framework metal centers (top), MOFs with defect sites (middle) and bimetallic MOFs (bottom); ③ application of metalloligands in the synthesis of MOFs (top) or MIXMOFs (bottom); ④ functional groups at the linker molecules of MOFs (top) and MIXMOFs (bottom); ⑤ immobilized metal complexes in MOFs (top) and MIXMOFs (bottom) *via* post-synthetic modification.

Due to their high specific surface areas, MOFs have been applied as porous host matrix for the encapsulation of metal nanoparticles, clusters or organometallic complexes (Scheme 12, ①). There are numerous studies on the deposition of metal nanoparticles on different framework structures and their consecutive application in catalysis.[187-197] The nanoparticles can be introduced into the framework structures *via* different preparation routes[188, 194, 197] including *e.g.* liquid phase infiltration, ion exchange and vapor phase deposition. Relevant metal@MOF materials, which have been applied in C-C coupling reactions, will be discussed in more detail in Chapter 1.5.2. Since this approach leads to the encapsulation of nanoparticles instead of defined single-sites, these systems are not discussed in detail in this thesis.

Another possibility to apply MOFs in catalysis is the utilization of unsaturated framework metal centers as active sites (Scheme 12, ②, top). The unsaturated coordination sites, which are not needed for the formation of the framework, are usually saturated by solvent molecules, which can be removed upon heating. Another option to obtain free coordination sites at a metal center is the introduction of a linker molecule, which is lacking a coordinating group, hence, creating a defect site in the resulting structure (Scheme 12, ②, middle).[97, 198] This approach might also result in changed electronical properties, a higher flexibility of the framework and larger cavities, which might be beneficial for applications in catalysis.[97] Catalytic applications of MOFs with unsaturated framework metal centers will be outlined in Chapter 1.4.2. Although the amount of catalyst material can be drastically reduced due to the high density of active centers in these frameworks, the high metal content might be problematic for expensive noble metals. The metal centers in such frameworks resemble homogeneous complexes, however, they have a given coordination sphere, which does rarely allow for dynamic changes.

An additional approach is the incorporation of the active centers into the organic linker molecules. There are three different methods to achieve such frameworks (Scheme 12, ③-⑤): First, metalloligands can be used as linker molecules for framework synthesis facilitating the direct incorporation of a metal complex (Scheme 12, ③). Such metalloligands are, for example, linker molecules based on salen complexes[199-203], bipyridine complexes[87] (also Chapter 1.3.3) or porphyrin complexes[204-207]. Metal-organic frameworks with salen complexes of manganese as linker molecules are of great interest for epoxidation reactions of alkenes, since they represent heterogeneous versions of the highly active Jacobsen catalyst[208-209]. *Via* this approach also chiral linkers can be incorporated in the framework structures enabling enantioselective reactions.[199-202] Furthermore, the aerobic epoxidation of stilbene

was accomplished with a series of lanthanide frameworks constructed from Mn-salen linkers (Scheme 13).[203]

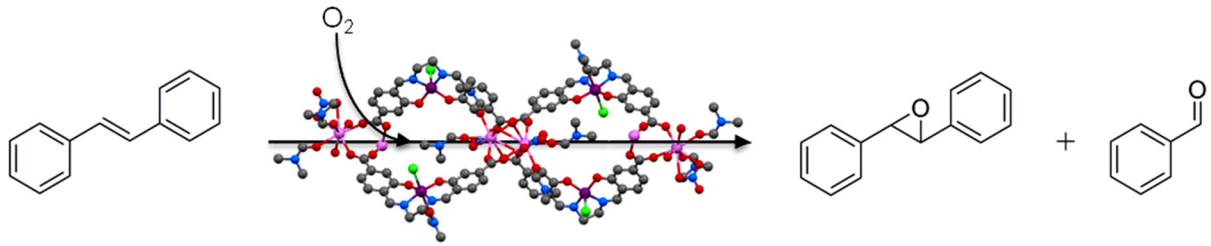

Scheme 13: Aerobic epoxidation of stilbene applying a lanthanide framework with Mn-salen linkers; Ln: pink, Mn: purple, O: red, N: blue, C: grey, Cl: green.

Second, organic groups at the linker molecules, which are not involved in the formation of the structure, might be catalytically active (Scheme 12, ④). Due to their basicity, amine-functionalized metal-organic frameworks (*e.g.* IRMOF-3, MIL-53-NH_2 and MIL-101-NH_2) were employed as catalysts primarily in base-catalyzed Knoevenagel condensation reactions[182, 210-215] (Scheme 14) but also for other transformations[128, 216].

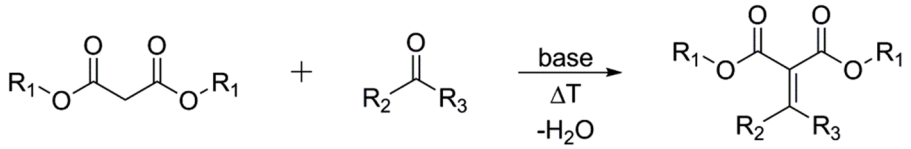

Scheme 14: Knoevenagel condensation reaction.

It is important to note that in some reports[210, 213, 215] on Knoevenagel reactions *N,N*-dimethylformamide (DMF) was utilized as a solvent, which is a nitrogen base that might also be able to catalyze the reaction. Although a high concentration of catalytically active centers seems to be advantageous, the application of MIXMOFs might be promising for some applications. The MIXMOF concept enables the dilution of functional groups in a framework and the tuning of various properties (*e.g.* thermal stability, basicity, surface area) and the material can, thus, be adjusted as needed for individual applications.[128, 130]

Another opportunity to accomplish the immobilization of defined metal complexes in the framework structure is the post-synthetic modification approach (Scheme 12, ⑤), which has already been discussed in Chapter 1.3.3. This approach is by far the most adjustable of those mentioned. Beside the ligand sphere of the complex, also the metal center can be adjusted individually to fit the target reaction. However, due to the immobilization of additional complexes in the porous structure blocking of the pore entrances can be problematic.[111, 170]

Dilution of the binding sites by applying mixed-linker MOFs or facilitating frameworks with a larger pore diameter might be beneficial to overcome those restrictions. Catalytic applications of the frameworks with immobilized metal complexes introduced by PSM are reviewed in Chapter 1.4.3.

1.4.2. Unsaturated framework metal centers

Several metal-organic frameworks with unsaturated framework metal centers have been applied in catalysis.[177, 185] This chapter focuses on the catalytic applications of the frameworks based on HKUST-1 (Scheme 5), MIL-101 (Scheme 15, left) and STA-12 (Scheme 15, right).

Each metal center in HKUST-1 is coordinated by one solvent molecule, which can be removed upon heating or substituted by a substrate molecule during catalysis (Scheme 6, Chapter 1.2.4). Framework materials based on HKUST-1 were applied as catalysts in a series of different reactions. The first report dates back to 2004 when Schlichte *et al.*[100] accomplished the phase pure synthesis of Cu-BTC and subsequently applied the framework in the cyanosilylation of benzaldehyde. However, during parameter optimization a low stability of the framework in certain solvents was observed and, therefore, only a yield < 60 % was achieved after three days.[100] Alaerts *et al.*[101] probed Cu-BTC for its activity in the isomerization of terpene derivatives. Although the copper precursor $Cu(NO_3)_2$ showed a higher activity compared to the solid catalyst, the selectivity was significantly increased after incorporation of the Cu^{2+} centers into the framework structure.[101] The catalytic activity of Cu-BTC in the Friedländer reaction for the synthesis of quinolines was studied by Pérez-Mayoral *et al.*[102, 217]. They observed a superior activity of Cu-BTC compared to conventional zeolite-based materials and explained the high conversion with the high loading of Lewis acidic sites and, especially, the presence of adjacent Cu^{2+} sites. Moreover, Cu-BTC was also compared to several other Lewis acidic frameworks and zeolites in different reactions including, *e.g.* Michael additions[109], click reactions[218] (Scheme 9), Knoevenagel condensation reactions[214] (Scheme 14) and the oxidation of benzylic alcohols[219].

Besides Cu-BTC, also the iron-containing framework based on HKUST-1 was used as a catalyst. Fe-BTC was studied in the Knoevenagel condensation reaction (Scheme 14).[214] Although the activity of Fe-BTC was slightly higher compared to zeolite-based catalysts, it was significantly lower than that of Cu-BTC, which might be due to the lower crystallinity of the iron-containing MOF.[214] Dhakshinamoorthy *et al.* tested Fe-BTC in the reduction of alkenes with hydrazine[220] and in the aerobic oxidation of benzyl amines[221] and alkanes[222].

Although the authors claimed an aerobic oxidation, it has to be noted that *N*-hydroxyphthalimide (NHPI) was enclosed in the framework structure, which is known to be a strong promoting additive.

HKUST-1 has also been synthesized with additional defect sites at the unsaturated metal centers by partially replacing the BTC linker molecules with pyridine-3,5-dicarboxylate (PyDC).[97, 137] Cu-BTC-PyDC[97] could be synthesized with up to 50 % of the defect linker PyDC while retaining the HKUST-1 structure, which was confirmed by X-ray diffraction and X-ray absorption data. Both Cu-BTC and Cu-BTC-PyDC were applied in the direct hydroxylation of aromatic compounds, such as toluene. However, due to the different electronic structure at the Cu^{2+} centers depending on the linker molecules the selectivity towards different products changed significantly.[97] For Ru-BTC-PyDC[137], beside a changed coordination sphere at the ruthenium centers due to incorporation of the defect linker, also a partial reduction of these centers was observed. The modified Ru-BTC-PyDC was more active in the hydrogenation of alkenes at ambient conditions than pure Ru-BTC and, therefore, the authors concluded that the defect sites beneficially influence the properties of the framework in this reaction.[137]

Another framework structure with unsaturated framework metal centers is MIL-101(Cr or Fe, Scheme 15, left), which has, for example, been investigated in the catalytic cyanosilylation of benzaldehyde[223], the synthesis of cyclic carbonates from epoxides and CO_2[224-225] and for the oxidation of hydrocarbons[224, 226-227]. The Kholdeeva group[227-228] applied MIL-101(Cr) and MIL-101(Fe) in the allylic oxidation of alkenes, which results in the formation of *α,β*-unsaturated ketones or alcohols. They observed that the iron version of MIL-101 was less stable compared to the chromium framework. Moreover, the product selectivity strongly depended on the framework metal centers. Whereas the chromium framework resulted in the formation of ketones, the iron compound strongly favored the formation of alcohols.[227] Zalomaeva *et al.*[225] applied MIL-101(Cr) in the formation of styrene carbonate and propene carbonate. High conversion and yield could be achieved at mild reaction conditions (8 bar, 25 °C), however, tetrabutylammonium bromide (TBAB) had to be added to the reaction as a promoting agent. Although a truly heterogeneous reaction pathway was established in hot filtration tests, the catalyst lost its porous structure and activity after several consecutive runs.[225]

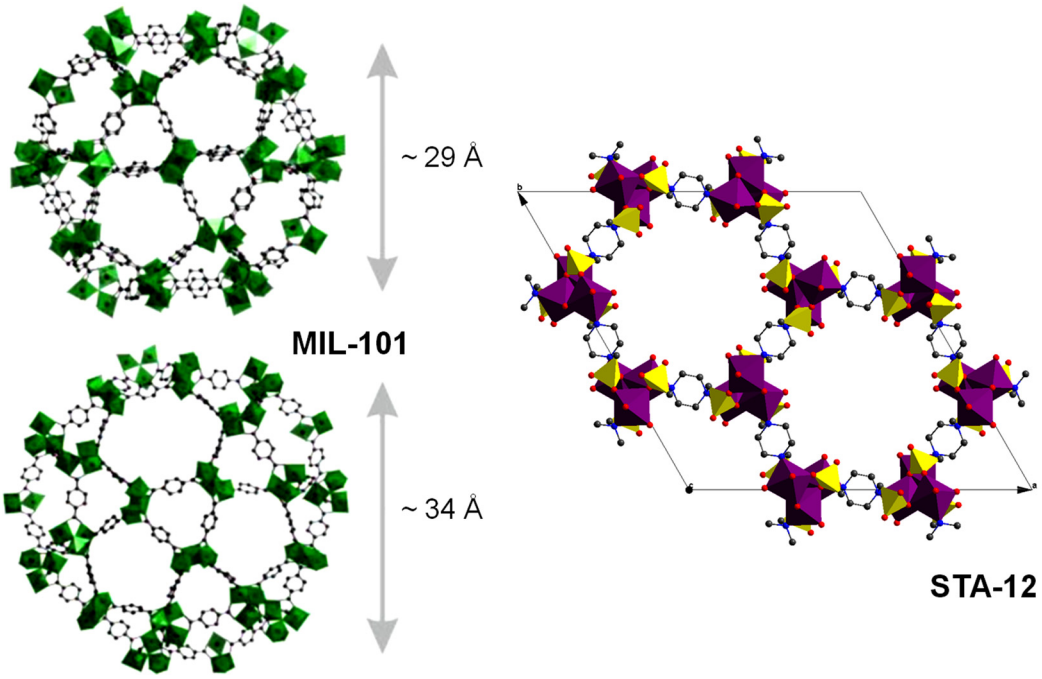

Scheme 15: Structures of MIL-101 (left, adapted with permission from [43], Copyright 2013 American Chemical Society) and STA-12 (right).

The framework STA-12(Co) with unsaturated Co^{2+} centers (Scheme 15, right) has been tested in the aerobic epoxidation of styrene and stilbene with low catalyst loadings of only 0.3 mol%.[229] Whereas stilbene was fully converted with a selectivity of nearly 90 % towards the epoxide, the conversion of styrene resulted in a very low selectivity, which was ascribed to oligomerization of the target product styrene oxide. The catalyst was reusable and no significant changes of the framework structure or leaching were observed.[229] The catalytic activity of the nickel form of STA-12 was probed in the intermolecular carbonyl ene reaction between alkenes and aldehydes.[109] In the reaction of α-methyl styrene and trifluoropyruvate, STA-12(Ni) yielded over 60 % of the product without significant loss of activity for at least three runs. The structure of the catalyst was retained throughout the cycles, and filtration tests suggested a heterogeneous reaction pathway.[109]

The metal-organic framework $[Pd(2\text{-pymo})_2]_n$[230], which is built from Pd^{2+} centers and 2-hydroxypyrimidinolate (pymo) linkers, was investigated for its activity in alkene hydrogenation[231-233], alcohol oxidation[231] and Suzuki coupling reactions[231]. The application of $[Pd(2\text{-pymo})_2]_n$ in Suzuki coupling reactions will be highlighted in Chapter 1.5.2. Opelt *et al.*[233] observed that in the hydrogenation reaction of a mixture of 1-octene and cyclododecene only 1-octene was hydrogenated in the first 4 h since the pores of the $[Pd(2\text{-pymo})_2]_n$ were too small for cyclododecene, which could consequently not reach the active sites. However, after 4 h the formation of palladium nanoparticles was detected, which

then also catalyzed the hydrogenation of cyclododecene.[233] A combined spectroscopic study of *in situ* infrared and X-ray absorption spectroscopy during hydrogenation of 1-octene revealed that the linker molecules were hydrogenated under the applied reaction conditions.[232] During this period the Pd^{2+} centers remained oxidized and the hydrogenation of 1-octene was nearly completed indicating that indeed the Pd^{2+} framework metal centers were the active species. However, Pd^0 nanoparticles were formed after the hydrogenation of the linker molecules was completed, thus, irreversibly destroying the framework structure. Obviously, the MOF was not stable in liquid phase hydrogenation reactions under the applied conditions.

1.4.3. Immobilized metal complexes

As already demonstrated in Chapter 1.3.3, the variety of immobilized complexes in MOFs and the resulting possibilities for applications of these frameworks is enormous. Therefore, only some selected examples will be discussed in this chapter.

Tanabe *et al.*[162] utilized UMCM-1-NH_2 equipped with an immobilized Fe^{3+} complex as Lewis acid in a Mukaiyama aldol reaction. The conversion after 24 h was < 60 % but the catalyst retained its activity over at least three cycles. The catalyst was size-selective for small silyl enol ethers, no iron leaching was detected and X-ray diffraction still showed an identical pattern after three cycles.[162] Dau *et al.*[234] immobilized a COD (1,5-cyclooctadiene) complex of Ir^+ on DMOF-1-dcppy (5,4'-phenylpyridine-dicarboxylate) and applied the framework as heterogeneous catalyst in the alkylation of amines. Under the applied reaction conditions, the catalyst achieved full conversion after approximately 30 h. X-ray diffraction patterns of the used catalyst showed that the framework was stable and hot filtration tests indicated no leaching of active species.[234]

A multitude of reports concern the application of various MOF-based catalysts in oxidation reactions[184] of *e.g.* alkenes[111, 171, 174] and alcohols[173]. Carson *et al.*[173] immobilized Ru^{3+} centers in the bipyridinedicarboxylate linkers of MOF-253 and applied the framework in the oxidation of primary and secondary alcohols. The oxidation was achieved with high yield and selectivity of approximately 90 % towards the corresponding aldehyde or ketone. The reaction was performed at low temperatures (< 40 °C) and the catalyst could be recycled six times without significant loss of activity. However, a strong oxidant ($PhI(OAc)_2$) was necessary.[173]

Bhattacharjee *et al.*[156] accomplished the immobilization of Mn^{2+} acetylacetonate complexes in IRMOF-3. The presence of the Mn^{2+} complex in the MOF structure was confirmed by IR and X-ray photoelectron spectroscopy (XPS). The resulting catalyst was tested in the

epoxidation of various alkenes with molecular oxygen, where it showed remarkable activity and selectivity towards the epoxide. However, two equivalents of trimethylacetaldehyde had to be applied as promoting agent to enable the use of O_2 as oxidant. The catalyst could be reused for at least three times without loss of activity and no leaching of active species could be detected.[156] Leus *et al.* also investigated the epoxidation of cyclohexene applying MIL-47-NH_2(V) modified with titanylacetylacetonate[171] and COMOC-4 with chelated Mn^{6+} ions at the bipyridinedicarboxylate linkers[174]. Using molecular oxygen, the yield of the epoxide was significantly higher for titanium-functionalized framework compared to pure MIL-53-NH_2(V).[171] Moreover, the leaching of vanadium, which was observed for the monometallic framework, could be prevented by addition of the Ti^{4+} complexes. The reason for this effect is, however, still unclear.[171] With Mo^{6+}-containing COMOC-4, a high selectivity towards the epoxide close to 100 % could be accomplished. The catalyst could be reused for at least three times without major loss of activity and no molybdenum leaching was detected. In this study, *tert*-butyl hydroperoxide (TBHP) had to be used instead of molecular oxygen to achieve the formation of the epoxide.[174] HKUST-1 with immobilized Mo^{6+} complexes (Chapter 1.3.3) has also been tested in the epoxidation of various alkenes with TBHP by Abednatanzi *et al.*[111] The catalyst achieved high conversion and selectivity close to 100 % and remained active in five consecutive runs. The turnover frequency (TOF) established for this catalyst is above the TOFs reported in literature for comparable Mo^{6+}-containing heterogeneous catalysts.[111]

1.5. C-C coupling reactions

C-C coupling reactions are interesting transformations for the synthesis of fine chemicals. Many of those reactions such as the Heck reaction (Scheme 16, ①), the Sonogashira reaction (Scheme 16, ②) or the Suzuki reaction (Scheme 16, ③) are readily catalyzed by palladium complexes. Immobilization of the active species in a solid material might enable easy separation and reuse of the catalyst and simplify the reaction process. Therefore, different methods were investigated to achieve truly heterogeneous catalysts for example by deposition of palladium nanoparticles (Chapter 1.5.1) or immobilization of palladium complexes on porous supports (*e.g.* C, Al_2O_3, zeolites). Recently, also palladium-containing metal-organic frameworks were applied in C-C coupling reactions, which will be discussed in Chapter 1.5.2.

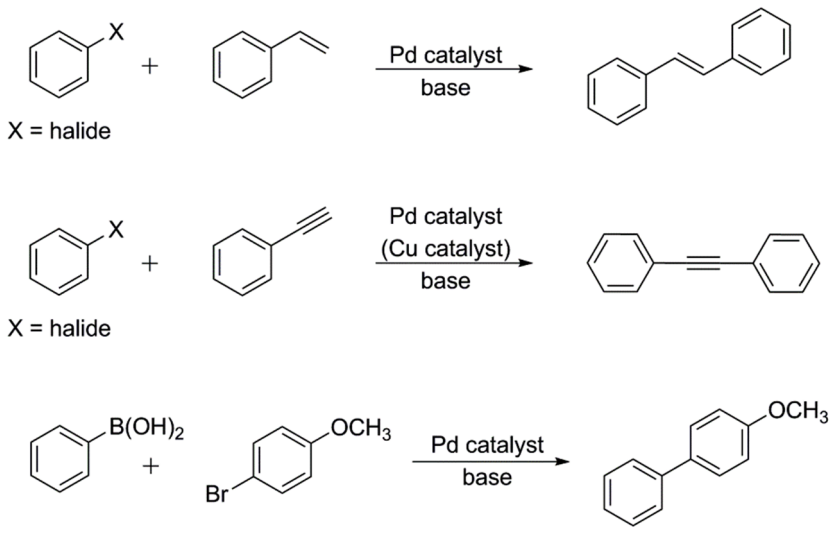

Scheme 16: C-C coupling reactions; ① Heck reaction, ② Sonogashira reaction, ③ Suzuki reaction.

1.5.1. Supported Pd catalysts in Heck reactions – a "quasi-homogeneous" mechanism

The Heck reaction (Scheme 16, ①) is a palladium catalyzed C-C coupling reaction between aryl halides and alkenes. Applying solid catalysts instead of the mainly utilized homogeneous complexes might have the advantage of easy separation and reuse. Therefore, the mechanism of the Heck reaction catalyzed by supported palladium nanoparticles has been extensively studied in the last couple of years applying various experimental and analytical methods.

Today it is widely accepted that not the palladium nanoparticles themselves but palladium complexes or clusters, which are *in situ* dissolved from the support, catalyze the reaction in a "quasi-homogenous" reaction pathway (Scheme 17).[235-239] Mononuclear palladium species are dissolved from the support by the oxidative addition of an aryl halide (Scheme 17, right bottom) and the reaction proceeds following the catalytic cycle known for homogeneous palladium catalysts. After the reaction is completed, the palladium species are reduced and redeposited on the support (Scheme 17, right top). The catalysts can be easily separated and most of them can be reused without significant loss of activity. However, sometimes growth of the Pd particles and, therefore, a change in the catalyst system is observed as a consequence of the dissolution-redeposition process. This undesired change can be prevented by a careful choice of the preparation method of the catalyst and the reaction conditions applied during catalysis.[237, 240] In literature, some supported systems were claimed to catalyze the Heck-type reaction of iodobenzene and alkenes in a truly heterogeneous manner. However, it is important to note that even negligible traces of palladium, which might be

below the detection limit of standard analysis methods, can be sufficient for the activation of reactive substrates such as aryl iodides and activated aryl bromides.[241] Similar "quasi-homogeneous" mechanisms were also reported for supported palladium catalysts in other C-C coupling reactions.

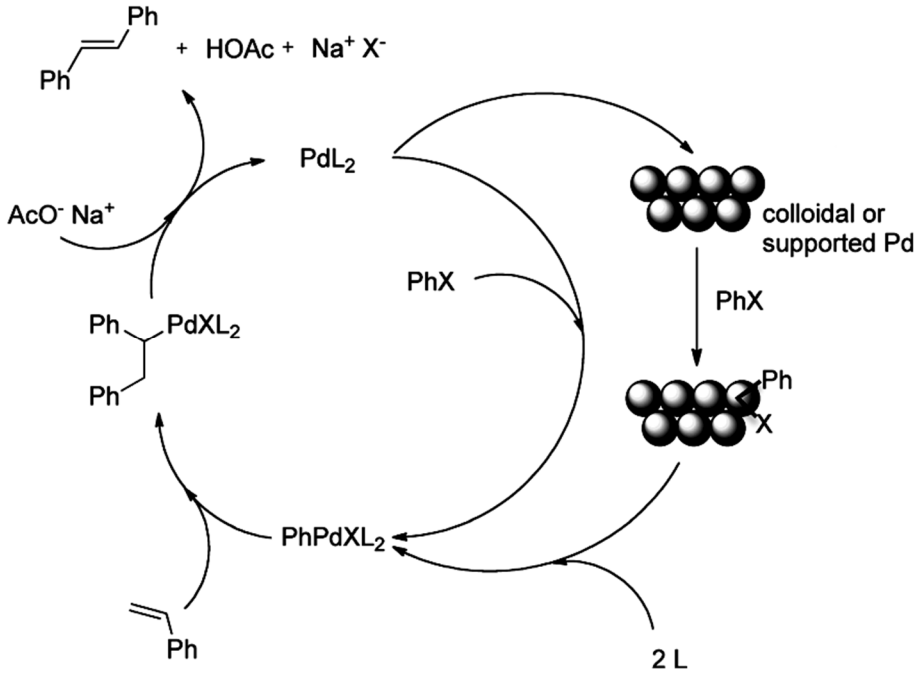

Scheme 17: Extended catalytic cycle of Heck reactions catalyzed by solid Pd species; adapted with permission from [238], Copyright 2011 American Chemical Society.

1.5.2. Metal-organic frameworks in C-C coupling reactions

In most reports of metal-organic frameworks applied in C-C coupling reactions, encapsulated palladium nanoparticles were utilized as active species.[189, 191, 193] There are only few examples so far, where MOFs with Pd^{2+} framework centers or Pd^{2+} complexes introduced by post-synthetic modification were tested for their activity in C-C coupling reactions.[87, 175, 231] Palladium nanoparticles were encapsulated into MOF-5 and probed for their activity in a Sonogashira reaction of iodobenzene with phenylacetylene derivatives by Gao *et al.*[189] The catalyst could not achieve the coupling of less reactive bromobenzene or chlorobenzene. Moreover, a drastic decrease in activity was observed after the second run, which was ascribed to oxidation and agglomeration of the palladium particles.[189] Another problem might be the low chemical stability of the MOF-5 framework. Huang *et al.*[191] encapsulated highly dispersed particles with a mean diameter of 3.1 nm in MIL-53-NH_2 *via* an ion exchange method with subsequent reduction of the palladium species. The loaded framework

was utilized as catalyst for the Suzuki coupling reaction of bromobenzene derivatives and arylboronic acid. Nearly full conversion was achieved in five consecutive runs after only 30 min at 40 °C.[191] The same group also deposited well dispersed palladium nanoparticles of identical size on mixed-linker MIL-53-NH_2.[193] The framework structure was retained and only a negligible loss of porosity was observed. The amine groups obviously stabilized the particles since the palladium species agglomerated immediately in amine-free MIL-53. The framework was active in the Heck-type C-C coupling reaction of bromobenzene derivatives and alkenes. However, a minor loss of activity and an increase in particle size were observed after several runs.[191] The mechanism of the metal-organic frameworks with encapsulated Pd nanoparticles is expected to be identical to the "quasi-homogeneous" mechanism of conventional supported catalysts.

There are a few examples, in which single-site palladium species incorporated in the MOF structure were utilized as the active species instead of nanoparticles supported on frameworks. This approach might facilitate alternative reaction pathways, since these palladium sites can be regarded as heterogeneous analogs of highly active homogeneous Pd complexes.

In the metal-organic framework $[Pd(2\text{-pymo})_2]_n$[230], the Pd^{2+} centers are surrounded by the 2-hydroxypyrimidinolate (pymo) linkers in a square planar coordination. The framework structure should not be affected by extension of the coordination sphere of the Pd^{2+} centers and was, hence, applied in the Suzuki coupling reaction between phenylboronic acid and 4-bromoanisole.[231] Under mild reaction conditions (40 °C, two days) the catalyst could be reused without significant loss of activity. The same conversion of approximately 90 % could be accomplished in only 5 h when the reaction mixture was heated to 150 °C. A hot filtration test under those conditions revealed no palladium leaching and the X-ray diffraction patterns were basically identical before and after the catalytic test.[231] However, utilizing MOFs with Pd^{2+} as framework metal centers might be problematic owing to the high costs caused by the high concentration of the noble metal.

Kim *et al.*[175] probed the catalytic activity of MIL-101(Cr) with a Pd^{2+} complex immobilized at the unsaturated metal centers for its catalytic activity in a Heck coupling reaction. Iodobenzene and acrylic acid were applied in this report and the authors claimed a heterogeneous reaction pathway.[175] It has to be noted that iodobenzene is activated quite easily due to the weak C-I bond and that even traces of leached palladium can catalyze the reaction. Still, the catalyst could be reused three times without losing its activity and no leaching of palladium was detected.[175]

Very recently, palladium doped UiO-67 (Scheme 4) was successfully synthesized by Chen *et al.*[87] using a mixed-linker approach. 10 % of the biphenyl-4,4'-dicarboxylate (BPDC) linker molecules were substituted by a metalloligand, namely 2,2'-bipyridine-5,5'-dicarboxyate with an immobilized Pd^{2+} complex. Due to the high dilution of the metalloligands, the Pd^{2+} centers should be well dispersed and isolated in the resulting framework structure. The modified MOF was applied in Heck and Suzuki reactions with chlorobenzene derivatives, which are, in general, difficult to activate because of the strong C-Cl bond. The MOF-based catalyst accomplished high conversion of those substrates and was reusable in at least five consecutive runs without significant loss of activity making this system a promising material for future research in C-C coupling reactions.[87]

1.6. Scope of the present thesis

Metal-organic frameworks (MOFs) are interesting novel materials for applications in catalysis since they feature structural motifs, which can be seen as heterogeneous analogs of highly active single-site complexes. Thus, they combine beneficial characteristics of both homogeneous (defined metal centers, high activity) and heterogeneous (easy separation and reuse) catalysts. The high variety in MOF topologies, linker molecules, framework metal centers and post-synthetic modification reactions should allow for a highly versatile catalyst design, which can be individually adjusted for specific applications. The aim of the presented thesis was to develop different concepts for the synthesis of novel single-site catalysts based on metal-organic frameworks and to perform first catalytic studies with those new materials. All metal-organic frameworks should be synthesized *via* a novel synthetic strategy at ambient pressure to enable easy scale-up, which is important for potential applications requiring large amounts of a material.

First, defined palladium complexes should be immobilized on MIL-53-NH_2(Al) (Chapter 2) *via* a two-step post-synthetic modification (PSM) reaction, which should be confirmed applying a multitude of characterization techniques (XRD, ATR-IR, TG, N_2 physisorption, AAS and XAS). The activity of the resulting catalyst materials should be probed in Heck-type C-C coupling reactions of bromo- or chlorobenzene with styrene. Since dissolved palladium complexes are known to be the catalytically active species in the presence of conventional heterogeneous catalysts (Chapter 1.5.1), the leaching of the novel MOF-based systems should be investigated. The palladium species immobilized in the frameworks can be regarded as heterogeneous counterparts of such dissolved complexes and, therefore, a reduction of leached species can be expected.

Since the high concentration of amine groups available for PSM might be problematic regarding the porosity of the modified materials, defined palladium complexes should also be immobilized in mixed-linker MIL-53-NH_2(x) (x = 40, 60, 80, Chapter 3). Applying the MIXMOF approach, a homogeneous distribution of accessible palladium complexes was expected, which should be ascertained employing various characterization techniques (XRD, ATR-IR, TG, N_2 physisorption, ^{1}H NMR, AAS and XAS). The novel materials should again be tested in Heck-type C-C coupling reactions of bromo- or chlorobenzene with styrene to compare them to the previous study and to gain insight into the influence of the amine percentage in the frameworks on the modification process and the catalytic results.

Applying metal-organic frameworks with larger pore dimensions is expected to broaden the scope of possible substrates applicable for post-synthetic modifications. Thus, more sophisticated metal complexes might be introduced into the framework structure or bulkier substrates might be utilized in the subsequent catalytic applications. Novel functionalized single- and mixed-linker frameworks based on DUT-5 should, consequently, be prepared to increase the pore dimensions of the resulting material (Chapter 4). After thorough characterization (XRD, ATR-IR, TG, TG-IR, N_2 physisorption, ^{1}H NMR) the functionalized mixed-linker frameworks should be applied in post-synthetic modification reactions for a "proof-of-principle" study using different substrates.

In addition, HKUST-1 with potentially free coordination sites at the framework metal centers should be modified by partial substitution of the Cu^{2+} centers with Ru^{3+} ions (Chapter 5). Ru^{3+} might be beneficial due to its favored octahedral coordination geometry and its similar ionic diameter, which should facilitate the incorporation into the HKUST-1 structure. The resulting material should be thoroughly characterized (XRD, ATR-IR, TG, N_2 physisorption, ICP-OES and XAS) to confirm the presence of Ru^{3+} in the framework structure and to exclude the formation of additional undesired phases. For future studies the resulting bimetallic framework might be promising for applications as bifunctional catalyst or in tandem reactions since both metal centers are versatile catalyst species.

2. Immobilization of Pd complexes on MIL-53-NH$_2$(Al)[242]

2.1. Motivation

Due to its remarkable properties, the metal-organic framework MIL-53-NH$_2$(Al)[56] is an attractive material for post-synthetic modification[163, 165] and catalytic applications[159, 210]. MIL-53-NH$_2$(Al) is thermally stable up to at least 350 °C and the structure is retained in organic solvents as well as diluted acids and bases. Owing to the high specific surface area (S_{BET} ~ 1000 m^2/g), the amine groups are accessible and can easily be utilized in a multitude of simple transformations with anhydrides[144, 146, 161-163], aldehydes[149, 152, 156, 158] as well as various other substrates[153-155, 164-165]. Therefore, in this study MIL-53-NH$_2$(Al) was chosen as starting material for the immobilization of well-defined mononuclear palladium complexes *via* a two-step post-synthetic modification reaction utilizing first maleic anhydride and then palladium acetate. The activity of the immobilized complexes should be tested in Heck-type C-C coupling reactions and is expected to be similar to comparable homogeneous systems, while separation and reuse should be feasible more easily. Thus, the resulting material might combine the beneficial characteristics of both homogeneous (high activity) and heterogeneous (easy separation and reuse) catalysts. In addition, leaching of active species, which is well-known for conventional supported catalysts in Heck-type C-C coupling reactions, might be reduced, since the catalyst already contains highly defined mononuclear palladium complexes.

In this Chapter the novel synthesis of MIL-53-NH$_2$(Al) at ambient pressure and its subsequent two-step post-synthetic modification (PSM) are highlighted. In addition, the characterization results (XRD, nitrogen physisorption, ATR-IR, AAS, XAS) after each synthetic step and the catalytic application of the resulting MIL-53-NH$_2$(Al)-Mal-Pd in Heck-type C-C coupling reactions are covered in detail.

2.2. Synthesis and post-synthetic modification

In contrast to the synthesis reported in literature[56], a non-solvothermal preparation route at ambient pressure was developed and applied in the synthesis of MIL-53-NH$_2$(Al). Instead of autoclaves, round bottom flasks could be used and, hence, scale-up of the reaction should be achievable more easily. This is an important requirement for the industrial fabrication of large amounts of a material that are needed for certain applications. MIL-53-NH$_2$(Al) was

synthesized using a solution of 2-aminobenzene-1,4-dicarboxylic acid (terephthalic acid, H$_2$ABDC) and Al(NO$_3$)$_3$*9H$_2$O (ratio 1:1) in DMF/H$_2$O, which was heated to 90 °C for 24 h (Scheme 18). As a reference, MIL-53-NH$_2$(Al) was also prepared *via* the solvothermal route known from literature.[56]

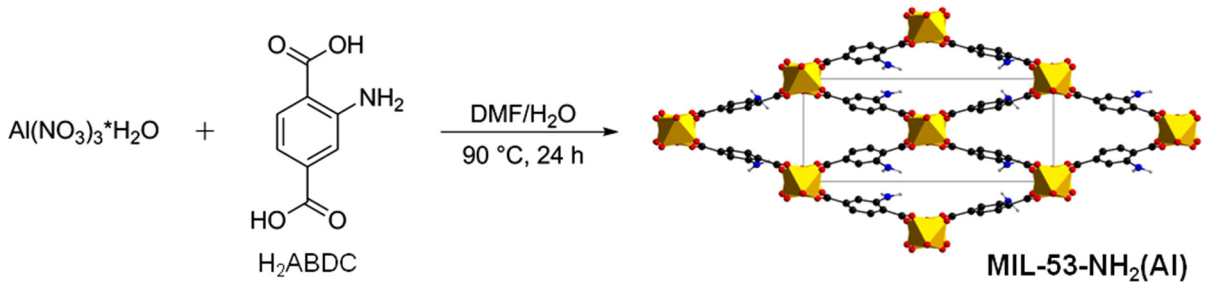

Scheme 18: Synthesis of MIL-53-NH$_2$(Al); grey: C, white: H, red: O, blue: N, yellow: Al.

After thorough characterization of MIL-53-NH$_2$(Al), the MOF was applied as starting material for a two-step post-synthetic modification (PSM) reaction, in which palladium complexes were immobilized on the amine groups of the framework structure (Scheme 19). In the first step the amine functionalities were modified with maleic anhydride, which resulted in the formation of an amide (MIL-53-NH$_2$(Al)-Mal) and in the second step this new side chain was utilized as chelating ligand to immobilize Pd^{2+} ions (MIL-53-NH$_2$(Al)-Mal-Pd). To optimize the PSM reaction, varying amounts of maleic anhydride (2 – 10 eq) and palladium acetate (0.25 – 1.5 eq) were applied. The amount of palladium acetate was calculated in regard to the literature value of 40 %[163] of the amine groups being successfully modified with maleic anhydride. The modified frameworks prepared with 0.25 eq (MIL-53-NH$_2$(Al)-Mal-Pd) and 1.5 eq (Pd@MIL-53-NH$_2$(Al)) of palladium acetate are discussed in detail in this Chapter.

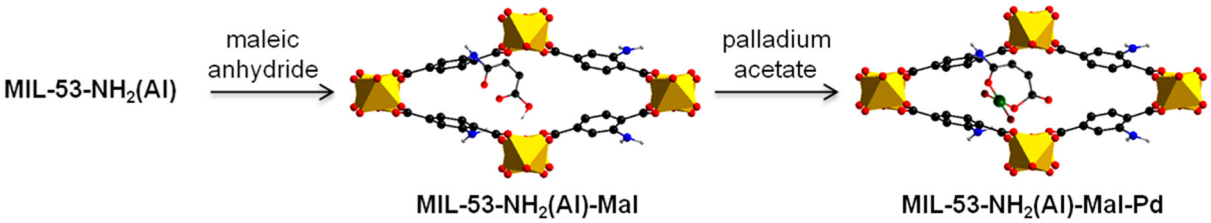

Scheme 19: Two-step post-synthetic modification of MIL-53-NH$_2$(Al) with, first, maleic anhydride and, second, palladium acetate; for clarity only one pore is shown; grey: C, white: H, red: O, blue: N, yellow: Al, green: Pd, brown: ligands.

All materials were thoroughly characterized after each synthetic step using X-ray diffraction (XRD), FT-IR spectroscopy (ATR mode) and nitrogen physisorption measurements (BET). The Pd-containing frameworks were additionally investigated by atomic absorption spectroscopy (AAS) and X-ray absorption spectroscopy (XAS).

2.3. Characterization

To analyze the crystal structure and to confirm the successful synthesis of MIL-53-NH$_2$(Al) under non-solvothermal reaction conditions, X-ray diffraction was applied. The diffractogram of MIL-53-NH$_2$(Al) matched the pattern reported in literature for MIL-53-NH$_2$(Al)_lt[56] perfectly. Obviously, a phase-pure framework without any residual acid molecules enclosed in the porous structure was obtained *via* the novel preparation route at ambient pressure. Thus, the additional activation steps described in literature[51, 56] for the materials synthesized under solvothermal conditions were not required, which clearly proves another advantage of the chosen synthetic approach. XRD further proved that the structure of MIL-53-NH$_2$(Al) (monoclinic, space group *Cc*) was retained throughout the modification process. In the diffractograms of the modified samples (Figure 2) a shift could be seen for most reflections, whereas the signals corresponding to distances perpendicular to the pore structure ((*hkl*) = (200) and (400)) remained at the same values for 2 Θ (9.28 ° and 18.62 °, respectively).

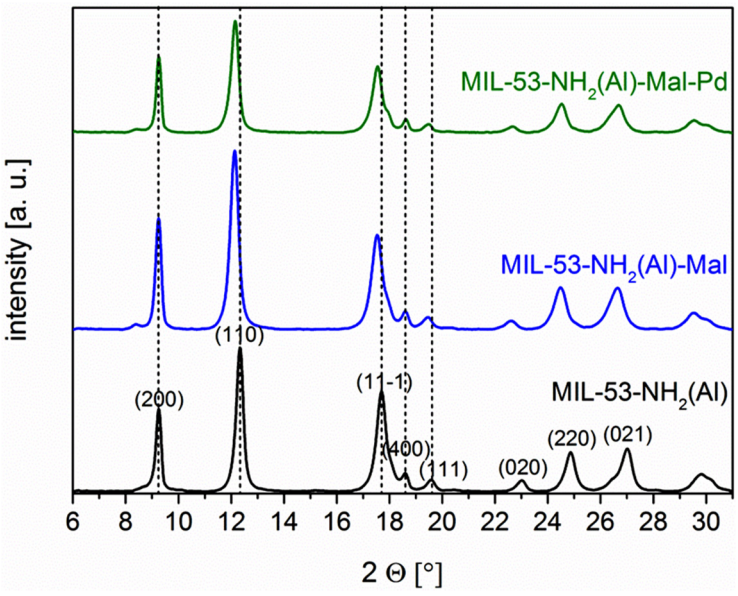

Figure 2: X-ray diffraction patterns of MIL-53-NH$_2$(Al) (black), MIL-53-NH$_2$(Al)-Mal (blue) and MIL-53-NH$_2$(Al)-Mal-Pd (green); dashed lines are added to illustrate whether or not the reflections were shifted after modification.

This observation was caused by the so called breathing effect of MIL-53-NH$_2$(Al), which describes the ability of the framework to change its pore geometry depending on the interactions with the substrate or guest molecules inside the pores.[51, 56] The different geometries of MIL-53(Al) were described in Chapter 1.2.2. Therefore, the observed shift of the reflections is an indication that post-synthetic modification of the amine groups in MIL-53-NH$_2$(Al) was achieved.

To optimize the reaction conditions for the first modification step with maleic anhydride, the reaction temperature (80 °C - 100 °C) and the ratio of maleic anhydride per amine group (2 - 10 eq) were varied. In the XRD patterns of those samples, the shift of the reflections increased with increasing temperature and ratio of maleic anhydride (Figure 3). The increasing shift indicated more distinct changes in the pore geometry of the frameworks and, thus, might also suggest a larger amount of introduced modified side chains, which means a higher degree of modification.

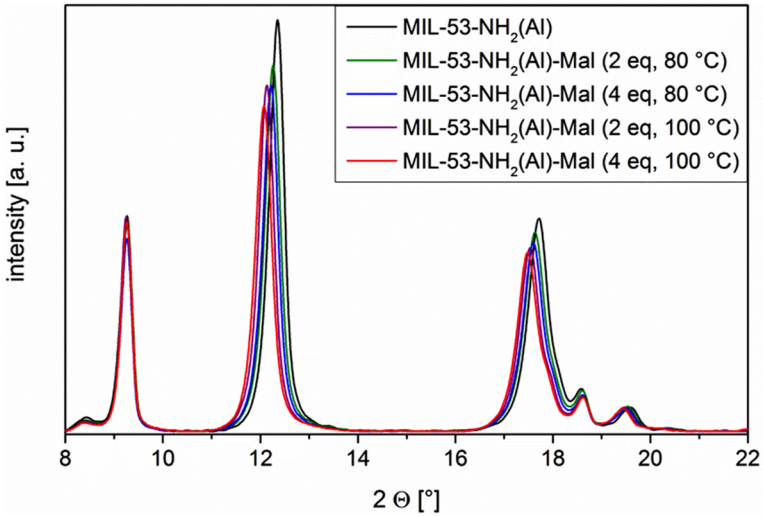

Figure 3: X-ray diffraction patterns of MIL-53-NH$_2$(Al)-Mal synthesized under different reaction conditions compared to the pattern of MIL-53-NH$_2$(Al).

The ATR-IR spectrum of MIL-53-NH$_2$(Al) synthesized at ambient pressure did not show a band around $\nu = 1680\ cm^{-1}$, which would correspond to protonated linker molecules. In contrast, a clear band could be found for the reference sample MIL-53-NH$_2$(Al)_as, prepared *via* the conventional synthesis route[56] using an autoclave (Figure 4). As already indicated by XRD, MIL-53-NH$_2$(Al) prepared *via* the novel synthesis route was free of unreacted precursor species, while the material prepared under solvothermal conditions required an additional activation step as described in literature[56] to remove residual acid molecules. Thus, besides

having the advantage of an easier scale-up, the synthesis at ambient pressure also resulted in materials of high purity so that the tedious purification was not necessary.

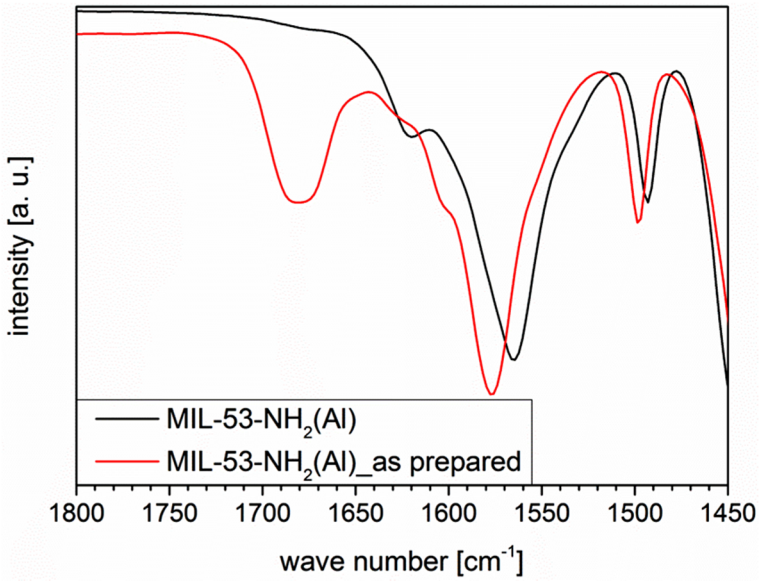

Figure 4: IR spectra of MIL-53-NH$_2$(Al) (black) synthesized at ambient pressure compared to the reference sample MIL-53-NH$_2$(Al)_as (red) containing free acid molecules after preparation in an autoclave.

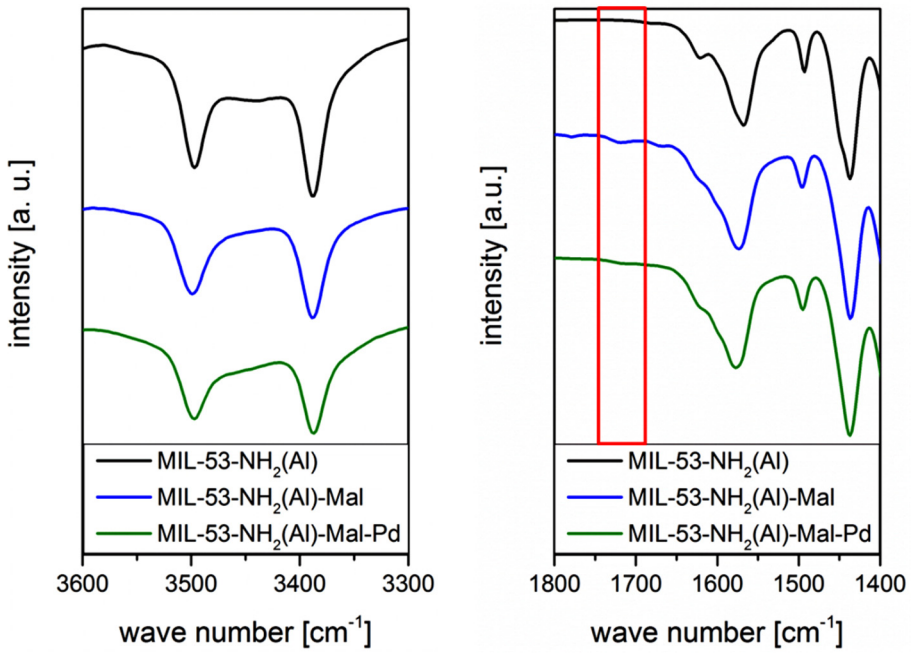

Figure 5: ATR-IR spectra of MIL-53-NH$_2$(Al) (black), MIL-53-NH$_2$(Al)-Mal (blue) and MIL-53-NH$_2$(Al)-Mal-Pd (green); left: N-H stretching vibrations of the amine groups (ν = 3498 cm^{-1} and ν = 3387 cm^{-1}); right: C=O stretching vibration of maleic anhydride (approx. ν = 1700 cm^{-1}).

The IR spectra of the modified frameworks indicated the successful formation of the amide functionality. The intensity of the N-H stretching vibrations of the amine group ($\nu = 3498$ cm^{-1} and $\nu = 3387$ cm^{-1}, Figure 5, left) decreased, while an additional weak band could be found around $\nu = 1700$ cm^{-1} (Figure 5, right), which was ascribed to the C=O vibration of the carbonyl groups introduced at the side chains of the framework structure. Notably, vibrations of residual maleic anhydride could not be observed, which strongly indicated successful modification.

Nitrogen physisorption measurements (Figure 6, Table 1), evaluated by the BET method, showed a high specific surface area of $S_{BET} = 980$ m^2/g for MIL-53-NH_2(Al). The observed step in the adsorption branch of the isotherm at $p/p_0 \approx 0.15$ has also been reported in literature for frameworks based on MIL-53 in physisorption measurements with nitrogen[56, 70] as well as other small molecules (CO_2[21, 67, 69], Xe[68]) and has been attributed to the breathing effect and the resulting change in pore geometry. The strong hysteresis between the adsorption and desorption isotherm has also been reported in literature.[56, 70]

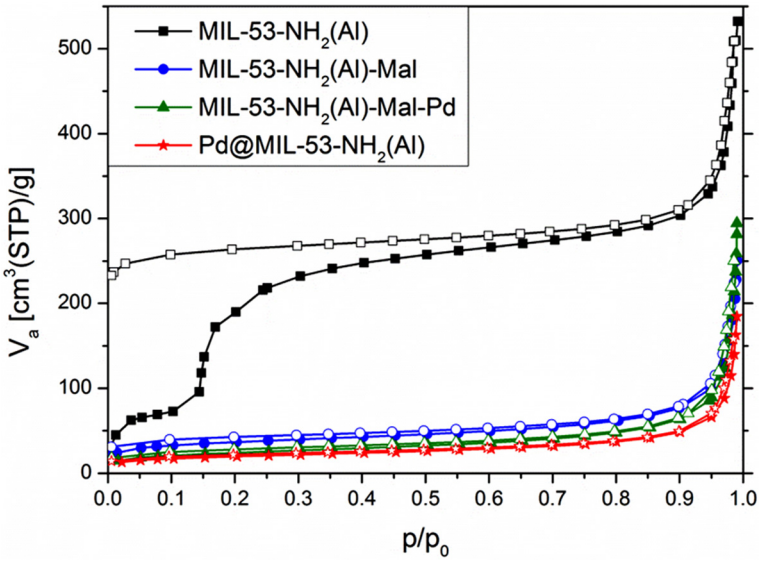

Figure 6: Adsorption (filled symbols) and desorption (open symbols) isotherms obtained from nitrogen physisorption measurements of MIL-53-NH_2(Al) (black), MIL-53-NH_2(Al)-Mal (blue), MIL-53-NH_2(Al)-Mal-Pd (green) and Pd@MIL-53-NH_2(Al) (red).

After the first modification step with maleic anhydride the specific surface area of MIL-53-NH_2(Al)-Mal decreased to $S_{BET} = 155$ m^2/g, which again proved the successful modification of the amine groups and, therefore, the formation of the chelating side chain. Increasing the amount of the Pd precursor applied in the second modification step, resulted in a decreasing specific surface area ($S_{BET} = 90$ - 65 m^2/g). This fact indicated that with

increasing amount of the Pd precursor either the amount or the nature of the immobilized species in the porous structure were different, which will be discussed later on employing atomic absorption and X-ray absorption spectroscopy. Based on the results from those studies, the materials were named MIL-53-NH_2(Al)-Mal-Pd, when 0.25 eq of the palladium precursor were applied, and Pd@MIL-53-NH_2(Al), when 1.5 eq were used.

Table 1: Specific surface areas and micropore volumes of MIL-53-NH_2(Al) and the modified framework materials obtained by nitrogen physisorption measurements.

sample	S_{BET} [m^2/g]	micropore volume [cm^3/g]
MIL-53-NH_2(Al)	980	0.39
MIL-53-NH_2(Al)-Mal	155	0.03
MIL-53-NH_2(Al)-Mal-Pd	90	0.01
Pd@ MIL-53-NH_2(Al)	65	0.01

Atomic absorption spectroscopy of digested samples (Chapter 7.2.7) was used to determine the metal content of the different Pd-containing framework materials. The results revealed a metal content of 2.1 wt% to 2.4 wt% independent of the amount of Pd precursor (0.25 – 1.5 eq) that was applied during the modification reaction. However, N_2 physisorption measurements revealed a decreasing specific surface area with increasing amount of the Pd precursor. This led to the hypothesis that high precursor amounts (1.0 – 1.5 eq, *e.g.* Pd@MIL-53-NH_2(Al)) resulted in the formation of undesired nanoparticles which blocked the pore system of the framework, whereas the requested immobilization of Pd complexes was achieved with small amounts of the precursor (0.25 – 0.5 eq, *e.g.* MIL-53-NH_2(Al)-Mal-Pd).
The hypothesis was tested using X-ray absorption spectroscopy (XAS) at the palladium K-edge (24350 eV). XANES (X-ray absorption near edge structure, Figure 7) spectroscopy supplies information about the oxidation state and geometry of the metal centers, whereas the local structure at the metal centers can be analyzed by EXAFS (extended X-ray absorption fine structure, Figure 8 and Figure 9). The analysis of the spectra revealed that, despite the similar Pd content, the Pd species incorporated in the frameworks were indeed different. Whereas the spectra for MIL-53-NH_2(Al)-Mal-Pd showed oxidized Pd^{2+} species, Pd^0 species were detected for Pd@MIL-53-NH_2(Al). The fitting parameters and results of the EXAFS analysis for both MIL-53-NH_2(Al)-Mal-Pd and Pd@MIL-53-NH_2(Al) are listed in Table 2.

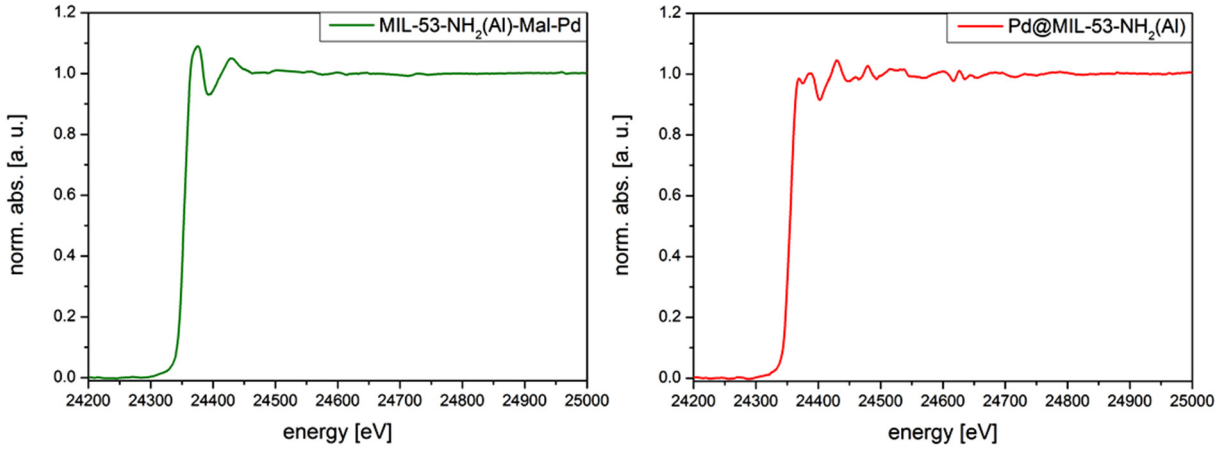

Figure 7: XAS spectra of MIL-53-NH$_2$(Al)-Mal-Pd (left) and Pd@MIL-53-NH$_2$(Al) (right) recorded at the palladium K-edge.

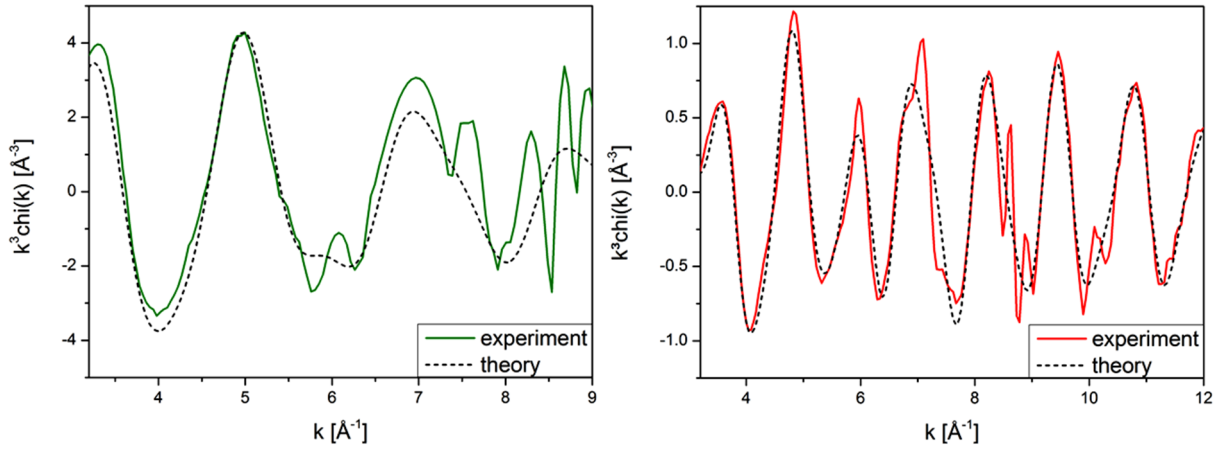

Figure 8: Experimental (solid line) and theoretically fitted (dotted line) k^{3}chi(k) of MIL-53-NH$_2$(Al)-Mal-Pd (left) and Pd@MIL-53-NH$_2$(Al) (right).

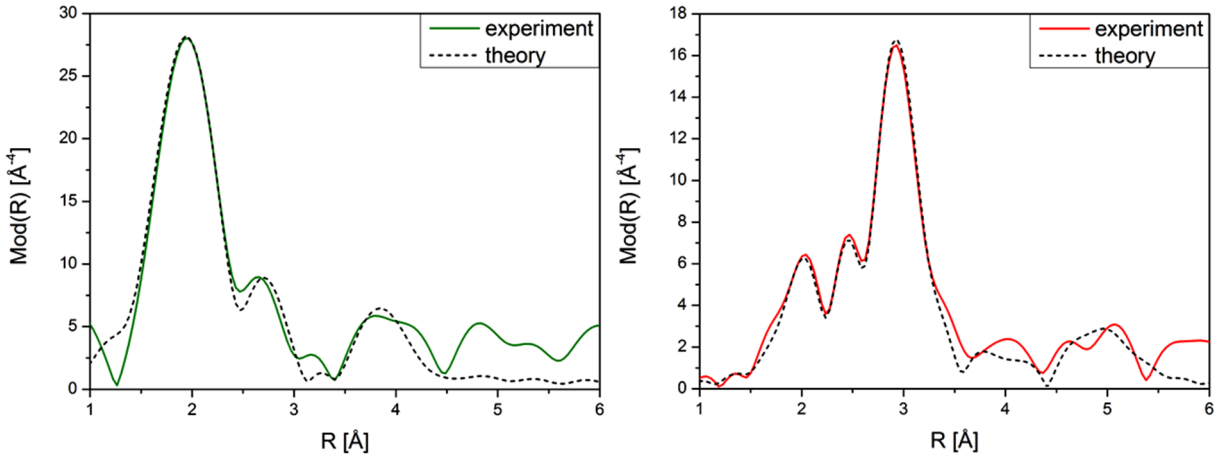

Figure 9: Experimental (solid line) and theoretically fitted (dotted line) Fourier transformed EXAFS spectra of MIL-53-NH$_2$(Al)-Mal-Pd (left) and Pd@MIL-53-NH$_2$(Al) (right).

Table 2: Fitting parameters of the EXAFS analysis and results for the spectra of MIL-53-NH_2(Al)-Mal-Pd and Pd@MIL-53-NH_2(Al).

sample	Abs-Bs[a]	N(Bs)[b]	R(Abs-Bs)[c] [Å]	σ[d] [Å]	R[e] [%] χ^2_{red}[f] E_f[g] [eV] Afac[h]
MIL-53-NH_2(Al)-Mal-Pd	Pd-O	3.9±0.3	2.008±0.020	0.107±0.010	35.48 18.9086*10^{-6} 7.108 0.800
	Pd-C	2.6±0.2	2.842±0.028	0.112±0.011	
	Pd-C	6.2±0.6	3.959±0.039	0.112±0.011	
Pd@MIL-53-NH_2(Al)	Pd-O	1.7±0.1	2.031±0.020	0.055±0.005	25.27 7.1680*10^{-6} 4.045 0.547
	Pd-Pd	5.0±0.5	2.741±0.027	0.074±0.007	
	Pd-C	8.4±0.8	2.898±0.028	0.112±0.011	
	Pd-Pd	3.6±0.3	3.803±0.038	0.112±0.011	
	Pd-Pd	5.3±0.8	4.745±0.047	0.084±0.008	

[a] Abs = X-ray absorbing atom, BS = backscattering atom; [b] number of backscattering atoms; [c] distance between absorbing and backscattering atom; [d] Debye–Waller-like factor; [e] fit index; [f] reduced χ^2 error (considers the error to the experiment as well as the number of independent points and the number of varied parameters); [g] Fermi energy that accounts for the shift between theory and experiment; [h] amplitude reducing factor.

In the first shell of MIL-53-NH_2(Al)-Mal-Pd, 3.9 oxygen atoms were found at a distance of 2.01 Å, which is consistent with a Pd^{2+} complex in a fourfold coordination. At a distance of 2.84 Å and 3.96 Å, two carbon shells were found, which originated from the backbone of the ligands coordinated to the Pd^{2+} ions. No palladium shells could be fitted for this Pd-containing framework, which led to the conclusion that in case of low precursor amounts (0.25 - 0.5 eq) the immobilization of defined mononuclear Pd^{2+} complexes was indeed successful (MIL-53-NH_2(Al)-Mal-Pd).

For Pd@MIL-53-NH_2(Al), only 1.7 oxygen atoms could be fitted in the first shell at a distance of 2.03 Å. Instead, three palladium shells were detected at 2.74 Å, 3.80 Å and 4.75 Å, which corresponded well to distances found in metallic palladium[232, 243]. Therefore, high amounts of the palladium precursor (1.0 - 1.5 eq) obviously promoted the formation of Pd^0 clusters, while only minor contributions of the targeted immobilized Pd^{2+} complexes were present (Pd@MIL-53-NH_2(Al)). The size of the deposited clusters could also be estimated from the evaluated EXAFS data. Most particles were in the range of 10-15 atoms but minor contributions of bigger clusters with up to about 100 atoms were found as well. According to those results mostly small particles were formed, but there was a broad size distribution of the deposited Pd nanoparticles.

2.4. Catalytic tests: Heck-type C-C coupling reaction

2.4.1. Parameter optimization

Pd containing catalysts are well known to be highly active in liquid phase C-C coupling reactions, such as the Heck reaction.[175, 193, 235-236] Thus, the modified metal-organic frameworks MIL-53-NH_2(Al)-Mal-Pd and Pd@MIL-53-NH_2(Al) were applied in the Heck-type coupling reaction of styrene with bromo- or chlorobenzene (Scheme 20).

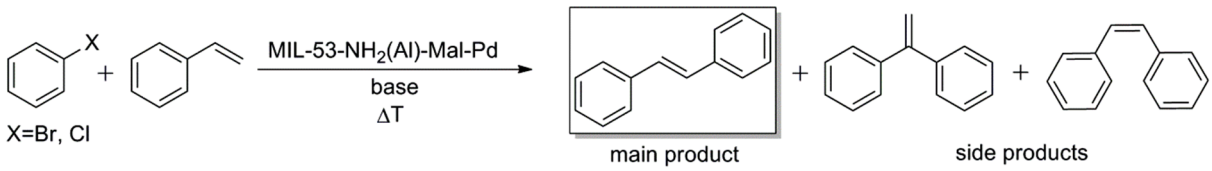

Scheme 20: Heck-type C-C coupling reaction of styrene and aryl halides.

MIL-53-NH_2(Al)-Mal-Pd with the targeted immobilized Pd^{2+} complexes was chosen for the optimization of the reaction parameters (temperature, reaction time, substrates, additives, bases). Under optimized conditions, MIL-53-NH_2(Al)-Mal-Pd was then compared to both a conventional supported catalyst (Pd@Al_2O_3) and a homogeneously dissolved Pd^{2+} salt (Pd(II) acetate).

First, MIL-53-NH_2(Al)-Mal-Pd was employed as catalyst in the reaction of styrene with bromobenzene under standard conditions known from literature.[244] Thus, the substrates were dissolved in *N*-methyl-2-pyrrolidone (NMP) in the presence of a base (sodium acetate) and then heated to 140 °C for 3 h. The applied conditions resulted in a conversion of 96 % and a selectivity of more than 90 % towards *trans*-stilbene (TON = 8240, Table 3, entry 1).

Next, the coupling of styrene with the less reactive substrate chlorobenzene was investigated. Due to the higher bond energy of C-Cl compared to the C-Br bond, the activation of chlorobenzene is more demanding. Since a longer reaction time might be necessary to achieve the conversion of chlorobenzene, the reaction time of the catalytic test was doubled to 6 h. However, no conversion of chlorobenzene and styrene could be observed at 140 °C without the addition of the promoting agent tetrabutylammonium bromide (TBAB). By adding an increasing amount of TBAB (2, 4 and 6 mmol) to the reaction mixture, a maximum conversion of 15 % and a yield of 11 % of *trans*-stilbene could be reached (Table 3, entries 3-6). As expected from literature reports[244], increasing the temperature from 140 °C to 160 °C and applying calcium hydroxide as a base instead of sodium acetate further

promoted the conversion of chlorobenzene. Applying the modified framework MIL-53-NH_2(Al)-Mal-Pd as a catalyst under optimized conditions (160 °C, $Ca(OH)_2$, 6 mmol TBAB, 6 h), a conversion of 22 % and a yield of 17 % of *trans*-stilbene were achieved (TON = 1740, Table 3, entry 8).

Table 3: Results of the catalytic tests.

	catalyst	substrate	base	temperature [°C]	TBAB[d] [mmol]	conversion [%]	yield [%]	TON
1	MIL-Pd[a]	PhBr[b]	NaOAc	140	-	96	88	8240
2	MIL-Pd[a]	PhBr[b]	NaOAc	160	-	98	88	8370
3	MIL-Pd[a]	PhCl[c]	NaOAc	140	-	1	0	10
4	MIL-Pd[a]	PhCl[c]	NaOAc	140	2	4	3	380
5	MIL-Pd[a]	PhCl[c]	NaOAc	140	4	7	6	680
6	MIL-Pd[a]	PhCl[c]	NaOAc	140	6	15	11	1120
7	MIL-Pd[a]	PhCl[c]	NaOAc	160	6	7	6	610
8	MIL-Pd[a]	PhCl[c]	$Ca(OH)_2$	160	6	22	17	1740
9	Pd@Al_2O_3	PhCl[c]	$Ca(OH)_2$	160	6	11	9	900
10	Pd(II)acetate	PhCl[c]	$Ca(OH)_2$	160	6	33	28	3100

[a] MIL-53-NH_2(Al)-Mal-Pd; [b] reaction conditions: bromobenzene (10 mmol), styrene (15 mmol), sodium acetate (12 mmol), Pd (0.01 mol%), N-methyl-2-pyrrolidone (NMP; 10 mL), 3 h; [c] reaction conditions: chlorobenzene (10 mmol), styrene (15 mmol), base (12 mmol), tetrabutylammonium bromide (TBAB), Pd (0.01 mol%), NMP (10 mL), 6 h; [d] tetrabutylammonium bromide.

Under the same conditions only 11 % conversion and 9 % yield (TON = 900) were reached with a conventional supported catalyst Pd@Al_2O_3 (Table 3, entry 9). The reaction with the homogeneous Pd^{2+} salt (Pd(II) acetate) resulted in a slightly higher conversion and yield of 33 % and 28 %, respectively (TON = 3100, Table 3, entry 10).

2.4.2. Hot filtration test, palladium leaching and reusability

In literature a "quasi-homogeneous" reaction mechanism is well-accepted for Heck-type C-C coupling reactions catalyzed by conventional heterogeneous catalysts, *e.g.* Pd@Al_2O_3 (see also Chapter 1.5.1).[235-239, 244] In this case, the reaction is exclusively catalyzed by homogeneous Pd complexes, which are dissolved from the supported bulk palladium. This reaction pathway should also be relevant for Pd@MIL-53-NH_2(Al), which also contains palladium nanoparticles. Since XAS proved the immobilization of defined palladium complexes into MIL-53-NH_2(Al)-Mal-Pd, the leaching of active species from the heterogeneous catalyst might not be necessary to achieve high conversion and, thus, might

result in a truly heterogeneous reaction pathway. To gather insight into the reaction mechanism and the leaching behavior of the catalyst materials, MIL-53-NH_2(Al)-Mal-Pd, Pd@MIL-53-NH_2(Al) and Pd@Al_2O_3 were applied in a hot filtration test. For the hot filtration test and the subsequent determination of the palladium leaching, the reaction of bromobenzene with styrene was chosen under optimized conditions (140 °C, NMP, sodium acetate, 3 h). To simplify catalyst separation, the catalysts were placed in a paper filter and removed from the reaction mixture after half an hour. The reaction was then resumed for another 2.5 h under the same reaction conditions and the results were compared to tests in which the catalyst was also put in a filter to exclude diffusion limitations but was not removed during the entire reaction time of 3 h.

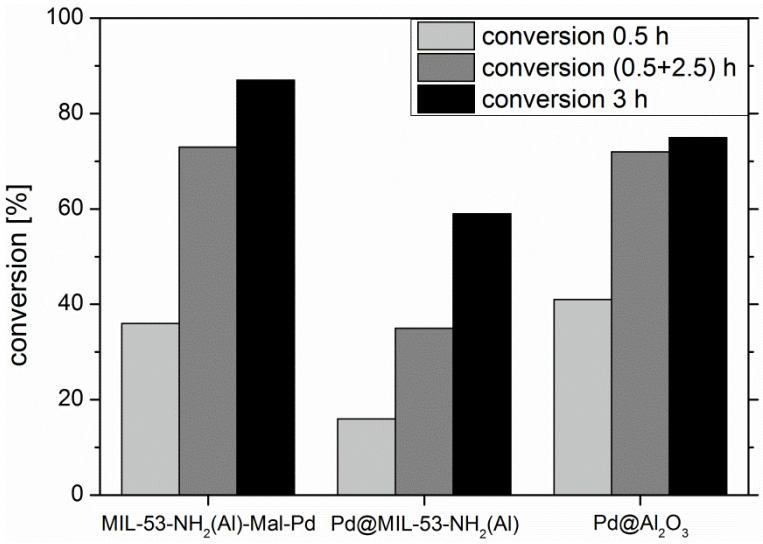

Figure 10: Results of the hot filtration test (light grey: after 0.5 h, dark grey: after 3 h) compared to a reaction with the catalyst (black); reaction conditions: NMP, 10 mmol bromobenzene, 15 mmol styrene, 12 mmol sodium acetate, 0.01 mol% catalyst, 140 °C.

Atomic absorption spectroscopy (AAS, Table 4) of the reaction mixture revealed that for MIL-53-NH_2(Al)-Mal-Pd with the targeted immobilized Pd^{2+} complexes only 1.7 % of the palladium were leached. Hence, the leaching was significantly lower than for Pd@MIL-53-NH_2(Al) and Pd@Al_2O_3 (2.8 % and 2.9 %, respectively), which both contained palladium nanoparticles. Nonetheless, applying MIL-53-NH_2(Al)-Mal-Pd resulted in the highest conversion and selectivity of 87 % and 92 %, respectively, and, therefore, it was the most active catalyst of those investigated in the C-C coupling reaction of bromobenzene and styrene under optimized conditions (Table 4). The conversion reached with the catalysts Pd@MIL-53-NH_2(Al) and Pd@Al_2O_3 after 3 h was only 59 % and 75 %, respectively,

although the amount of leached palladium was nearly twice the amount leached from MIL-53-NH_2(Al)-Mal-Pd.

Table 4: Results of the hot filtration test and for the leaching of palladium determined by atomic absorption spectroscopy.

catalyst material	conversion (hot filtration test, 0.5 h) [%]	conversion (hot filtration test, 3 h) [%]	conversion (3 h with catalyst) [%]	Pd leaching [%]
MIL-53-NH_2(Al)-Mal-Pd	36	73	87	1.7
Pd@ MIL-53-NH_2(Al)	16	35	59	2.8
Pd@Al_2O_3	41	72	75	2.9

For all tested catalysts, the reaction still proceeded after filtration of the catalyst, indicating that leached palladium species take part in the catalytic reaction. However, while the conversions achieved by MIL-53-NH_2(Al)-Mal-Pd and Pd@Al_2O_3 in the hot filtration test were identical, the results of the tests without catalyst removal revealed a significant difference between the two materials (Table 4 and Figure 10). For the conventional heterogeneous catalyst Pd@Al_2O_3, there was no obvious difference in conversion whether the catalyst was filtered off or remained in the mixture (72 % and 75 %, respectively), confirming the expected "quasi-homogeneous" pathway. In contrast, the conversion in the presence of MIL-53-NH_2(Al)-Mal-Pd was considerably higher when the catalyst was retained in the mixture compared to the filtration experiment (87 % and 73 %, respectively). Those results strongly indicate additional contributions of a heterogeneous reaction pathway, thus, proving the hypothesis that immobilized complexes allow for an alternative reaction pathway. For Pd@MIL-53-NH_2(Al) the conversion also increased when the catalyst remained in the reaction mixture for the entire time (59 % compared to 35 % in the hot filtration test). However, the overall activity of this catalyst was significantly lower than that of the catalyst with the targeted immobilized complexes as well as that of the conventional heterogeneous catalyst.

The results of the hot filtration test clearly indicate contributions of a truly heterogeneous reaction pathway for MIL-53-NH_2(Al)-Mal-Pd with defined immobilized Pd^{2+} complexes in addition to the "quasi-homogeneous" pathway established for conventional catalysts. Moreover, the analysis of the palladium leaching proved that leaching of palladium species could be minimized by immobilization of complexes in the metal-organic framework MIL-53-NH_2(Al) (1.7 %) compared to conventional heterogeneous catalysts, which contain

supported palladium nanoparticles (2.9 %). To further diminish the leaching of active species, the synthesis of improved chelating ligands with stronger coordination to the palladium centers might be beneficial.

MIL-53-NH_2(Al)-Mal-Pd was applied in three consecutive coupling reactions of bromobenzene with styrene under standard conditions (140 °C, NMP, sodium acetate, 3 h). To ensure easy separation and reuse, the catalyst was again placed in a paper filter. Before the catalyst was applied in the successive reactions, it was thoroughly washed with NMP and dried over night at room temperature. Nonetheless the activity of MIL-53-NH_2(Al)-Mal-Pd decreased significantly after the first run. While a conversion of more than 80 % was achieved in the first run, the conversion of the second and third run was only 22 %. This significant decrease might have been due to either deactivation of the catalyst or blocking of the filter by the base (sodium acetate), which did not dissolve completely in the reaction mixture, thus, hindering the conversion of bromobenzene.

2.5. Conclusion

Well defined mononuclear Pd^{2+} complexes were successfully immobilized at the amine functionalities of the metal-organic framework MIL-53-NH_2(Al) *via* a two-step post-synthetic modification reaction using maleic anhydride and palladium acetate. X-ray diffraction patterns proved that under the applied synthetic conditions (ambient pressure, 90 °C) a crystalline material with MIL-53 structure could be prepared effectively and that the framework structure was retained throughout the modification process. ATR-IR verified that there were no residual precursor species in the pore system, thus, confirming that further purification steps, which have been reported in literature for solvothermal syntheses, were not necessary. An additional band in the ATR-IR spectra and the decreased specific surface area (from 980 m^2/g to 90 m^2/g) strongly indicated that the modification was successful. Evaluation of the XAS data confirmed that the targeted Pd^{2+} complexes were immobilized when low amounts (0.25 – 0.5 eq) of the palladium precursor were used in the second modification step. In contrast, too high amounts of the precursor (> 1 eq) mainly resulted in the additional formation of palladium nanoparticles in the pores of MIL-53-NH_2(Al).

The catalytic potential of the Pd-containing frameworks was demonstrated in a Heck-type C-C coupling reaction of styrene with bromo- or chlorobenzene, where they exhibited high activity. For the two tested aryl halides (bromo- and chlorobenzene, respectively) turnover numbers (TONs) of 8240 and 1740 could be achieved after 3 h and 6 h, respectively, under optimized reaction conditions. To get some insight into the reaction mechanism, a hot

filtration test was conducted and the leaching behavior of the catalysts was investigated. The results of the hot filtration tests strongly pointed towards contributions of a truly heterogeneous reaction pathway for the catalyst MIL-53-NH_2(Al)-Mal-Pd with immobilized Pd^{2+} complexes, whereas in systems catalyzed by supported catalysts with nanoparticles exclusively homogeneously dissolved species were active. Additionally, the leaching of palladium species was significantly lower for the novel framework based catalyst (1.7 %) compared to that of a common heterogeneous reference catalyst (2.9 %).

In summary, the new catalyst system MIL-53-NH_2(Al)-Mal-Pd with immobilized mononuclear Pd^{2+} complexes was highly active *via* a partly heterogeneous reaction pathway, in which the leaching of palladium could be drastically minimized.

3. Immobilization of Pd complexes on mixed-linker MIL-53-NH$_2$(x)[245]

3.1. Motivation

The results presented in Chapter 2[242] demonstrate that MIL-53-NH$_2$(Al)-Mal-Pd lost most of its high specific surface area throughout the modification process (decrease from 980 m²/g to 90 m²/g). The drastic decrease was most probably caused by an exclusive modification of the amine groups on the outer surface resulting in blocking of the pore entrances.[242] Mixed-linker metal-organic frameworks based on MIL-53-NH$_2$(Al) with a defined ratio of functionalized und unfunctionalized linker molecules are an interesting alternative starting material. Due to the lower amount of amine groups and, hence, possible sites for post-synthetic modification the immobilized complexes should be well distributed in the framework and pore blocking should be minimized. Due to the higher porosity expected for modified MIXMOFs, the active centers inside the framework should also be accessible. Moreover, the porous material with well distributed active centers might be more active in catalysis compared to the surface-functionalized material.

In this Chapter the synthesis of mixed-linker frameworks MIXMIL-53-NH$_2$(x) (where x is the percentage of amine groups), their post-synthetic modification and the characterization results (XRD, nitrogen physisorption, ATR-IR, ^{1}H NMR, AAS, XAS) after each synthetic step are presented. In addition, the resulting MIL-53-NH$_2$(x)-Mal-Pd were applied in Heck-type C-C coupling reactions of styrene and aryl halides and the results of those studies are highlighted. Furthermore, the characterization data and catalytic results are compared to the findings observed for MIL-53-NH$_2$(100)-Mal-Pd[242] (Chapter 2).

3.2. Synthesis and post-synthetic modification

The mixed-linker frameworks MIL-53-NH$_2$(x) (x = 40, 60, 80) were prepared at ambient pressure based on the synthetic protocoll developed for pure MIL-53-NH$_2$(100)[242] (Chapter 2.2). “(x)” indicates the initial percentage of 2-aminobenzene-1,4-dicarboxylate (2-aminoterephthalate, ABDC) applied during the syntheses of the mixed-linker frameworks. The amount of DMF in the solvent mixture had to be increased for the syntheses of the mixed-linker MOFs in order to fully dissolve the linker molecules 2-aminobenzene-1,4-dicarboxylic acid (2-aminoterephthalic acid, H$_2$ABDC) and especially

benzene-1,4-dicarboxylic acid (terephthalic acid, H_2BDC). Heating the solution of the two linker molecules (defined ratio of 2:3, 3:2 or 4:1) and $Al(NO_3)_3*9H_2O$ in DMF/H_2O to 90 °C for 24 h resulted in the formation of MIL-53-NH_2(x). (Scheme 21).[245]

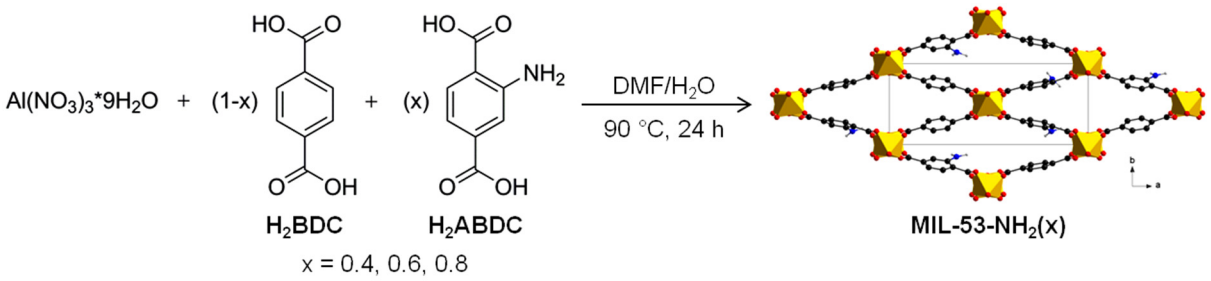

Scheme 21: Synthesis of mixed-linker MIL-53-NH_2(x) (x = 40, 60, 80); grey: C, white: H, red: O, blue: N, yellow: Al.

After thorough characterization of the starting materials defined Pd^{2+} complexes were immobilized at the amine groups of the mixed-linker metal-organic frameworks *via* a two-step post-synthetic modification reaction (Scheme 22) previously optimized for pure MIL-53-NH_2(100)[242]. In the first step maleic anhydride (4 eq) was applied to create a chelating side chain (MIL-53-NH_2(x)-Mal), which could be employed to bind Pd^{2+} centers in a second step (0.25 eq, MIL-53-NH_2(x)-Mal-Pd).

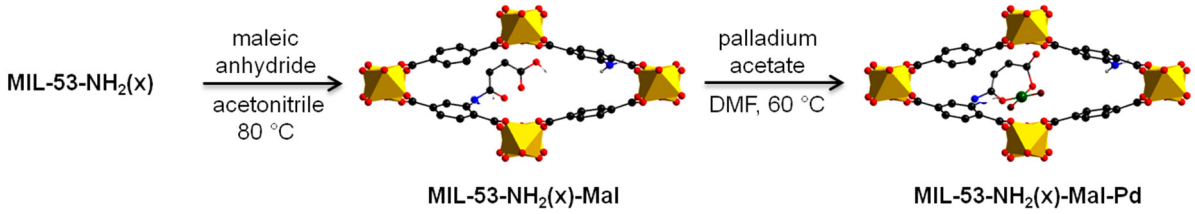

Scheme 22: Two-step post-synthetic modification of MIL-53-NH_2(x) (x = 40, 60, 80) with, first, maleic anhydride and, second, palladium acetate; for clarity only one pore is shown; grey: C, white: H, red: O, blue: N, yellow: Al, green: Pd, brown: ligands.

All novel materials were characterized in detail by X-ray diffraction (XRD), FT-IR spectroscopy (ATR mode), nitrogen physisorption measurements (BET) and nuclear magnetic resonance spectroscopy (^{1}H NMR) after each synthetic step. In addition, X-ray absorption spectroscopy (XAS) and atomic absorption spectroscopy (AAS) were applied to analyze the Pd-containing frameworks.

3.3. Characterization

3.3.1. Mixed-linker MIL-53-NH2(x)

The X-ray diffraction patterns of all materials were compared to prove that the structure of the mixed-linker frameworks is isoreticular to pure MIL-53-NH2(100). The diffractograms shown in Figure 11 confirmed the successful formation of crystalline MIXMILs with MIL-53-NH2(Al)_lt structure. Again, additional purification steps to remove residual acid molecules were not necessary.

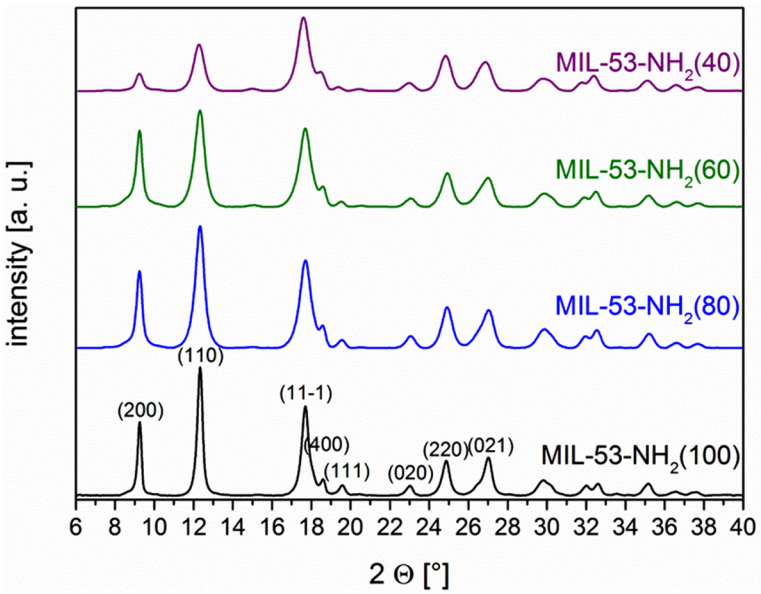

Figure 11: X-ray diffraction patterns of MIL-53-NH2(x) with x = 40 (purple), 60 (green), 80 (blue) compared to pure MIL-53-NH2(100) (black).

To verify the linker ratio in the MIL-53-NH2(x) materials qualitatively, infrared spectra of all samples were recorded in the attenuated total reflectance mode (ATR-IR, Figure 12).

Two prominent effects could be observed in those spectra. First, the intensity of the N-H stretching vibrations around $\nu = 3498$ cm^{-1} and $\nu = 3387$ cm^{-1} decreased when the amount of the amine-functionalized linker was reduced in the synthesis of the framework materials (Figure 12, left). Second, the wave numbers of the aromatic C-H bending vibrations of 2-aminoterephthalate and terephthalate differed because of the changed substitution patterns at the aromatic rings, which resulted in two distinguishable signals for the two linker molecules (Figure 12, right). The band of 2-aminoterephtalate emerged at $\nu = 775$ cm^{-1}, while the signal at $\nu = 753$ cm^{-1} originated from the terephthalate linker.

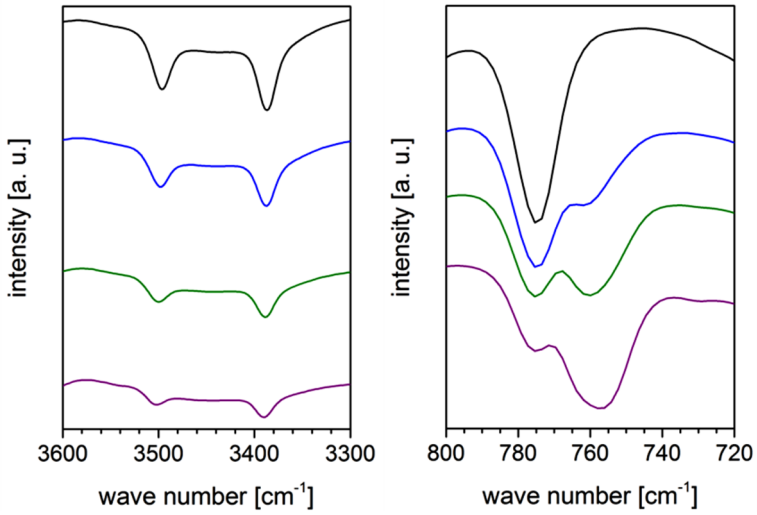

Figure 12: ATR-IR spectra of MIL-53-NH$_2$(40) (purple), MIL-53-NH$_2$(60) (green), MIL-53-NH$_2$(80) (blue) and MIL-53-NH$_2$(100) (black).

Moreover, no band was detected around $\nu = 1680$ cm^{-1}, which would correspond to the C=O vibration of protonated H$_2$BDC or H$_2$ABDC, confirming again that no residual acid molecules were present in the pore system. The observed trends in the IR spectra strongly indicated the successful incorporation of both linker molecules into the mixed-linker metal-organic frameworks in defined ratio, while at the same time definitely excluding the presence of unreacted precursor species.

^{1}H NMR spectra of digested samples (Chapter 7.2.6) were recorded to quantify the linker ratio of 2-aminoterephthalate and terephthalate and to determine if the linker ratio applied during synthesis matched the ratio in the resulting materials. The mixed-linker MIL-53-NH$_2$(x) materials are chemically very stable and, therefore, a concentrated solution of sodium hydroxide in D$_2$O was required to dissolve the samples. Since ATR-IR spectra showed that there were no residual acid molecules present in the pores, the linker ratio determined by NMR could be directly correlated to the actual composition of the mixed-linker frameworks. The BDC linker molecules were visible as one singlet corresponding to four H-atoms and for ABDC two doublets and one singlet were observed, which each originated from one H-atom. The ^{1}H NMR spectra of MIL-53-NH$_2$(x) with x = 40, 60, 80 and the assignment of the signals are shown in Figure 13. The ratios found by integration of the NMR spectra matched the ratios applied during synthesis very well (Table 5), which confirmed that both linker molecules were incorporated into the MIL-53 structure with the same preference.

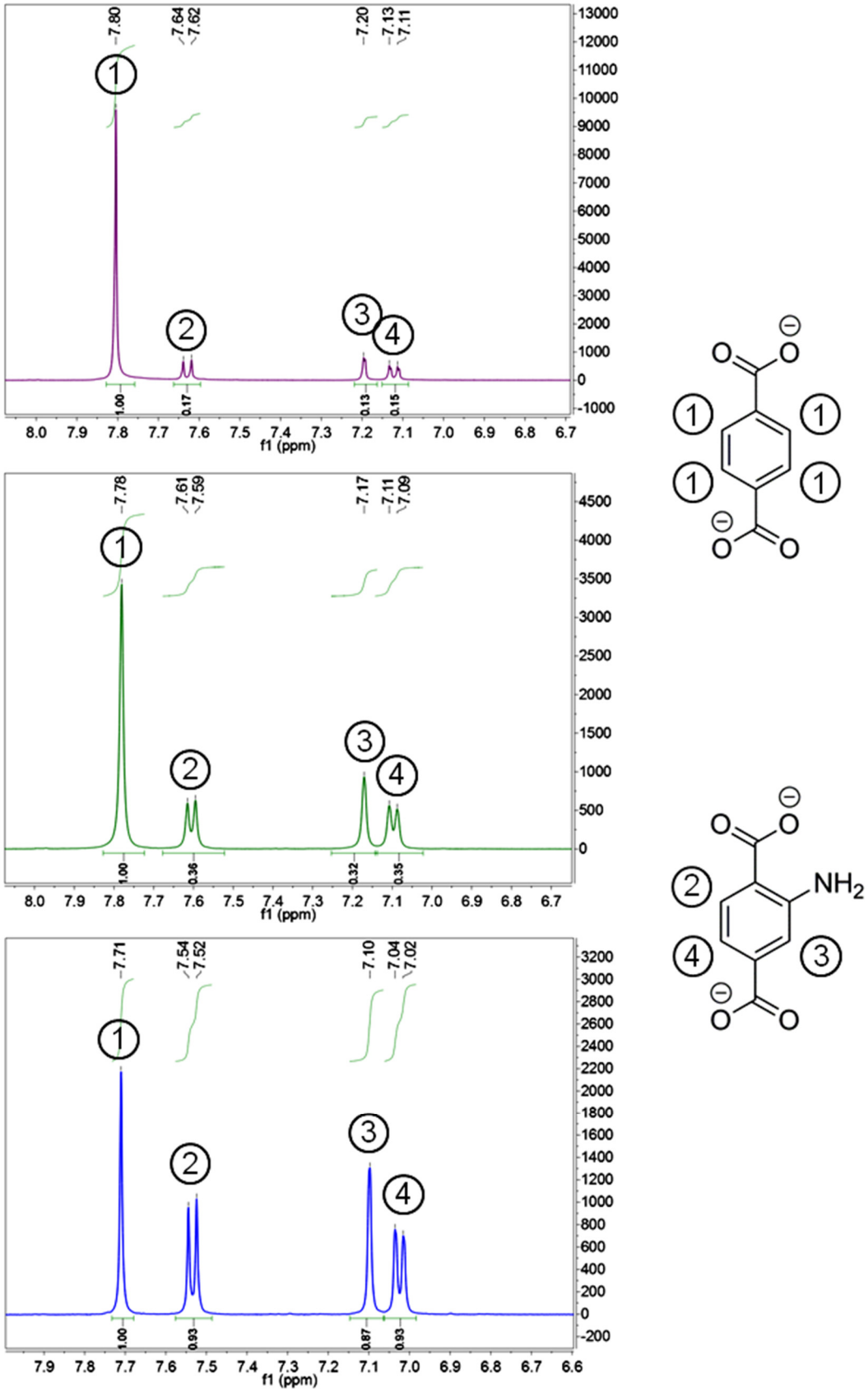

Figure 13: NMR spectra of digested samples: MIL-53-NH$_2$(40) (purple), MIL-53-NH$_2$(60) (green) and MIL-53-NH$_2$(80) (blue); the linker molecules BDC (top) and ABDC (bottom) and the assignment of the signals are shown on the right.

Table 5: Theoretical and measured linker ratios.

material	ABDC : BDC	
	applied	determined
MIL-53-NH$_2$(80)	4 : 1	3.7 : 1.0
MIL-53-NH$_2$(60)	3 : 2	2.8 : 2.0
MIL-53-NH$_2$(40)	2 : 3	2.0 : 3.0

To prove a mainly homogeneous distribution of the two linker molecules in the framework structure and to exclude the formation of core-shell particles, three additional samples were prepared. For all three materials an initial linker ratio of 1:1 was applied during synthesis, but the reaction time was varied between 8 h, 24 h and 72 h. Whereas the crystallinity of the materials increased with longer reaction time (confirmed by XRD, Figure 14), evaluation of the ^{1}H NMR spectra of the three samples confirmed a linker ratio of 1:1 independent of the reaction time. This observation supports the successful formation of mixed-linker metal-organic frameworks with homogeneously distributed amine-functionalized linker molecules rather than the formation of core-shell particles. Lescouet *et al.* previously published a more detailed study on the distribution of the different linker molecules in mixed-linker MIL-53(Al), where they also concluded a homogeneous incorporation of both linker molecules into the framework structure.[135]

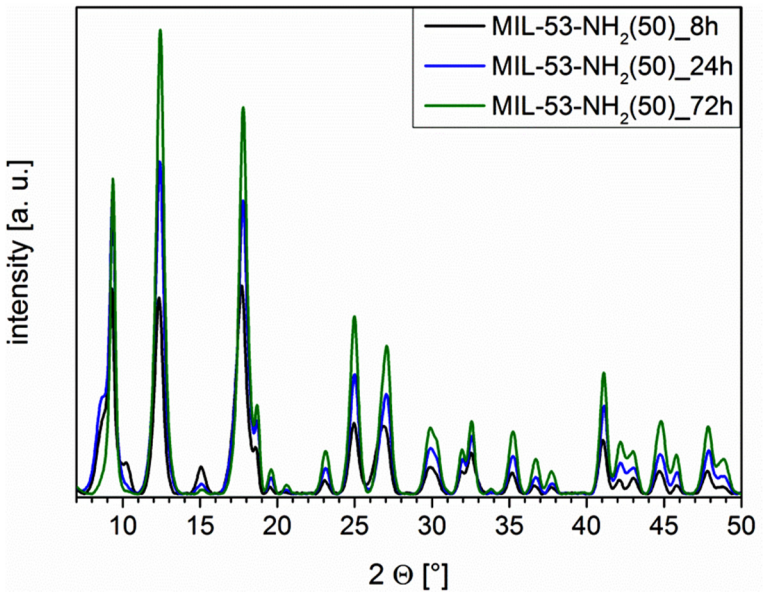

Figure 14: X-ray diffraction patterns of MIL-53-NH$_2$(50) after a reaction time of 8 h (black), 24 h (blue) and 72 h (green).

Table 6: Micropore volumes of mixed-linker MIL-53-NH$_2$(x) and pure MIL-53-NH$_2$(Al) determined by nitrogen physisorption measurements.

material	MIL-53-NH$_2$ (100)	MIL-53-NH$_2$ (80)	MIL-53-NH$_2$ (60)	MIL-53-NH$_2$ (40)
micropore volume [cm^3/g]	0.39	0.17	0.22	0.30

The micropore volumes of the mixed-linker MIL-53-NH$_2$(x) derived from nitrogen physisorption measurements were lower than that obtained for pure MIL-53-NH$_2$(Al) (Table 6). The micropore volume of MIL-53-NH$_2$(100) was 0.39 cm^3/g whereas those of the mixed-linker materials ranged from 0.17 cm^3/g to 0.30 cm^3/g (for MIL-53-NH$_2$(80) and MIL-53-NH$_2$(40), respectively). The decreased micropore volumes might be a consequence of a higher disorder or slightly reduced crystallinity in the frameworks caused by the introduction of the second linker.

3.3.2. Modified MIL-53-NH$_2$(x)

Since the micropore volume of pure MIL-53-NH$_2$(100) drastically decreased from 0.39 cm^3/g to only 0.01 cm^3/g throughout the modification process with maleic anhydride and palladium(II) acetate (Table 7, Figure 15 and Chapter 2.3)[242], the mixed linker metal-organic frameworks were applied in the two-step post-synthetic modification reaction under the same conditions[245].

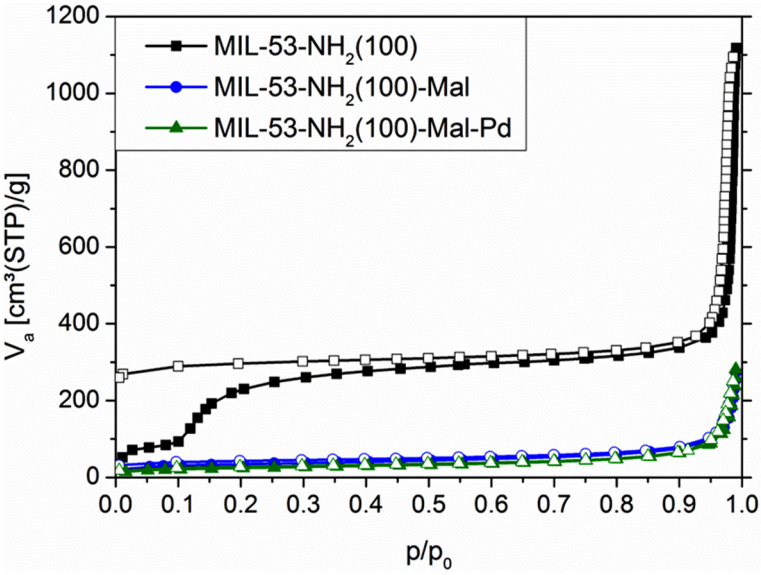

Figure 15: Adsorption (filled symbols) and desorption (open symbols) isotherms of MIL-53-NH$_2$(Al) throughout the modification process.

^{1}H NMR of the MIL-53-NH$_2$(x) materials revealed that the targeted ratio of amine functionalities was indeed present in the MOFs (Table 5) and both linker molecules were uniformly distributed in the samples (Chapter 3.3.1). Hence, the immobilized Pd^{2+} complexes should also be well distributed in the porous structure and pore blocking should be minimized.

Table 7: Micropore volumes of mixed-linker MIL-53-NH$_2$(x) and pure MIL-53-NH$_2$(100) before and after post-synthetic modification determined by nitrogen physisorption measurements.

material	micropore volume [cm^3/g]		
	unmodified	maleic anhydride	palladium acetate
MIL-53-NH$_2$(100)	0.39	0.03	0.01
MIL-53-NH$_2$(80)	0.17	0.08	0.08
MIL-53-NH$_2$(60)	0.22	0.20	0.10
MIL-53-NH$_2$(40)	0.30	0.12	0.11

Nitrogen physisorption measurements of modified MIL-53-NH$_2$(x) were performed to corroborate this hypothesis. The obtained data showed that in contrast to MIL-53-NH$_2$(100)-Mal-Pd (0.01 cm^3/g) the modified mixed-linker MOFs remained highly porous throughout the modification process (Table 7). The micropore volumes of MIL-53-NH$_2$(x)-Mal-Pd increased from 0.08 cm^3/g to 0.11 cm^3/g with decreasing amount of amine functionalities (from x = 80 to x = 40). Thus, the micropore volumes of the modified MIXMILs are one order of magnitude larger than that of MIL-53-NH$_2$(100)-Mal-Pd.

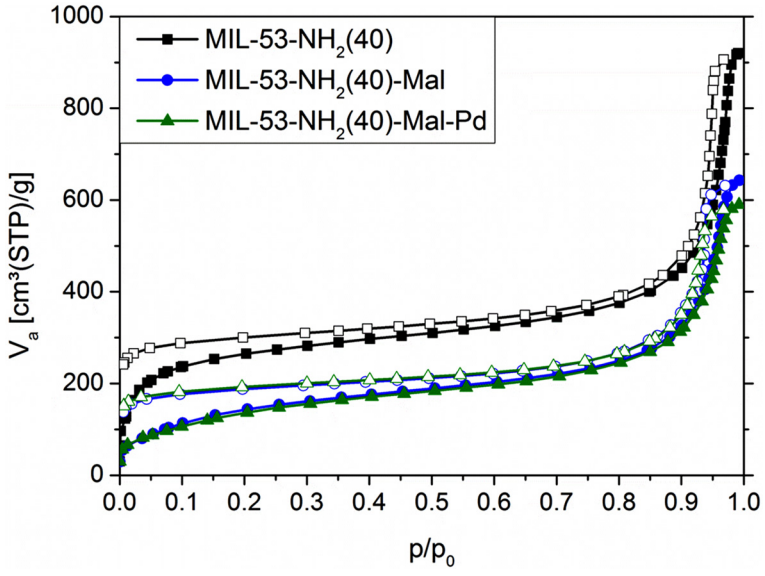

Figure 16: Adsorption (filled symbols) and desorption (open symbols) isotherms of MIL-53-NH$_2$(40) throughout the modification process.

The adsorption and desorption isotherms for MIL-53-NH$_2$(40) before and after each modification step are exemplarily depicted in Figure 16. The results explicitly illustrate that the blocking of the pore system was minimized, which was most probably due to the dilution and homogeneous distribution of the amine groups in the framework structure, thus, proving the advantages of applying the mixed-linker approach.

The X-ray diffraction patterns of the modified mixed-linker materials revealed that the MIL-53 structure was retained throughout the modification process. A unique characteristic of frameworks based on MIL-53 is the so-called breathing effect[4, 51, 56], which describes the ability of the material to change its pore geometry depending on the interactions with guest molecules present inside the pore system. This behavior can be monitored by XRD and was also observed for the modified MIL-53-NH$_2$(x)-Mal and MIL-53-NH$_2$(x)-Mal-Pd materials (Figure 17). The reflections which describe distances perpendicular to the pores and are, thus, not affected by the breathing effect ((*hkl*) = (200) and (400)) remained at the same 2 Θ positions (2 Θ = 9.28° and 18.62°, respectively), while a shift occurred for all other reflections. The same observation has been made for single-linker MIL-53-NH$_2$(100)-Mal-Pd (Chapter 2.3).

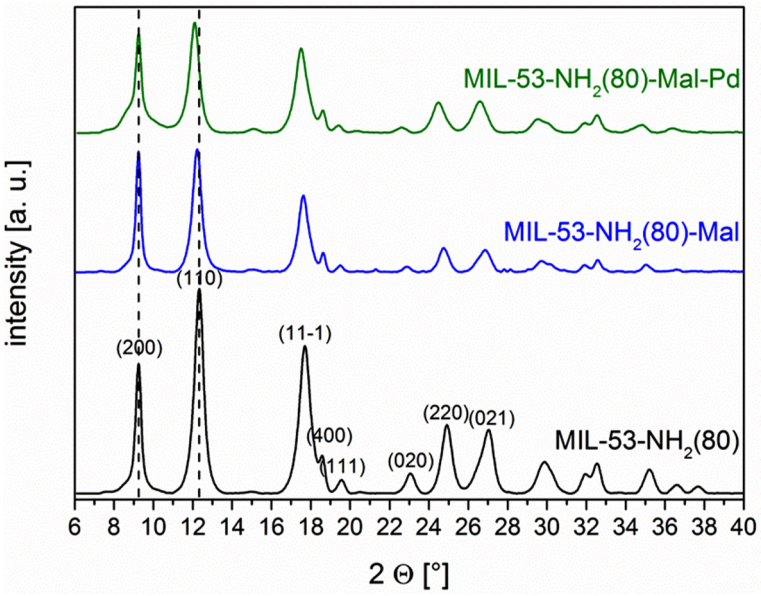

Figure 17: X-ray diffraction patterns of MIL-53-NH$_2$(80) before (black) and after each modification step (1st step blue, 2nd step green).

Hence, the observed shift provided qualitative proof of the successful modification of the mixed-linker frameworks based on MIL-53-NH$_2$. Moreover, the position of the second

reflection ((*hkl*) = (110), Table 8) might be a qualitative indication for the degree of modification.

Table 8: Position of the reflection (*hkl*) = (110) in the diffractograms throughout the modification process of MIL-53-NH$_2$(x) (x = 100, 80, 60, 40).

x	position of (*hkl*) = (110) [°]		
	MIL-53-NH$_2$(x)	MIL-53-NH$_2$(x)-Mal	MIL-53-NH$_2$(x)-Mal-Pd
100	12.32	12.13	12.12
80	12.33	12.22	12.10
60	12.33	12.27	12.21
40	12.31	12.28	12.23

The ATR-IR spectra recorded for the modified mixed-linker metal-organic frameworks also clearly indicate the successful formation of the amide. First, the intensity of the N-H stretching vibrations (ν = 3498 cm^{-1} and ν = 3387 cm^{-1}) decreased after modification of the amine group with maleic anhydride and, second, an additional band around $\nu \approx 1700$ cm^{-1} (C=O vibration, Figure 18) confirmed the presence of the inserted carbonyl functionalities.

NMR spectra of the digested materials were recorded for all samples after the reaction with maleic anhydride to quantify the modification degree of the amine groups. The spectra of MIL-53-NH$_2$(x)-Mal (x = 40, 60, 80) are shown in Figure 19. The signals around 6.29 ppm and 5.78 ppm correspond to the two H atoms of the newly introduced side chain, and the integrated areas could be directly correlated to those of the three H atoms of the amine linker (around 7.47 ppm, 7.03 ppm and 6.96 ppm).

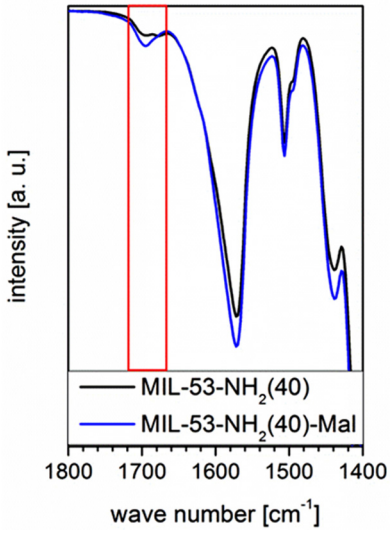

Figure 18: ATR-IR spectra of MIL-53-NH$_2$(40) (black) and MIL-53-NH$_2$(40)-Mal (blue).

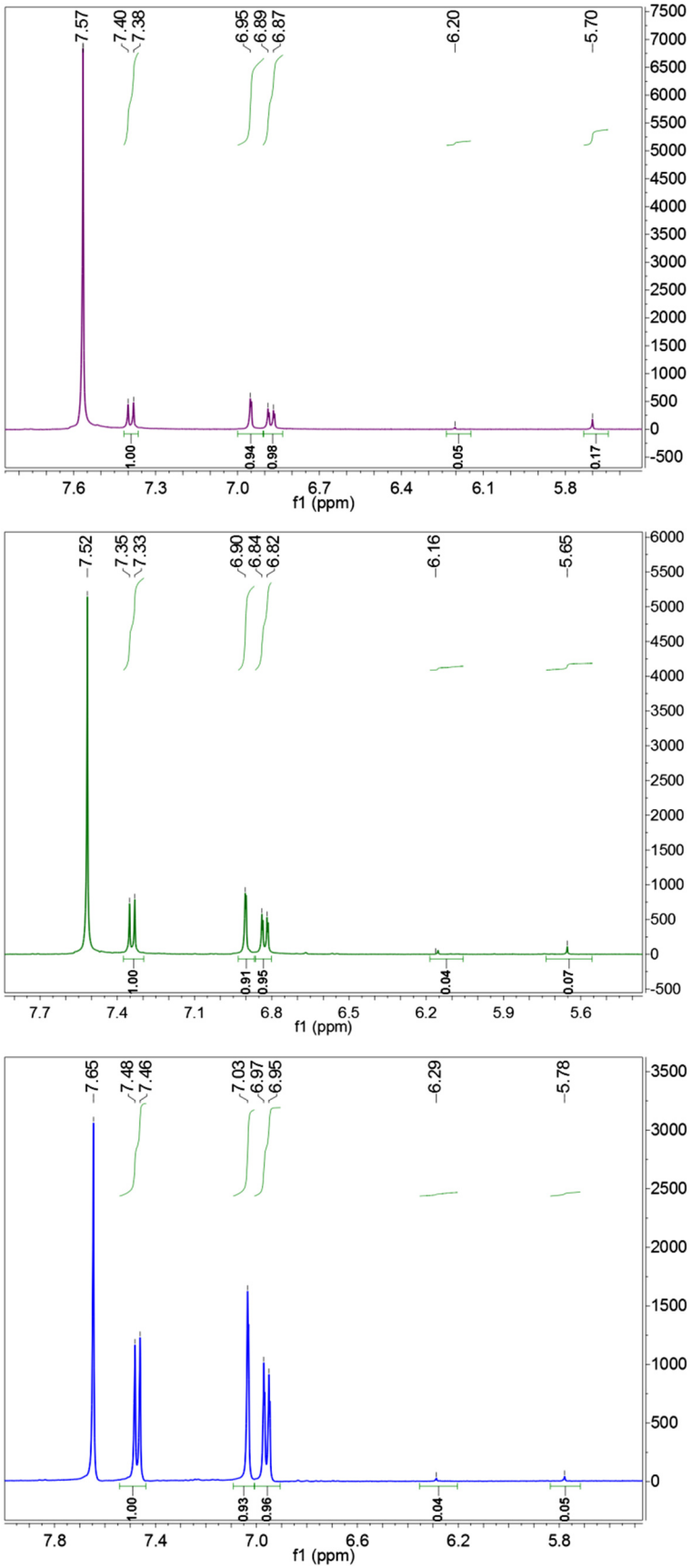

Figure 19: NMR spectra of digested samples after modification with maleic anhydride: MIL-53-NH_2(40)-Mal (purple), MIL-53-NH_2(60)-Mal (green) and MIL-53-NH_2(80)-Mal (blue).

Table 9: Modification degree per amine group and overall modification degree of the frameworks after reaction with maleic anhydride as determined by NMR spectroscopy.

	degree of modification [%]	
	per amine group	of the framework
MIL-53-NH2(100)-Mal	5	5
MIL-53-NH2(80)-Mal	5	4
MIL-53-NH2(60)-Mal	6	4
MIL-53-NH2(40)-Mal	11	5

The evaluation of all spectra revealed that the modification degree per amine group increased from 5 % to 11 % with decreasing degree of functionalization (from x = 100 to x = 40, respectively). However, the overall modification degree, which is the total number of modified linker molecules per framework, did not vary substantially and amounted to approximately 4 – 5 % (Table 9). Although the overall modification degree was comparable for all modified materials, the mixed-linker frameworks remained highly porous throughout the modification process, thus, proving that blocking of the pores could be minimized by applying the mixed-linker approach. Notably, a higher degree of modification of approximately 40 % has been reported in literature for MIL-53-NH2(Al)[163], which was probably achieved due to a 15 times higher amount of maleic anhydride used by these authors. Moreover, the authors did not report any specific surface areas or micropore volumes after the post-synthetic modification reaction.

Although NMR studies revealed that the overall modification degree was independent of the amine content of the starting materials, smaller shifts of the reflection (*hkl*) = (110) (Table 8) were observed in the XRD patterns of the MIXMILs, which indicated a less extensive "breathing". Additionally, the micropore volumes derived from N_2 physisorption measurements were substantially higher for the mixed-linker MOFs indicating that pore blocking was prevented. Considering all the data suggested a homogeneous distribution of the introduced side chains in the mixed-linker metal-organic frameworks, whereas mostly the linker molecules at the pore entries were modified in pure MIL-53-NH2(100) resulting in a more pronounced change in the pore geometry.

The palladium loading of the modified mixed-linker frameworks was determined by atomic absorption spectroscopy (AAS). Although the same amount of palladium acetate was applied for the modification (0.25 eq), the Pd content of the MIXMILs (x = 80 – x = 40) could be increased to 2.8 wt% - 3.1 wt% compared to a Pd loading of only 2.1 wt% for MIL-53-NH2(100)-Mal-Pd (Table 10).

Table 10: Palladium loading of MIL-53-NH_2(x)-Mal-Pd determined by AAS measurements.

	palladium loading [wt%]
MIL-53-NH_2(100)-Mal-Pd	2.1
MIL-53-NH_2(80)-Mal-Pd	2.8
MIL-53-NH_2(60)-Mal-Pd	2.9
MIL-53-NH_2(40)-Mal-Pd	3.1

The increased palladium loading of MIL-53-NH_2(x)-Mal-Pd compared to the pure material was in contrast to the similar overall modification degrees, found for all modified frameworks. This contradiction might be explained by the high porosity of the mixed-linker materials and, thus, the better accessibility of the chelating side chains inside the porous structure. Another possible explanation was the additional formation of undesired palladium nanoparticles, which would also have increased the palladium loading of the resulting materials.

Since the nature of the palladium species immobilized in MIL-53-NH_2(100) was strongly dependent on the synthetic conditions, the parameters optimized in this previous study[242] (Chapter 2.2 and 2.3) were applied for the synthesis of MIL-53-NH_2(100)-Mal-Pd. Thus, low amounts of the palladium precursor (0.25 eq) were applied during the second modification step to prevent the formation of additional palladium nanoparticles and instead achieve immobilization of defined Pd^{2+} complexes. Because a modification degree of 40 % has been reported in literature for the modification of MIL-53-NH_2(Al) with maleic anhydride[163], the amount of applied palladium precursor was calculated in regard to a theoretical value of 40 % of all linker molecules being modified. However, NMR spectra of the MIL-53-NH_2(x)-Mal materials later revealed that the overall modification degree of the materials reported herein was only 5 %. Thus, the applied amount of the palladium precursor was equivalent to 2 eq instead of the assumed 0.25 eq. The excess of palladium precursor compared to chelating side chains might promote the additional deposition of undesired palladium nanoparticles on the porous frameworks.

To exclude the possible formation of palladium nanoparticles and to affirm the successful immobilization of the targeted Pd^{2+} complexes, X-ray absorption spectra (XAS) were recorded at the Pd K-edge (24350 eV). Conclusions about the oxidation state and geometry of the metal centers can be gathered by XANES spectroscopy, and EXAFS analysis of the spectra provides information about their local environment.

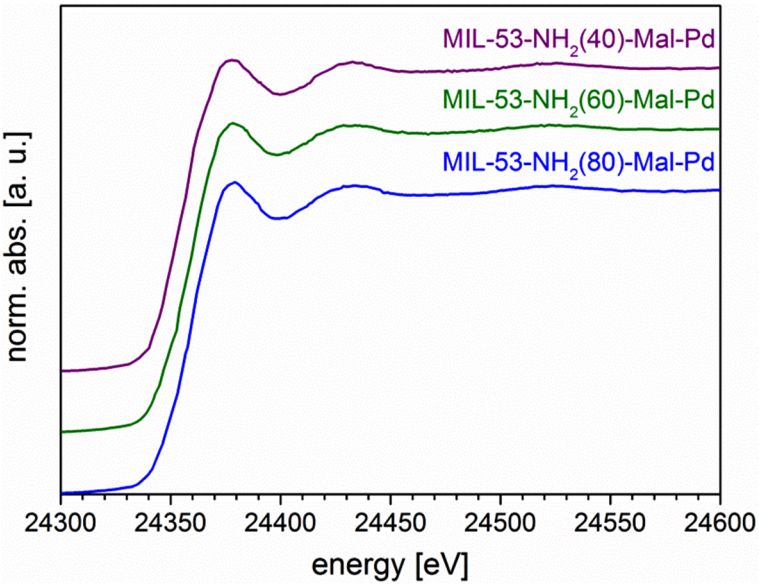

Figure 20: Normalized and self-absorption corrected X-ray absorption spectra of MIL-53-NH2(80)-Mal-Pd (blue), MIL-53-NH2(60)-Mal-Pd (green), and MIL-53-NH2(40)-Mal-Pd (purple).

The XANES spectra of the three MIL-53-NH2(x)-Mal-Pd samples (Figure 20) all showed a double-peak structure characteristic for Pd^{2+}[232], thus, indicating a successful immobilization of the targeted palladium complexes.

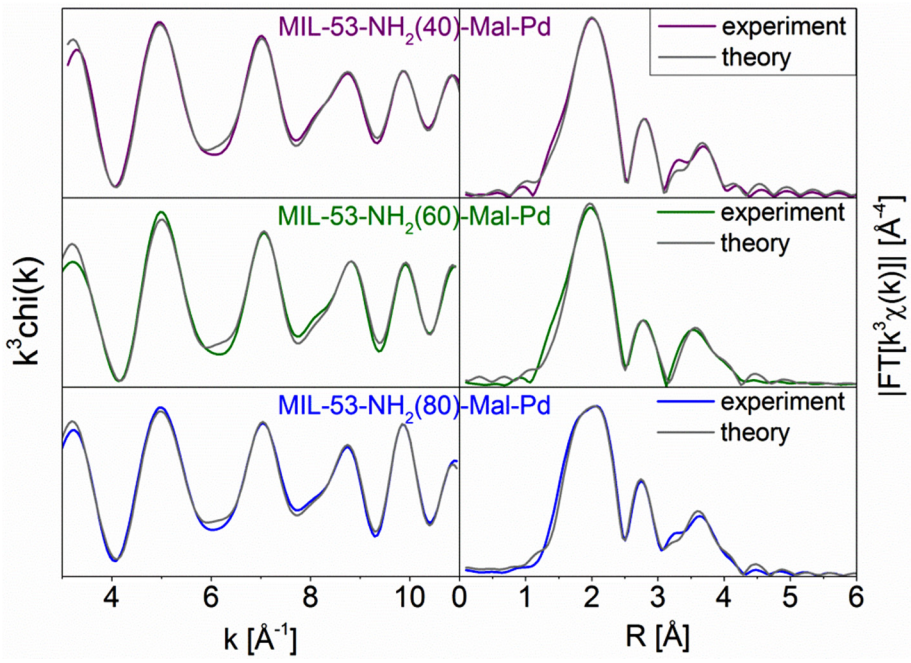

Figure 21: Fourier-filtered EXAFS spectra (left) and corresponding Fourier-transformed functions (right) of the samples MIL-53-NH2(80)-Mal-Pd (blue), MIL-53-NH2(60)-Mal-Pd (green), and MIL-53-NH2(40)-Mal-Pd (purple); the theoretical fit is shown in grey.

The EXAFS spectra of all modified mixed-linker MOFs also looked quite similar (Figure 21). Three different models were used for EXAFS analysis: the first model assumed the presence of mainly isolated Pd^{2+} centers, the second described large metallic palladium clusters and the third model was a mixture of the two. The results for the palladium-containing mixed-linker MOFs fitted with all three models are listed in Table 11. The R-factor, which represents the percental deviation between experiment and the theoretical fit, was used to determine the quality of a fit as well as the corresponding model.

The first model assuming isolated Pd^{2+} centers[242] with oxygen in the first shell at a distance of 2.01 Å and two carbon shells around 2.85 Å and 3.80 Å resulted in very high R-factors of 27.49 % (MIL-53-NH_2(40)-Mal-Pd), 35.86 % (MIL-53-NH_2(60)-Mal-Pd) and 35.85 % (MIL-53-NH_2(80)-Mal-Pd). The R-factors for the second model, which was used to describe metallic palladium clusters with oxygen in the first shell at 2.01 Å and two palladium shells at 2.64 Å and 3.60 Å, were also high (21.06 % for MIL-53-NH_2(40)-Mal-Pd, 21.93 % for MIL-53-NH_2(60)-Mal-Pd and 22.57 % for MIL-53-NH_2(80)-Mal-Pd). The third model, which combines the isolated Pd^{2+} centers and the palladium clusters, resulted in considerably smaller R-factors of 9.96 % (MIL-53-NH_2(40)-Mal-Pd), 12.77 % (MIL-53-NH_2(60)-Mal-Pd) and 9.19 % (MIL-53-NH_2(80)-Mal-Pd). Therefore, this mixed model was applied for the final EXAFS analysis of the Fourier transformed spectra. The structural parameters resulting from EXAFS analysis were identical within the experimental error for all three materials and the type and numbers of fitted shells as well as the distances obtained for the adjusted backscatterers were very similar.

Four oxygen atoms, corresponding to the two carboxyl groups of the introduced chelating side group and two additional acetate or H_2O ligands, could be fitted in the first shell between 1.90 Å and 2.08 Å. Two shells corresponding to the carbon scaffold of the modified side chains were detected at distances around 2.89 Å and 3.95 Å. Those three shells in combination with the double-peak structure observed in the XANES spectra proved the successful immobilization of the targeted Pd^{2+} complexes into the mixed-linker frameworks. However, two additional palladium shells were found around 2.66 Å and 3.59 Å suggesting the presence of a few undesired palladium clusters. The low coordination numbers found in those two shells (Table 11) and a contraction in the Pd-Pd distances (2.66 Å and 3.59 Å) compared to metallic palladium (2.74 Å and 3.83 Å[232, 243]) strongly indicated that only very small particles were present in the modified frameworks. Furthermore, no reflections corresponding to metallic palladium particles could be detected by XRD, which also supported this hypothesis.

Table 11: Fitting parameters of the EXAFS analysis and results for the spectra of MIL-53-NH_2(40)-Mal-Pd, MIL-53-NH_2(60)-Mal-Pd and MIL-53-NH_2(80)-Mal-Pd; parameters are shown for the three different models used for the fitting: isolated Pd^{2+} centers, small Pd clusters and a mixture of both.

material	fitting model	Abs-Bs[a]	N(Bs)[b]	R(Abs-Bs)[c] [Å]	σ[d] [Å]	R[e] [%] Ef[f] [eV] Afac[g]
MIL-53-NH_2(40)-Mal-Pd	isolated Pd^{2+} centers	Pd-O	2.7±0.2	2.020±0.020	0.112±0.011	27.49 -5.502 0.6897
		Pd-C	1.0±0.1	2.861±0.028	0.032±0.003	
		Pd-C	1.3±0.1	3.813±0.038	0.032±0.003	
	Pd clusters	Pd-O	3.0±0.3	2.027±0.020	0.112±0.011	21.06 -6.405 0.6145
		Pd-Pd	0.2±0.02	2.651±0.026	0.045±0.004	
		Pd-Pd	0.2±0.02	3.612±0.036	0.039±0.003	
	mixed model	Pd-O	2.0±0.1	1.929±0.0192	0.067±0.006	**9.96** -5.034 0.4222
		Pd-O	1.8±0.1	2.077±0.0207	0.032±0.003	
		Pd-Pd	0.2±0.02	2.670±0.0267	0.055±0.005	
		Pd-C	2.0±0.2	2.894±0.0289	0.110±0.011	
		Pd-Pd	0.5±0.05	3.592±0.0359	0.032±0.003	
		Pd-C	2.0±0.2	3.941±0.0394	0.050±0.005	
MIL-53-NH_2(60)-Mal-Pd	isolated Pd^{2+}	Pd-O	2.4±0.2	2.010±0.020	0.100±0.010	35.86 -10.070 0.7283
		Pd-C	1.2±0.1	2.849±0.028	0.032±0.003	
		Pd-C	1.3±0.1	3.786±0.037	0.032±0.003	
	Pd clusters	Pd-O	2.7±0.2	2.007±0.020	0.100±0.010	21.93 -9.617 0.6641
		Pd-Pd	0.3±0.03	2.645±0.026	0.067±0.006	
		Pd-Pd	0.3±0.03	3.580±0.035	0.032±0.003	
	mixed model	Pd-O	1.7±0.08	1.891±0.0189	0.032±0.003	**12.77** -8.871 0.3633
		Pd-O	2.7±0.2	2.048±0.0204	0.032±0.003	
		Pd-Pd	0.7±0.07	2.658±0.0265	0.087±0.008	
		Pd-C	1.5±0.1	2.852±0.0285	0.112±0.011	
		Pd-Pd	1.0±0.1	3.587±0.0358	0.045±0.004	
		Pd-C	3.1±0.3	3.956±0.0395	0.045±0.004	
MIL-53-NH_2(80)-Mal-Pd	isolated Pd^{2+}	Pd-O	2.6±0.2	2.000±0.020	0.112±0.011	35.85 -4.999 0.6952
		Pd-C	1.4±0.1	2.839±0.028	0.032±0.003	
		Pd-C	2.0±0.2	3.805±0.038	0.032±0.003	
	Pd clusters	Pd-O	3.7±0.3	2.006±0.020	0.112±0.011	22.57 -5.686 0.4860
		Pd-Pd	0.3±0.03	2.631±0.026	0.032±0.003	
		Pd-Pd	0.5±0.05	3.612±0.036	0.050±0.005	
	mixed model	Pd-O	1.7±0.08	1.908±0.0190	0.050±0.005	**9.19** -6.113 0.4346
		Pd-O	2.0±0.2	2.072±0.0207	0.032±0.003	
		Pd-Pd	0.3±0.03	2.640±0.0264	0.032±0.003	
		Pd-C	2.0±0.2	2.914±0.0291	0.112±0.011	
		Pd-Pd	0.7±0.07	3.605±0.0360	0.032±0.003	
		Pd-C	2.0±0.2	3.963±0.0396	0.039±0.003	

[a] Abs = X-ray absorbing atom, BS = backscattering atom; [b] number of backscattering atoms; [c] distance between absorbing and backscattering atom; [d] Debye–Waller-like factor; [e] fit index; [f] Fermi energy that accounts for the shift between theory and experiment; [g] amplitude reducing factor.

3.4. Catalytic tests: Heck-type C-C coupling reaction

Since MIL-53-NH$_2$(100)-Mal-Pd was a highly active catalyst for Heck-type C-C coupling reactions of aryl halides and alkenes (Chapter 2.4), the palladium containing MIXMOFs were applied in the same reactions (Scheme 23) under optimized conditions to evaluate their catalytic activity and compare them to MIL-53-NH$_2$(100)-Mal-Pd. The higher specific surface area and the homogeneous distribution of the Pd^{2+} complexes in the MIXMOFs might have a beneficial influence on their catalytic behavior.

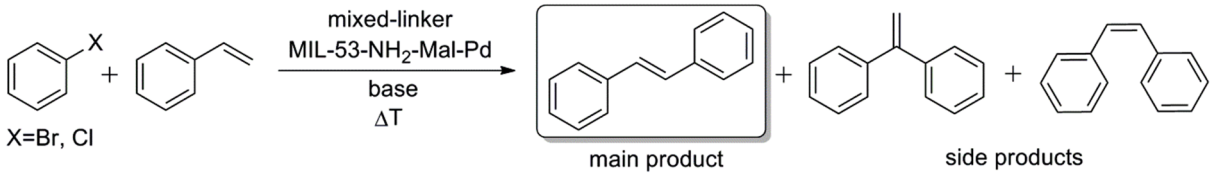

Scheme 23: Heck-type C-C coupling reaction of aryl halides and styrene catalyzed by palladium-containing mixed-linker MOFs.

3.4.1. Activity of MIL-53-NH$_2$(x)-Mal-Pd

Under the applied optimized conditions all catalyst materials exhibited comparable activity (conversion and TONs) in the C-C coupling reactions of bromo- or chlorobenzene with styrene independent of their amine content.

Table 12: Results of the catalytic tests.

	catalyst	substrate	conversion [%]	yield [%]	selectivity [%]	TON
1	MIL-53-NH$_2$(100)-Mal-Pd	PhBr[a]	96	88	92	8240
2	MIL-53-NH$_2$(80)-Mal-Pd	PhBr[a]	94	86	92	8710
3	MIL-53-NH$_2$(60)-Mal-Pd	PhBr[a]	93	86	93	8370
4	MIL-53-NH$_2$(40)-Mal-Pd	PhBr[a]	91	84	93	8630
5	MIL-53-NH$_2$(100)-Mal-Pd	PhCl[b]	22	17	78	1740
6	MIL-53-NH$_2$(80)-Mal-Pd	PhCl[b]	21	18	84	1980
7	MIL-53-NH$_2$(60)-Mal-Pd	PhCl[b]	19	16	84	1730
8	MIL-53-NH$_2$(40)-Mal-Pd	PhCl[b]	18	15	83	1690

[a] reaction conditions: bromobenzene (10 mmol), styrene (15 mmol), sodium acetate (12 mmol), Pd (0.01 mol%), N-methyl-2-pyrrolidone (NMP; 10 mL), 140 °C, 3 h; [b] reaction conditions: chlorobenzene (10 mmol), styrene (15 mmol), calcium hydroxide (12 mmol), tetrabutylammonium bromide (TBAB; 6 mmol), Pd (0.01 mol%), NMP (10 mL), 160 °C, 6 h.

In the reaction of bromobenzene with styrene not only the conversions (91 - 96 %, TONs = 8240 - 8710, Table 12, entries 1-4) but also the selectivity towards *trans*-stilbene (92 - 93 %) were quite similar for all applied catalysts. Although in the coupling of chlorobenzene with styrene the conversions (18 - 22 %, TONs = 1690 - 1980, Table 12, entries 5-8) were again comparable, the selectivity towards *trans*-stilbene was slightly higher for the mixed-linker catalysts (84 %, Table 12, entries 6-8) than the pure MIL-53-NH_2(100)-Mal-Pd (78 %, Table 12, entry 5).

The micropore volume determined for MIL-53-NH_2(100)-Mal-Pd was very low (0.01 cm^3/g), which strongly indicated that the active palladium complexes were mainly located at the outer surface of the MOF. In contrast, the micropore volumes of the mixed linker MIL-53-NH_2(x)-Mal-Pd materials were significantly higher (0.08 - 0.11 cm^3/g), thus, indicating a good distribution of the immobilized Pd^{2+} complexes in the porous structures. Since comparable TONs were observed for the palladium-containing mixed-linker MOFs and MIL-53-NH_2(100)-Mal-Pd, the catalytic activity was not affected significantly by the higher micropore volumes and the homogeneous dispersion of the active centers in the mixed-linker frameworks. However, this observation also indicated that beside the Pd^{2+} complexes immobilized on the outer surface of MIL-53-NH_2(x)-Mal-Pd (x = 80, 60, 40) also those inside the porous structure could be reached and were catalytically active in the C-C coupling reaction. In the future, additional catalytic studies with substrates of different sizes might provide valuable data to further validate this claim and to investigate a possible size- or shape-selectivity of the novel MOF-based catalysts.

3.4.2. Hot filtration test

As already discussed in Chapter 1.5.1 and Chapter 2.4.2 a “quasi-homogeneous” reaction mechanism is well-accepted for conventional heterogeneous catalysts in Heck-type C-C coupling reactions.[235-239, 244] In this case the reaction is catalyzed exclusively by Pd complexes dissolved from the supported bulk palladium. In the present study, the palladium species are already incorporated in the solid catalyst material as defined Pd^{2+} complexes. Consequently, the leaching of active species from the heterogeneous catalyst might not be required resulting in a truly heterogeneous reaction pathway. However, a minor amount of small palladium particles was also deposited in the porous structure (XAS), which might result in contributions of a “quasi-homogeneous” reaction pathway in the catalytic reaction.

To test this hypothesis, hot filtration experiments were performed using the coupling reaction of bromobenzene and styrene under optimized conditions. In those tests, the catalyst was

placed in a paper filter to enable easy separation of the powder. The catalyst was removed from the reaction after 30 min and the reaction was then resumed for another 2.5 h under the same conditions. Since the paper filter might cause external diffusion limitations, a control experiment was performed, in which the catalyst was also placed in a paper filter but was not removed from the reaction mixture for 3 h.

Table 13: Results of the hot filtration test and the control experiment with catalyst.

material	conversion (hot filtration test after 0.5 h) [%]	conversion (hot filtration test after 3 h) [%]	conversion (3 h with catalyst) [%]
MIL-53-NH$_2$(40)-Mal-Pd	30	64	77
MIL-53-NH$_2$(60)-Mal-Pd	27	74	84
MIL-53-NH$_2$(80)-Mal-Pd	22	65	85

In a previous study[242] (Chapter 2.4.2), a partly heterogeneous reaction pathway was observed for MIL-53-NH$_2$(100)-Mal-Pd, which was in contrast to the widely accepted "quasi-homogeneous" reaction pathway known for conventional supported palladium catalysts.

In the hot filtration tests performed with the palladium-containing mixed-linker MOFs conversion and yield still increased even after catalyst removal (Table 13 and Figure 22).

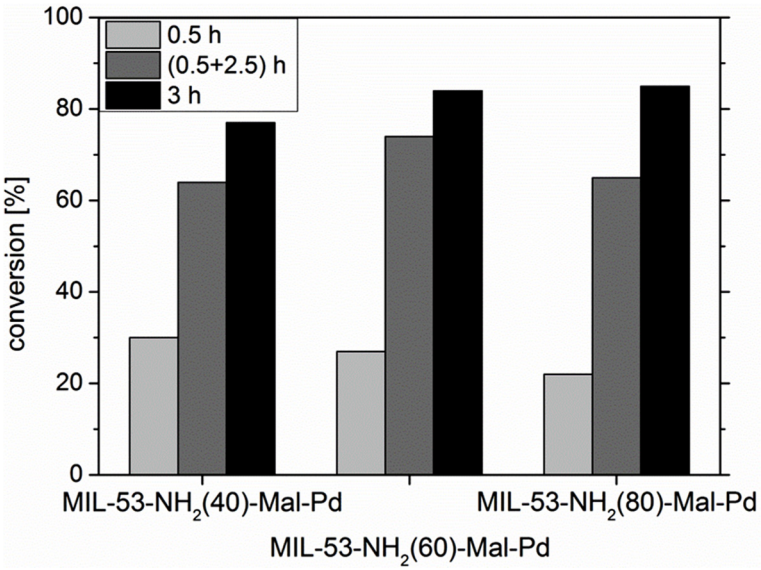

Figure 22: Results of the hot filtration test (light grey: after 0.5 h, dark grey: after 3 h) compared to a reaction with the catalyst (black); reaction conditions: NMP, 10 mmol bromobenzene, 15 mmol styrene, 12 mmol sodium acetate, 0.01 mol% catalyst, 140 °C.

Nevertheless, the conversion reached in the hot filtration test (64 - 74 %) was considerably lower than the conversion achieved in the control experiment without catalyst removal (77 - 85 %, Table 13 and Figure 22). Those results verified the hypothesis that for the novel catalysts, based on MIXMILs, contributions of a truly heterogeneous reaction pathway are feasible. The remaining activity after the catalyst had been removed might be due to leached species originating from the minor amount of small palladium nanoparticles enclosed in MIL-53-NH_2(x)-Mal-Pd or very small catalyst particles, which could not be held back by the paper filter.

3.5. Conclusion

Mixed-linker metal-organic frameworks based on MIL-53-NH_2(Al) with defined ratios of terephthalate and 2-aminoterephthalate as linker molecules were successfully synthesized at ambient pressure. The X-ray diffraction patterns confirmed that the structure of the novel materials was isoreticular to that of pure MIL-53-NH_2(Al). Moreover, ^{1}H NMR spectra revealed that the linker ratio applied during synthesis and the ratio in the resulting MOFs matched very well, thus, confirming that both terephthalate and 2-aminoterephthalate linkers were built into the framework with the same preference. The formation of core-shell particles could be excluded by variation of the reaction time and analyses of the resulting materials. Although longer reaction times led to a higher crystallinity of the frameworks, the linker ratio was constant and in good agreement with the initially applied ratio. ^{1}H NMR spectra of the frameworks modified with maleic anhydride uncovered that the modification degree per amine group steadily increased with declining percentage of 2-aminoterephthalate linkers in the MIL-53-NH_2(x)-Mal samples (5 - 11 % for x = 100 and x = 40, respectively), but the overall modification degree was, indeed, the same for all frameworks (approx. 5 %). Nitrogen physisorption measurements confirmed that the mixed-linker frameworks modified *via* a two-step PSM reaction with maleic anhydride and palladium acetate remained highly porous throughout the modification process. A micropore volume of up to 0.11 cm^3/g could be retained for the modified MIXMILs, whereas MIL-53-NH_2(100)-Mal-Pd almost entirely lost its porosity (0.01 cm^3/g). Obviously, blocking of the porous structure, which was observed for the fully functionalized framework, could be effectively prevented by diluting the amine functionalities in the mixed-linker frameworks. Although the palladium content of the MIL-53-NH_2(x)-Mal-Pd samples was considerably higher (around 3.0 wt%) compared to that of MIL-53-NH_2(100)-Mal-Pd (2.1 wt%), EXAFS analysis confirmed the successful

immobilization of defined Pd^{2+} complexes for all materials and only minor contributions of small palladium clusters were detected.

All novel materials were applied as catalysts in Heck-type C-C coupling reactions of bromo- or chlorobenzene and styrene, where they exhibited high activities (TON ≈ 8490 and 1790 for BrBz and ClBz, respectively). In the coupling of bromobenzene and styrene the selectivity towards *trans*-stilbene was similar for all catalysts (93 %), but the selectivity towards *trans*-stilbene in the coupling of chlorobenzene and styrene was slightly higher for the mixed-linker catalysts (84 %) compared to that established for MIL-53-NH_2(100)-Mal-Pd (78 %). The similar activities found for all catalysts independent of their porosity indicated that the Pd^{2+} complexes in the pores of the mixed-linker catalysts could be reached due to the high micropore volumes, while for MIL-53-NH_2(100)-Mal-Pd the complexes were immobilized exclusively on the outer surface. In addition, the results of the hot filtration test clearly showed contributions of a truly heterogeneous reaction pathway, comparable to that discovered for MIL-53-NH_2(100)-Mal-Pd.

The results of this study led to the conclusion that mixed-linker metal-organic frameworks are, indeed, interesting materials for the post-synthetic immobilization of defined metal complexes and subsequent application as heterogeneous catalysts in liquid phase reactions. Owing to their defined porous structure, they might also be promising for shape- or size-selective catalysis. To further reduce the leaching of active species, it might be advantageous to develop better ligand systems and to apply lower amounts of the palladium precursor in the modification reaction, thus, preventing the formation of nanoparticles.

4. Single- and mixed-linker DUT-5 with additional functional groups[246]

4.1. Motivation

Applying the mixed-linker frameworks MIXMIL-53-NH_2(x) (Chapter 3)[245] instead of fully functionalized MIL-53-NH_2(Al) (Chapter 2)[242] as starting materials for the immobilization of defined palladium complexes increased the specific surface area of the resulting catalyst materials from approx. 90 m²/g up to ca. 500 m²/g. However, the terephthalate linkers are relatively short resulting in a comparatively small pore diameter of < 1 nm for the mixed-linker MIL-53-NH_2 materials. In order to broaden the scope of potential guest molecules for applications such as post-synthetic modification, catalysis and separation, it might be beneficial to design metal-organic frameworks with a larger pore diameter. This approach might allow the immobilization of more sophisticated metal complexes during post-synthetic modification, which could reduce the leaching of active species during catalysis. In addition, larger pore dimensions might also be advantageous for the conversion of bulkier substrates or for the application of the framework in size- and shape-selective catalysis. DUT-5[52] (Chapter 1.2.3) features high chemical and thermal stability, which is an important requirement for the application in modification reactions and catalysis. Moreover, DUT-5 is isoreticular to MIL-53-NH_2(Al)_ht, but due to elongated linker molecules the pore dimensions are increased from 8.5 Å x 8.5 Å (MIL-53_ht[51]) to 22.7 Å x 19.2 Å (DUT-5[52]).
This Chapter covers the synthesis of fully functionalized and mixed-linker metal-organic frameworks based on DUT-5 with biphenyl-4,4'-dicarboxylate linkers bearing an additional amine, alkyne, nitro or azide group. Moreover, an unfunctionalized DUT-5 was prepared as reference and for comparison with previous reports[52]. Extensive characterization data (XRD, nitrogen physisorption, ATR-IR, ^{1}H NMR, TG, TG-IR) are presented and a number of post-synthetic modification reactions of MIXDUT-5-amine(50) and MIXDUT-5-alkyne(50) are introduced as "proof-of-principle" studies.

4.2. Synthesis of functionalized biphenyl-4,4'-dicarboxylic acids

Additional side groups are requested at the linker molecules to tune the properties of metal-organic frameworks and to utilize them for post-synthetic modification reactions. To

synthesize functionalized metal-organic frameworks based on DUT-5, the organic linker biphenyl-4,4'-dicarboxylic acid had to be equipped with an additional functional group.
The syntheses of the functionalized linker molecules were performed by the Bräse group (Institute of Organic Chemistry, KIT). Biphenyl-4,4'-dicarboxylic acid molecules with one additional amine (H_2amineBPDC), alkyne (H_2alkyneBPDC), nitro (H_2nitroBPDC) or azide group (H_2azideBPDC) were successfully prepared following the synthetic protocol depicted in Scheme 24. The strategy was developed in order to minimize the reaction steps and, thus, the four linker molecules could be prepared in a total of only eight steps.

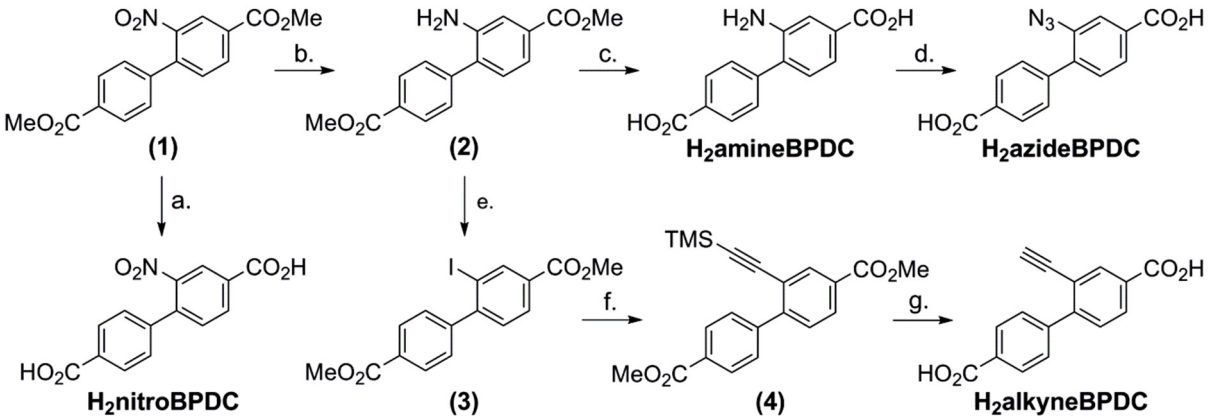

(a) KOH, THF/H_2O, reflux, 74%; (b) Pd/C, H_2, THF, r.t., 91%; (c) KOH, THF/H_2O, reflux, 95%; (d) *t*BuONO, THF, then TMS-N_3, 0°C to r.t., 97%; (e) $NaNO_2$, aq. HCl, 0°C, then NaI, 0°C, 64%; (f) TMSA, $PdCl_2(PPh_3)_2$, CuI, Et_3N/THF, r.t., 91%; (g) KOH, THF/H_2O, r.t., 92%.

Scheme 24: Synthetic protocol of the multi-step preparation of functionalized biphenyl-4,4'-dicarboxylic acid molecules; reaction conditions are listed underneath the Scheme.

4.3. Synthesis of functionalized DUT-5 and mixed-linker MIXDUT-5-functionality(x)

Fully functionalized metal-organic frameworks based on DUT-5 (DUT-5-functionality) were synthesized at ambient pressure using a solution of the functionalized biphenyl-4,4'-dicarboxylic acid molecules and $Al(NO_3)_3$*$9H_2O$ (ratio 0.54 mmol : 0.7 mmol) in *N,N*-dimethylformamide (DMF), which was heated to 120 °C for 24 h. An unfunctionalized DUT-5 was synthesized under the same reaction conditions at ambient pressure to compare it to DUT-5 reported in literature[52], which was synthesized under solvothermal conditions. The novel synthetic strategy at ambient pressure should enable easy scale-up, which is an important task regarding industrial applications and the provision of larger amounts of a material.

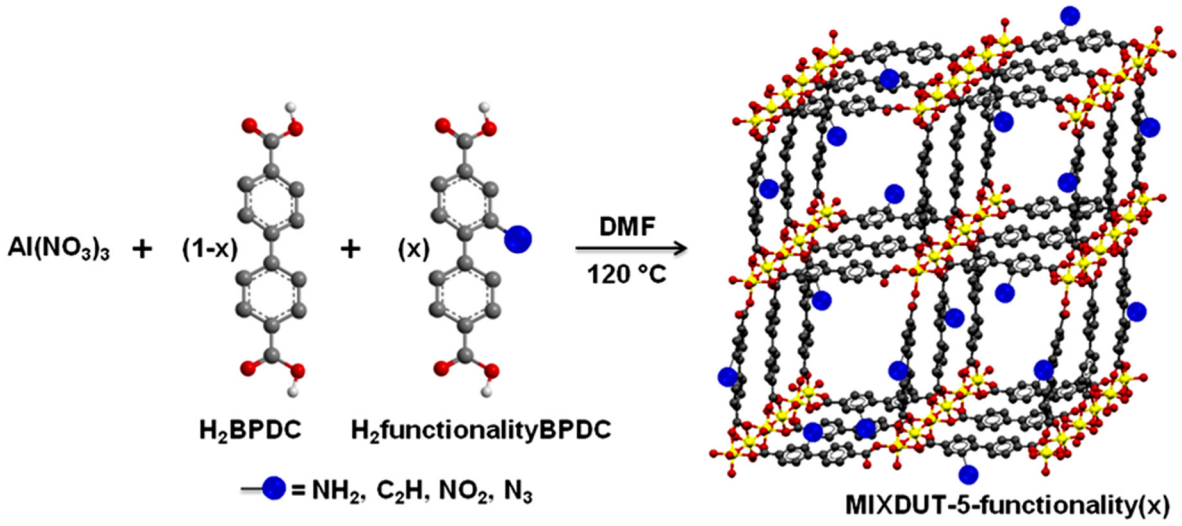

Scheme 25: Synthesis of MIXDUT-5-functionality(x); x = 25, 50, 75; x represents the percentage of functionalized linker initially applied during synthesis.

The mixed-linker MOFs (MIXDUT-5-functionality(x), x = 25, 50, 75) were prepared accordingly but with a defined mixture (1:3, 1:1, 3:1) of functionalized and unfunctionalized biphenyl-4,4'-dicarboxylic acid linkers (Scheme 25). "x" represents the percentage of the functionalized linker initially applied during synthesis. Moreover, a framework containing three different linker molecules was prepared using H_2BPDC, H_2amineBPDC and H_2alkyneBPDC in a ratio of 1:1:1 (MIXDUT-5-amine(33)-alkyne(33)). Since all reactions were – in contrast to the solvothermal route reported in literature[52] – carried out at ambient pressure, scale-up should be simplified.

4.4. Characterization

All materials were thoroughly characterized by X-ray diffraction (XRD), FT-IR spectroscopy (attenuated total reflection (ATR) mode), nitrogen physisorption measurements (BET), thermogravimetric analysis (TG), thermogravimetric analysis coupled with FT-IR spectroscopy (TG-IR) and nuclear magnetic resonance spectroscopy (^{1}H NMR).

4.4.1. Functionalized single-linker DUT-5

The XRD pattern of DUT-5 prepared at ambient pressure was in very good agreement with the diffractogram reported in literature[52] for a DUT-5 material synthesized under solvothermal conditions. Obviously the novel preparation route at ambient pressure was successful and resulted in a crystalline metal-organic framework with an identical structure.

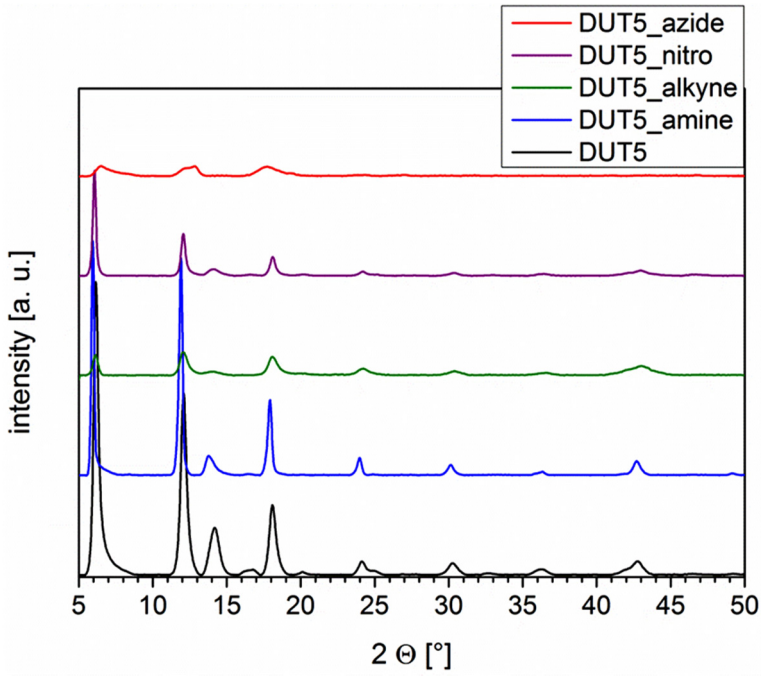

Figure 23: X-ray diffraction patterns of DUT-5 and of the fully functionalized materials based on DUT-5.

The XRD patterns (Figure 23) also confirmed that the structures of the functionalized frameworks were isoreticular to DUT-5, hence, proving that the additional functionalities did not prevent the formation of the framework structure. The diffractogram of the azide-functionalized material was, however, less intense and the reflections were considerably broader compared to the other novel materials indicating a decreased crystallinity or amorphous contributions.

To rule out the presence of residual precursor species or solvent molecules (*e.g.* free acid molecules or *N,N*-dimethylformamide) in the porous framework structure, ATR-IR spectra were recorded. The additional groups of the novel functionalized linker molecules should also be visible in the spectra confirming the successful incorporation of the functionalized linker molecules into the framework structure and the stability of the groups under the applied reaction conditions. No bands corresponding to the C=O vibrations of either free acid molecules or DMF (around 1680 cm^{-1}) were observed in the IR spectra, which indicated that the porous structure should not be blocked by any guest molecules and that the functional groups should be accessible for post-synthetic modification reactions.

In the spectra of the amine-functionalized framework (Figure 24, left) the N-H stretching vibrations were visible around $\nu = 3485\ cm^{-1}$ and $\nu = 3380\ cm^{-1}$. The C≡C-H stretching vibration of the alkyne-functionalized material (Figure 24, right) had a comparatively low intensity but could still be observed around $\nu = 3290\ cm^{-1}$. The characteristic bands of the

nitro functionality around $\nu = 1533\ cm^{-1}$ and $\nu = 1355\ cm^{-1}$ were also visible in the corresponding spectrum (Figure 27). Since no residual acid molecules were detected in any of the spectra, the additional bands of the functional groups indeed originate from linker molecules incorporated into the framework structure. Those observations proved that the amine-, alkyne- and nitro-functionalized linker molecules were successfully built into the framework structures and that the functional groups were stable under the applied reaction conditions.

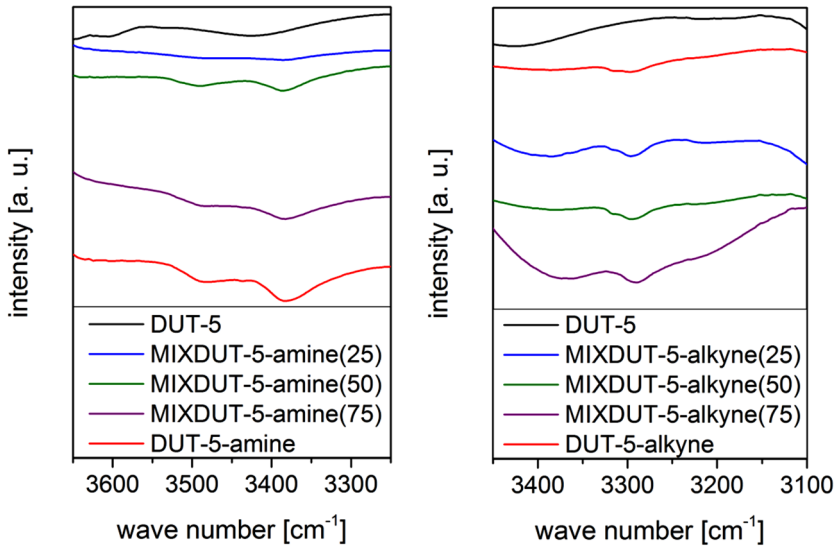

Figure 24: ATR-IR spectra of mixed-linker MIXDUT-5-amine(x) (left) and MIXDUT-5-alkyne(x) (right) compared to the fully functionalized materials (red) and DUT-5 (black).

However, a band originating from the N_3 group in the azide-functionalized framework, expected at approximately 2100 cm^{-1}, was not visible in the corresponding spectrum (Figure 25, right). Evidently, the azide group was not stable under the given reaction conditions. Instead, an additional band was detected around $\nu = 3436\ cm^{-1}$ (Figure 25, left) suggesting the transformation of the biphenyl-4,4'-dicarboxylic acid to the corresponding carbazole compound (Figure 25). Recently, the conversion of H_2azideBPDC to the corresponding carbazole has also been published for the azide-functionalized metal-organic framework UiO-67 at temperatures > 80 °C.[91] The transformation into the carbazole compound resulted in a slightly bent molecule and a different linker geometry. Due to this changed linker geometry, the formation of a DUT-5-like structure might have been hindered, which would also explain the low crystallinity observed in the diffraction pattern of DUT-5-azide. Owing to the observed decomposition of the azide group, the synthesis of DUT-5-azide was also performed at lower temperatures (80 °C and 100 °C) and with a lower Al precursor to linker

ratio (1:1 instead of 1.40:1.07). However, a crystalline material with an isoreticular and porous structure could not be obtained under any of the probed reaction conditions.

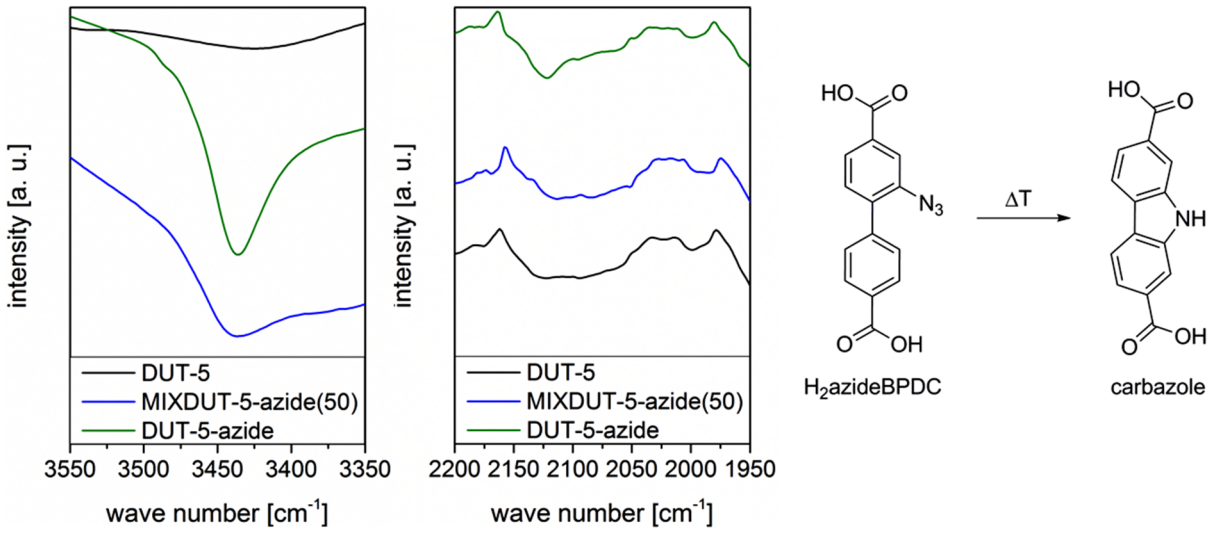

Figure 25: ATR-IR spectra of mixed-linker MIXDUT-5-azide(50) (blue) compared to the fully functionalized DUT-5-azide (green) and DUT-5 (black); formation of the carbazole is schematically shown beside the spectra.

Nitrogen physisorption measurements were carried out to determine the specific surface areas and the accessible pore volumes of the fully functionalized samples (Table 14). In literature, a specific surface area of S_{BET} = 1613 m²/g and a pore volume of 0.81 cm³/g have been reported for DUT-5.[52] Those values matched the specific surface area of S_{BET} = 1880 m²/g and the micropore volume of 0.61 cm³/g established for DUT-5 in the present study very well. The combined results from XRD, ATR-IR and N_2 physisorption measurements proved that the synthesis of DUT-5 at ambient pressure was successful without the need of solvothermal conditions in an autoclave, hence, simplifying the scale-up of the reaction.

Table 14: Specific surface areas and micropore volumes of DUT-5 and fully functionalized DUT-5.

material	S_{BET} [m²/g]	micropore volume [cm³/g]
DUT-5	1880	0.61
DUT-5-amine	1570	0.58
DUT-5-alkyne	1270	0.40
DUT-5-nitro	550	0.15
DUT-5-azide	540	0.16

The specific surface areas and the micropore volumes detected for DUT-5-amine (S_{BET} = 1570 m²/g) and DUT-5-alkyne (S_{BET} = 1270 m²/g) were slightly lower but again confirmed that the formation of a porous DUT-5 structure with the functionalized linker molecules H_2amineBPDC and H_2alkyneBPDC was accomplished. The specific surface areas and micropore volumes measured for the fully azide- and nitro-functionalized frameworks were, however, significantly lower (S_{BET} = 540 m²/g and S_{BET} = 550 m²/g, respectively). Those results in combination with the lower crystallinity observed in the XRD patterns indicated that the generation of an extended three-dimensional structure was not successful with those linker molecules.

Table 15: Thermal stability of functionalized single-linker frameworks based on DUT-5 in air.

material	thermal stability [°C]
DUT-5	450
DUT-5-amine	370
DUT-5-alkyne	390
DUT-5-nitro	340
DUT-5-azide	370

The thermal stability of the novel materials in air (Table 15) was investigated by thermogravimetric analyses (TG) and determined by considering the TG, DTG (first derivative of the TG curve) and DTA (differential thermal analysis) curves. A thermal stability of up to 450 °C was established for DUT-5, which matched the value reported in literature[52] (430 °C) very well. The thermal stabilities of the functionalized DUT-5 samples in air were slightly lower but still comparatively high (> 340 °C) for metal-organic frameworks. The fully functionalized frameworks were stable up to 340 °C (DUT-5-nitro), 370 °C (DUT-5-amine and DUT-5-azide) and 390 °C (DUT-5-alkyne), respectively.

4.4.2. Mixed-linker frameworks based on DUT-5

The XRD patterns confirmed that the structures of the mixed-linker frameworks (Figure 26) were also isoreticular to DUT-5 confirming that the additional functionalities or the presence of various linker molecules did not prevent the formation of the framework structure. As has been observed for the single-linker material, the diffractogram of the azide-functionalized material was again less intense with broadened reflections suggesting a decreased crystallinity or amorphous contributions.

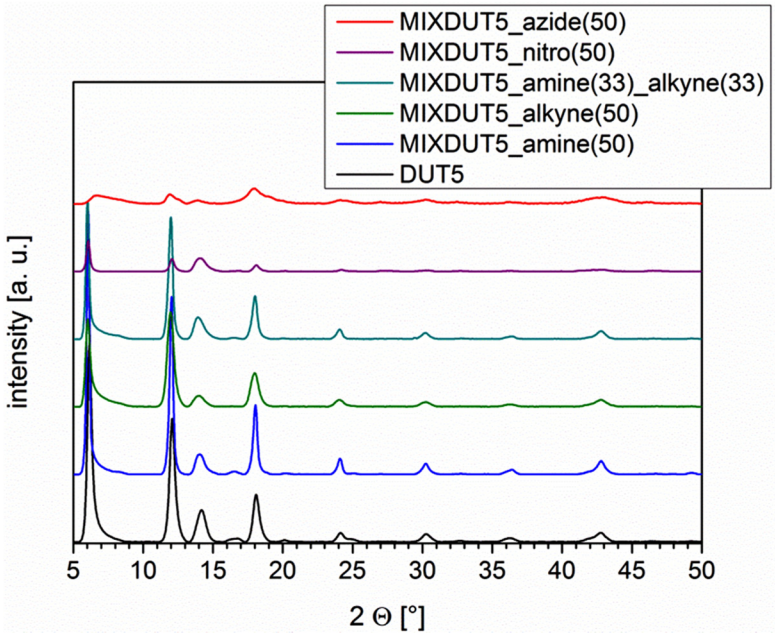

Figure 26: X-ray diffraction patterns of DUT-5 and of the mixed-linker metal-organic frameworks based on DUT-5.

ATR-IR spectra were recorded to rule out the presence of residual precursor species or solvent molecules (*e.g.* free acid molecules or *N,N*-dimethylformamide) in the porous framework structure and to confirm the successful incorporation of the functionalized linker molecules into the framework. No bands originating from the C=O vibrations of either free acid molecules or DMF were observed in the IR spectra again indicating that the functional groups should be accessible for post-synthetic modification reactions. Due to the absence of residual acid molecules, the observed bands correlate to linker molecules incorporated in the framework structure.

The N-H stretching vibrations of the amine group (around $\nu = 3485$ cm^{-1} and $\nu = 3380$ cm^{-1}, Figure 24, left), the C≡C-H stretching vibration of the alkyne-functionalized materials (around $\nu = 3290$ cm^{-1}, Figure 24, right) and the characteristic bands of the nitro functionality (around $\nu = 1533$ cm^{-1} and $\nu = 1355$ cm^{-1}, Figure 27) were visible in the corresponding spectra. The observed bands confirmed that the amine-, alkyne- and nitro-functionalized linker molecules were successfully incorporated into the mixed-linker frameworks and that the functional groups were stable under the applied reaction conditions as expected from the results for the single-linker materials.

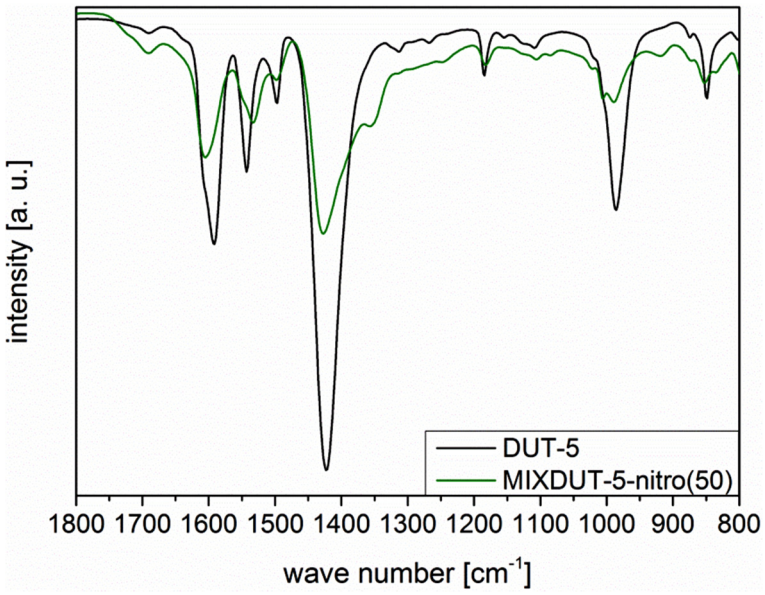

Figure 27: ATR-IR spectra of mixed-linker MIXDUT-5-nitro(50) (green) compared to DUT-5 (black).

No band originating from the N_3 group in the azide-functionalized framework was visible in the corresponding spectrum (Figure 25) confirming again that the azide group was not stable under the given reaction conditions. The additional band corresponding to the carbazole around $\nu = 3436$ cm^{-1} was also detected explaining the low crystallinity seen in the diffraction pattern of MIXDUT-5-azide(50).

Nitrogen physisorption measurements were carried out to determine the specific surface areas and the accessible pore volumes of the mixed-linker samples (Table 16). The specific surface areas of the MIXDUT-5-amine(x) materials (x = 25, 50, 75) were in the range of S_{BET} = 1600 m²/g to S_{BET} = 1630 m²/g and, therefore, in between the values established for DUT-5 (S_{BET} = 1880 m²/g) and the fully functionalized DUT-5-amine (S_{BET} = 1570 m²/g). Obviously, the specific surface area could be tuned depending on the number of amine-functionalized linker molecules incorporated in the mixed-linker frameworks. Although a similar tendency was observed for MIXDUT-5-azide(50), MIXDUT-5-nitro(50) and MIXDUT-5-amine(33)-alkyne(33), the specific surface areas determined for MIXDUT-5-alkyne(25) and MIXDUT-5-alkyne(75) were considerably lower (S_{BET} = 650 m^2/g and S_{BET} = 970 m^2/g, respectively) than the values established for both single-linker MOFs. There is not yet an explanation for this inconsistent trend in the series of the alkyne-functionalized frameworks. The syntheses of MIXDUT-5-alkyne(x) (x = 25, 50, 75) were repeated several times but nitrogen physisorption measurements of the different samples always resulted in comparable inconsistent values for the specific surface areas.

Table 16: Specific surface areas and micropore volumes of MIXDUT-5-functionality(x) materials; x: amount of functionalized linker molecules applied in the synthesis in mol%.

material	S_{BET} [m^2/g]	micropore volume [cm^3/g]
MIXDUT-5-amine(25)	1600	0.54
MIXDUT-5-amine(50)	1630	0.58
MIXDUT-5-amine(75)	1630	0.59
MIXDUT-5-alkyne(25)	650	0.17
MIXDUT-5-alkyne(50)	1350	0.42
MIXDUT-5-alkyne(75)	970	0.29
MIXDUT-5-nitro(50)	700	0.22
MIXDUT-5-azide(50)	820	0.25
MIXDUT-5-amine(33)- alkyne(33)	1630	0.56

Table 17: Thermal stability of fully functionalized and mixed-linker frameworks based on DUT-5 in air.

material	thermal stability [°C]
DUT-5	450
MIXDUT-5-amine(25)	420
MIXDUT-5-amine(50)	400
MIXDUT-5-amine(75)	390
DUT-5-amine	370
MIXDUT-5-alkyne(25)	440
MIXDUT-5-alkyne(50)	420
MIXDUT-5-alkyne(75)	400
DUT-5-alkyne	390
MIXDUT-5-amine(33)-alkyne(33)	410
MIXDUT-5-nitro(50)	380
DUT-5-nitro	340
MIXDUT-5-azide(50)	400
DUT-5-azide	370

The thermal stability of the materials could be tuned by introducing varying amounts of the functionalized linker molecules (Table 17). For the MIXDUT-5-amine(x) series (Figure 28), the thermal stability was steadily reduced from 420 °C to 390 °C ($x = 25$ and $x = 75$, respectively) with increasing amount of amine groups incorporated in the structure. A comparable trend has previously also been reported in literature for mixed-linker MOFs based on MIL-53(Al).[132] A similar behavior was observed for the alkyne-, nitro- and azide-functionalized DUT-5 samples as well as the MIXDUT-5-amine(33)-alkyne(33) framework containing three different linkers. The steady trend of the thermal stability

depending on the theoretical number of functional groups in the frameworks is a qualitative proof for the actual incorporation of both linker molecules in the ratio that was initially applied during synthesis.

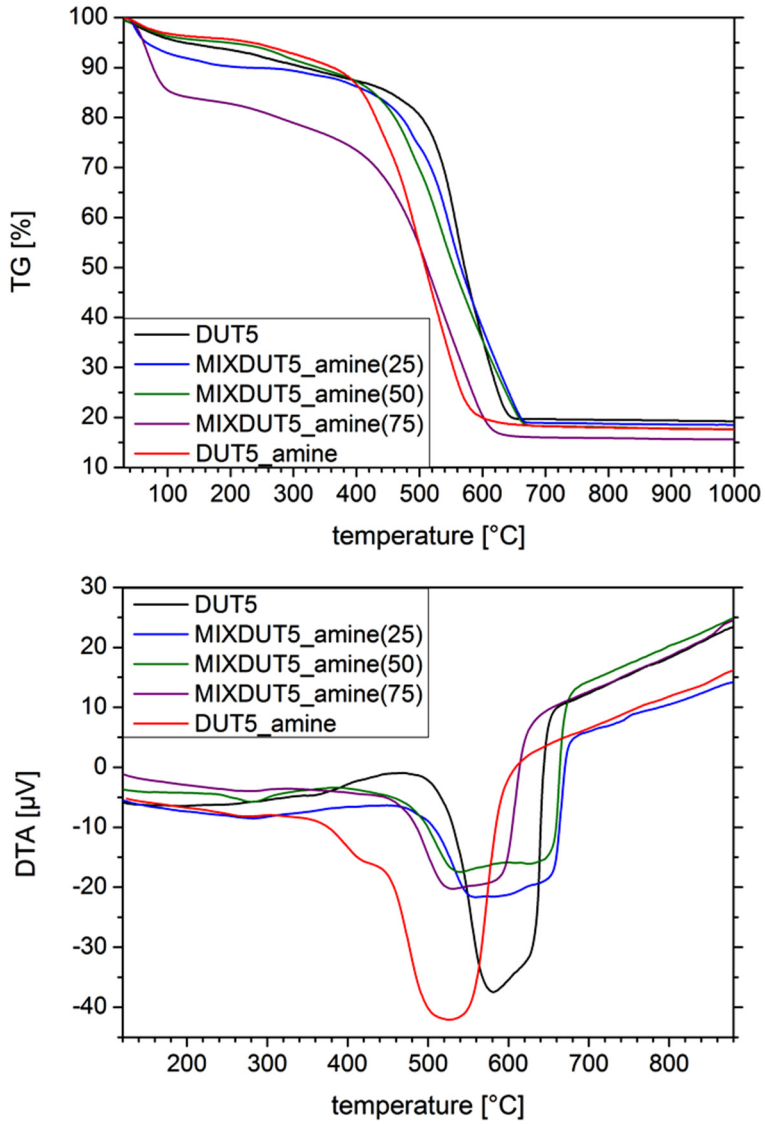

Figure 28: Thermogravimetric analysis (top) and differential thermal analysis (bottom) of DUT-5 (black), DUT-5-amine (red) and MIXDUT-5-amine(x) carried out in air.

Fourier-transformed infrared spectroscopy (FT-IR) was coupled with TG analysis to quantify the actual ratio of H_2amineBPDC and H_2BPDC linker molecules in the mixed-linker MIXDUT-5-amine(x) (x = 25, 50, 75) frameworks. The combustion of the linker molecules during TG analysis in air resulted in the formation of CO_2, H_2O and in case of the amine-functionalized linker molecules also NO_2.

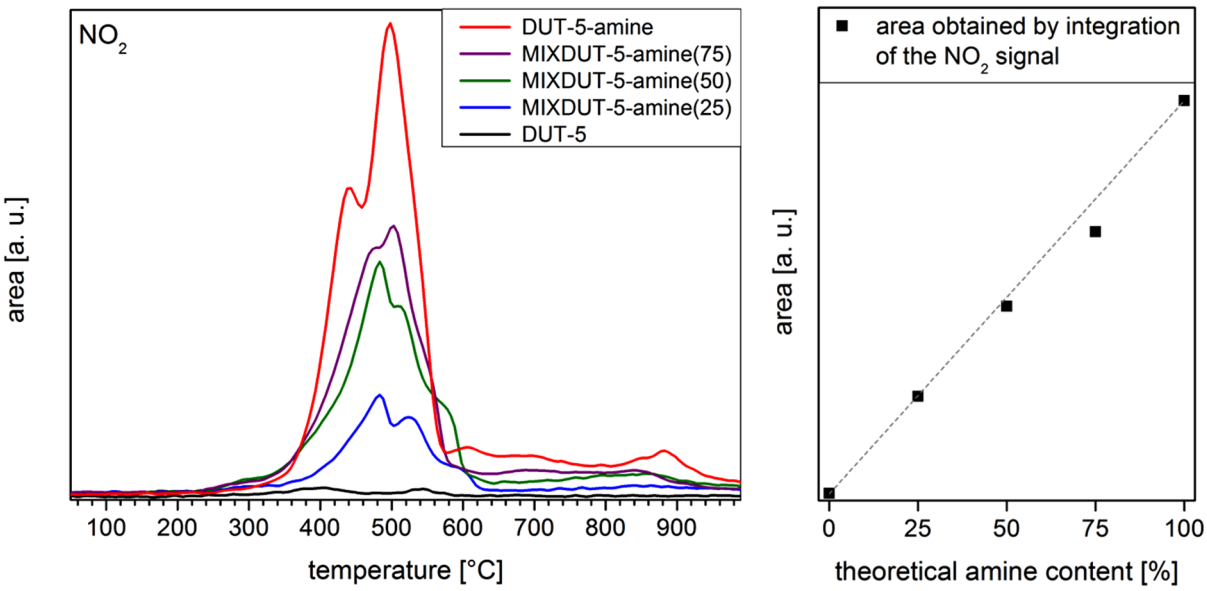

Figure 29: Integrated area of the NO_2 signal detected by TG-IR (left) and correlation of those areas to the theoretical amine content in MIXDUT-5-amine(x) (x = 25, 50, 75), DUT-5-amine (red) and DUT-5 (black); dotted line added to guide the eye.

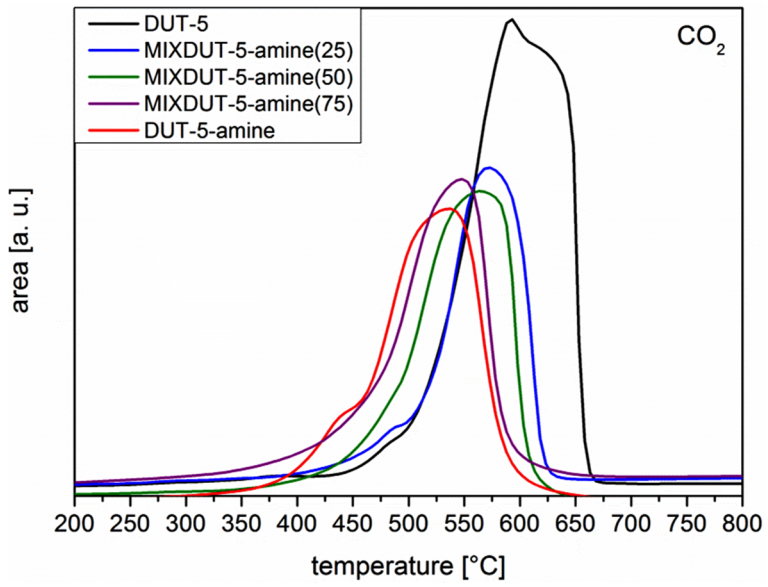

Figure 30: Integrated area of the CO_2 signal detected by TG-IR for MIXDUT-5-amine(x) (x = 25, 50, 75), DUT-5-amine (red) and DUT-5 (black).

The NO_2 signal detected by FT-IR (Figure 29, left) was integrated over the whole temperature range and could be directly related to the ratios of the amine-functionalized linker in the frameworks because no residual free acid molecules were present in the porous structure (ATR-IR). It was found that the areas steadily increased with increasing ratio of amineBPDC in the frameworks (Figure 29, right). Evidently, the linker ratio applied during synthesis and

the ratio actually incorporated in the mixed-linker frameworks matched very well. In addition, the CO_2 band in the spectra of the mixed-linker MIXDUT-5-amine(x) frameworks was also integrated and a shift to lower temperatures was observed for the maximum of the integrated peak area when the functionalization degree increased (Figure 30). This fact also corroborated the steady decrease of the thermal stability of the partially functionalized MOFs with increasing amine content.

To further quantify the linker ratio in the different mixed-linker frameworks based on DUT-5, ^{1}H NMR spectra of digested samples were recorded. This method has previously been used to determine the linker ratio of terephthalate and 2-aminoterephthalate in mixed-linker MIL-53-NH_2(x) and in that case the initially applied ratio and the actual ratio in the frameworks were in very good agreement.[245] Since no residual free acid molecules were present in the porous structure of the materials based on DUT-5 (ATR-IR), the linker ratio established by NMR was directly related to the linker ratio effectively incorporated in the framework.

For MIXDUT-5-nitro(50) the ^{1}H NMR spectrum (Figure 31) confirmed that both employed linker molecules (H_2BPDC and H_2nitroBPDC) were built into the framework structure with the same preference. For BPDC two doublets, which each corresponded to four H-atoms, were detected. One singlet and two doublets, each originating from one H-atom, and two doublets, each corresponding to two H-atoms, were found for nitroBPDC. Integration of the peaks revealed that the initial linker ratio and the ratio detected by NMR of the dissolved sample matched perfectly.

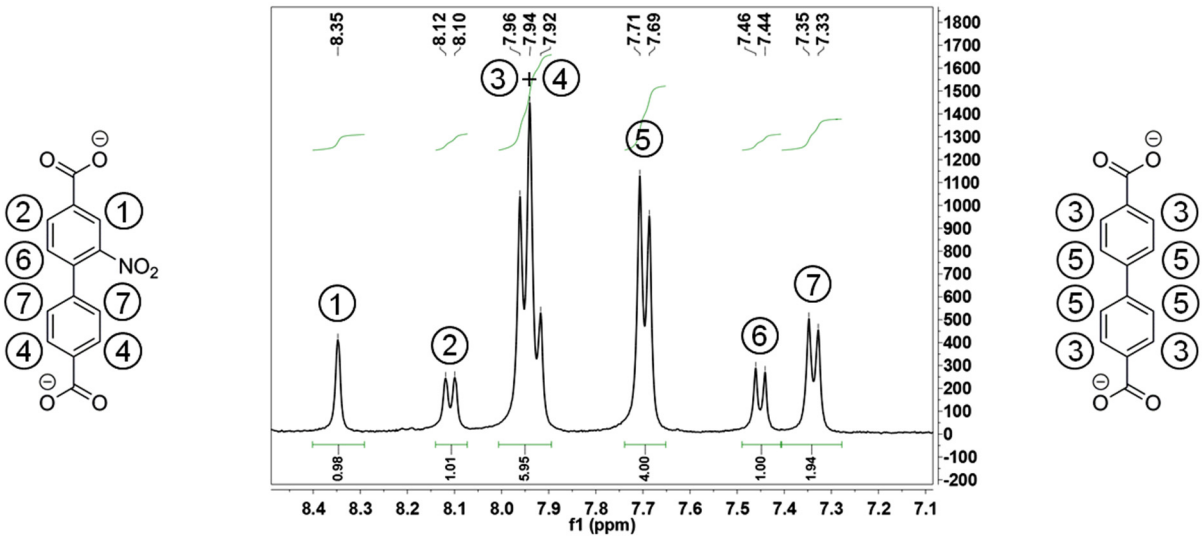

Figure 31: NMR spectrum of dissolved MIXDUT-5-nitro(50), the linker molecules nitroBPDC (left) and BPDC (right) and the assignment of the signals.

For the amine-, alkyne- and azide-functionalized MIXDUTs the quantification with NMR, however, proved difficult due to the strong overlap of the signals of the different linker molecules in the aromatic region. Another issue might be the reaction of a small fraction of the amine groups with the solvent *N,N*-dimethylformamide, which has previously been observed in the synthesis of amine-functionalized UiO-67.[92] However, for MIXDUT-5-amine(x) the determination of the linker ratio was accomplished by TG-IR measurements. The signals in the spectra of the alkyne- and azide-functionalized materials could qualitatively be correlated to the different linker molecules and confirmed again that both linker molecules were present in the MIXDUT materials.

4.5. Post-synthetic modification of functionalized DUT-5

After thorough characterization MIXDUT-5-amine(50) and MIXDUT-5-alkyne(50) were applied in a number of post-synthetic modification reactions. In a previous study, the post-synthetic modification of MIL-53-NH_2(Al) with maleic anhydride resulted in a drastic decrease of the specific surface area from 980 m^2/g to 150 m^2/g.[242] This drop could be minimized by applying mixed-linker MIL-53-NH_2(x) frameworks as the starting materials in the modification process. In this case, the specific surface area after the reaction with maleic anhydride was still approximately 500 m^2/g.[245] Post-synthetic modification of MIXDUT-5-amine(50) and MIXDUT-5-alkyne(50) should result in an even higher porosity after PSM owing to the longer linker molecules and the resulting increased pore diameter of the frameworks. Due to the larger pore diameter of the DUT-5 materials compared to the samples based on MIL-53, post-synthetic modification should also be feasible with more complex and bulkier substrates, thus, broadening the scope of PSM. Employing mixed-linker metal-organic frameworks based on DUT-5 instead of the fully functionalized framework further has the advantage of reducing the production cost since the synthesis of the functionalized linker molecules is expensive and time consuming.

4.5.1. Post-synthetic modification of MIXDUT-5-amine(50)

Maleic anhydride (MIXDUT-5-amine(50)-Mal), salicylaldehyde (MIXDUT-5-amine(50)-Sal) and 2-pyridinecarboxaldehyde (MIXDUT-5-amine(50)-Pyal) were chosen for the modification (Scheme 26) because they result in the formation of three different chelating ligands. In future studies, these introduced side chains might be utilized for the immobilization of defined metal centers to obtain novel single-site catalysts.

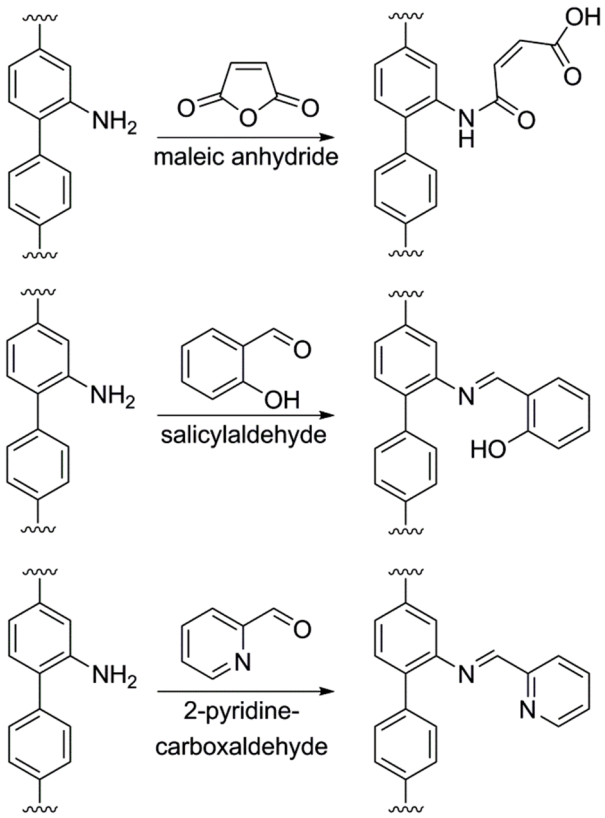

Scheme 26: Post-synthetic modification of MIXDUT-5-amine(50) with maleic anhydride (top), salicylaldehyde (middle) and 2-pyridinecarboxaldehyde (bottom).

Whereas MIXDUT-5-amine(50)-Mal has chelating side chains, which can bind metal ions *via* two oxygen atoms, MIXDUT-5-amine(50)-Sal bears one oxygen and one nitrogen atom and MIXDUT-5-amine(50)-Pyal can complex metal ions *via* two nitrogen atoms. The different coordinating sites of the introduced ligands most probably influence the strength of the bonds between the modified frameworks and the immobilized metal ions. Since leaching of active species is a problem that needs to be addressed for all heterogeneous catalysts, optimizing the chelating ligand, which connects the active centers to the porous framework, might be beneficial to minimize leaching. Moreover, the chelating ligands have varying geometries, which also might influence their ability to bind different metal ions.

X-ray diffraction patterns of the three modified frameworks (Figure 32) confirmed that the structures were stable throughout the modification process under the given reaction conditions and that the materials remained highly crystalline.

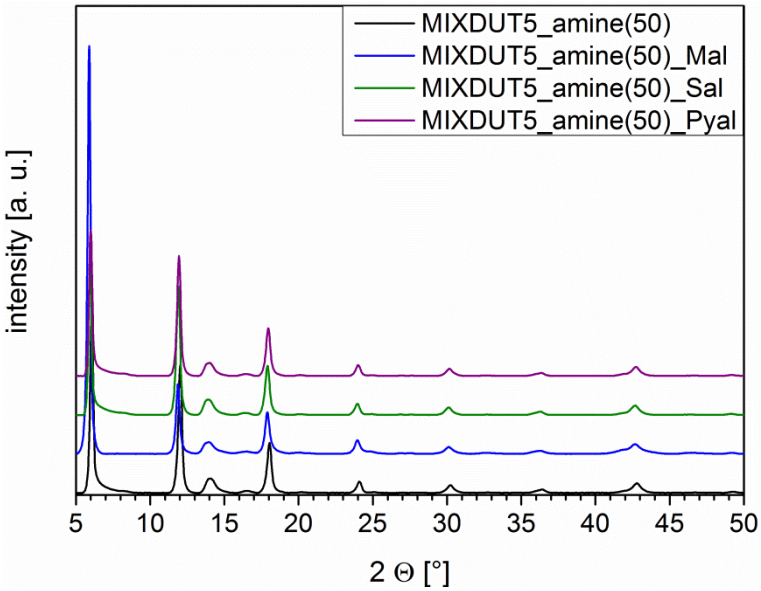

Figure 32: X-ray diffraction patterns of modified MIXDUT-5-amine(50)-mod and of MIXDUT-5-amine(50).

The hypothesis that for MIXDUT-5-amine(50) the high specific surface area would be retained throughout the modification process was probed by nitrogen physisorption measurements (Table 18). For MIXDUT-5-amine(50)-Sal and MIXDUT-5-amine(50)-Pyal the specific surface area was barely affected (S_{BET} = 1610 m^2/g and S_{BET} = 1600 m^2/g, respectively), whereas a decrease from S_{BET} = 1630 m^2/g to S_{BET} = 1200 m^2/g was observed for the framework modified with maleic anhydride.

Table 18: Specific surface areas and micropore volumes of modified MIXDUT-5-amine(50) compared to the starting material MIXDUT-5-amine(50).

material	S_{BET} [m^2/g]	micropore volume [cm^3/g]
MIXDUT-5-amine(50)	1630	0.58
MIXDUT-5-amine(50)-Mal	1200	0.43
MIXDUT-5-amine(50)-Sal	1610	0.64
MIXDUT-5-amine(50)-Pyal	1600	0.59

However, the specific surface area of MIXDUT-5-amine(50) was only reduced by approximately 25 % after the modification with maleic anhydride, while MIL-53-NH_2(40)[245] with smaller pores lost about 50 % of its porosity in the same reaction under equal modification conditions. Due to the preserved high specific surface areas, the formed chelating side chains should be accessible for the future immobilization of metal ions.

Owing to the carbonyl group introduced into MIXDUT-5-amine(50)-Mal by the PSM reaction, an additional band around ν = 1690 cm^{-1} was visible in the ATR-IR spectrum. In

contrast, no changes were observed in the spectra of MIXDUT-5-amine(50)-Sal and MIXDUT-5-amine(50)-Pyal. The intensity of the N-H stretching vibrations has already been very low in the starting material MIXDUT-5-amine(50) and, therefore, the accomplished modification could not be proven based on a reduction of the intensity of those bands.

4.5.2. Post-synthetic modification of MIXDUT-5-alkyne(50)

There are a few examples for the modification of alkyne groups in MOFs applying a click reaction with an azide to form 1,2,3-triazole derivates.[166, 247] For a first test, MIXDUT-5-alkyne(50) was utilized as starting material in a post-synthetic copper catalyzed click reaction with 2-pyridine azide (MIXDUT-5-alkyne(50)-Pyaz, Scheme 27).

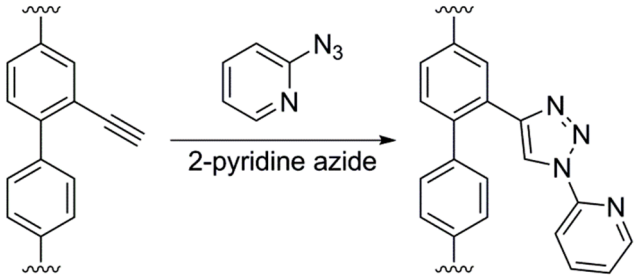

Scheme 27: Post-synthetic modification of MIXDUT-5-alkyne(50) with 2-pyridine azide.

However, the X-ray diffraction pattern revealed that the crystallinity of MIXDUT-5-alkyne(50)-Pyaz was considerably reduced indicating that the framework structure was not stable under the applied reaction conditions. This observation was further corroborated by the significant drop of the specific surface area to S_{BET} = 250 m^2/g after the modification. A possible reason for the insufficient stability of the framework under the given reaction conditions might be the basicity of 2-pyridine azide. Obviously, the reaction pathway for the post-synthetic modification of alkyne-functionalized metal-organic frameworks *via* click reactions has to be optimized to accomplish the stability of the framework during PSM.

4.6. Conclusion

Four biphenyl-4,4'-dicarboxylic acid molecules functionalized with an additional amine, alkyne, nitro or azide group, which have been prepared by the Bräse group (Institute of Organic Chemistry, KIT), were successfully applied as linker molecules in the synthesis of novel metal-organic frameworks based on DUT-5 under ambient pressure. The X-ray

diffraction patterns confirmed that the functionalized MOFs were isoreticular to the targeted DUT-5 structure although the crystallinity of the azide-functionalized framework was very low. ATR-IR spectra verified that the amine, alkyne and nitro group were incorporated in the resulting materials and, therefore, stable under the applied reaction conditions. The band of the azide group was not visible, but an additional band was observed instead indicating the decomposition of the azide-functionalized biphenyl-4,4'-dicarboxylate to the corresponding carbazole. Due to this transformation, the linker molecule has a bent geometry, which was probably the reason for the low crystallinity of the resulting material. Nitrogen physisorption measurements revealed that DUT-5-amine and DUT-5-alkyne were highly porous (1570 m^2/g and 1270 m^2/g, respectively), while the specific surface area of the nitro-functionalized framework (550 m^2/g) was lower. Thermogravimetric analyses proved that all four functionalized MOFs were stable in air up to at least 370 °C.

Based on the synthetic route successfully employed for the fully functionalized materials, mixed-linker metal-organic frameworks were synthesized with a defined ratio of biphenyl-4,4'-dicarboxylate and the functionalized linker molecules. The benefit of this approach was the possibility to tune the properties of the frameworks depending on the number of functionalized linker molecules incorporated into the materials. For the amine-functionalized series, nitrogen physisorption measurements revealed a steady decrease of the specific surface area from 1880 m^2/g to 1570 m^2/g with increasing amine content. Moreover, the thermal stability of all novel materials could be increased by decreasing the percentage of the additional functionalities in the framework structure, which was detected by thermogravimetric analysis. The incorporation of the amine, alkyne and nitro groups into the MIXDUTs was qualitatively confirmed by ATR-IR spectroscopy, which also proved the absence of any residual precursor species in the pores (*e.g.* free acids, DMF). For MIXDUT-5-nitro(50) the quantification of the linker ratio was achieved by ^{1}H NMR spectroscopy. Integration of the corresponding signals verified that the linker ratio applied during synthesis and the actual ratio in MIXDUT-5-nitro(50) matched perfectly. The linker ratio in the amine-functionalized materials could be confirmed by thermogravimetric analysis coupled with FT-IR spectroscopy (TG-IR). The measurements proved that for the MIXDUT-5-amine(x) series the linker ratios in the framework materials were in very good agreement with the ratios initially employed during synthesis. The observations made for MIXDUT-5-nitro(50) and MIXDUT-5-amine(x) (x = 25, 50, 75) strongly indicated that H_2BPDC as well as the functionalized linker molecules were incorporated into the framework structure with the same preference.

MIXDUT-5-amine(50) was then applied in post-synthetic modification reactions with maleic anhydride, salicylaldehyde and 2-pyridinecarboxaldehyde. The diffraction patterns of the modified samples showed that the structure and crystallinity of the frameworks were retained throughout the modification process. Most importantly, the modified frameworks remained highly porous with specific surface areas ranging between 1200 m^2/g for MIXDUT-5-amine(50)-Mal and 1600 m^2/g for MIXDUT-5-amine(50)-Sal and MIXDUT-5-amine(50)-Pyal. Obviously, the pore blocking previously observed for MIL-53-NH_2-Mal (150 m^2/g) and mixed-linker MIL-53-NH_2(50)-Mal (approximately 500 m^2/g) could be minimized by using mixed-linker frameworks based on DUT-5 with bigger pore dimensions.

In summary, the straightforward synthesis of highly porous metal-organic frameworks based on DUT-5 with an additional functional group or chelating side chain was accomplished. Due to their defined structure and properties, the novel materials are interesting materials for future applications, *e.g.* the immobilization of defined metal complexes, heterogeneous catalysis and gas separation/adsorption.

5. Bimetallic Cu-Ru-BTC[248]

5.1. Motivation

Bifunctional materials are advantageous for applications in catalytic transformations, in which two different active centers are required. Additionally, also tandem reactions might be accessible by the introduction of a second functionality into a catalyst material, thus, simplifying the workup procedure. Cu-BTC[53] (also known as HKUST-1 or $Cu_3(BTC)_2$) is one of the best investigated metal-organic frameworks, which has been synthesized with a number of different framework metal centers (Chapter 1.2.4). Since the potentially unsaturated metal centers in the framework structure are accessible after removal of the solvent molecules coordinated to the Cu^{2+} centers, it is an interesting material for catalytic applications.[97, 102, 214, 217, 249] To introduce a second functionality into the framework structure, a second type of metal ion[140, 143] can be introduced. In this chapter the synthesis and thorough characterization (XRD, ATR-IR, ICP-OES, XAS, nitrogen physisorption, TG) of the novel bimetallic framework Cu-Ru-BTC, which is based on HKUST-1, are presented.[248] Ruthenium was chosen as second metal since it is a versatile metal for various catalytic applications[173, 250-252]. As a reference a pure Cu-BTC framework was synthesized under comparable reaction conditions.

5.2. Synthesis and Composition

Cu-Ru-BTC (Scheme 28) was prepared using $Cu(NO_3)_2*3H_2O$ and $RuCl_3*xH_2O$ in a molar ratio of 4:1 and the organic linker molecule benzene-1,3,5-tricarboxylic acid (H_3BTC) applying a direct preparation route at ambient pressure[248] similar to a synthesis which has previously been reported for pure Cu-BTC[97]. The reference Cu-BTC was prepared after the synthetic protocol described in literature.[97]

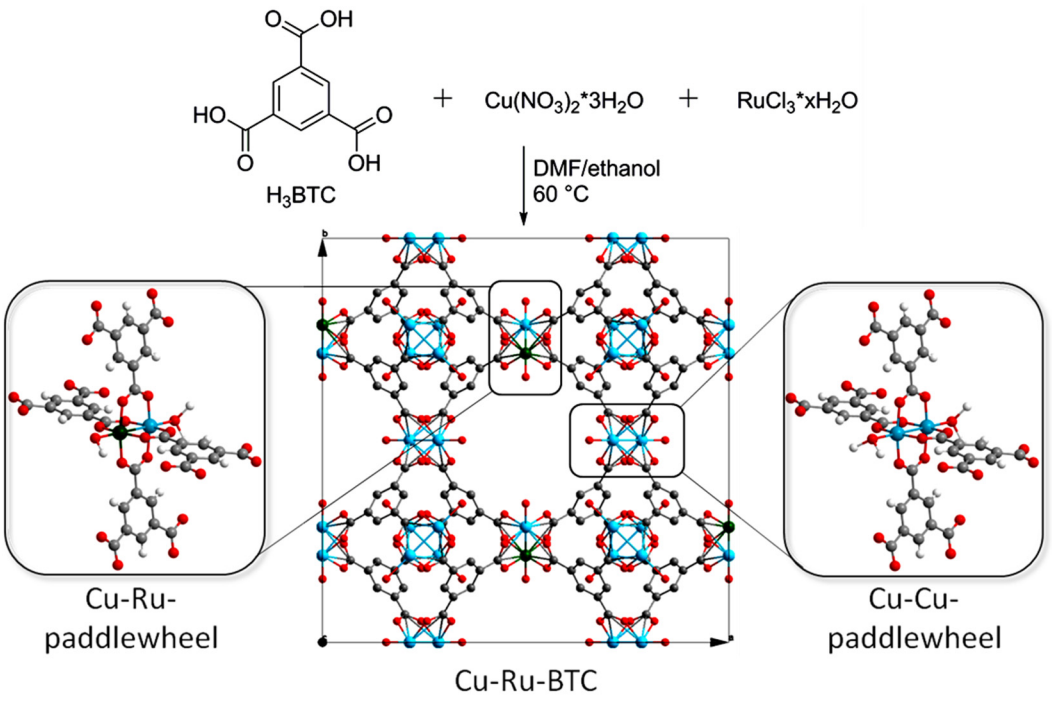

Scheme 28: Schematic synthesis of Cu-Ru-BTC and targeted structure including Cu-Ru paddlewheels (left) and Cu-Cu paddlewheels (right); blue: Cu, green: Ru, grey: C, red: O, white: H.

Optical emission spectrometry (ICP-OES, Table 19) revealed that only 3.2 wt% of ruthenium were incorporated compared to 23 wt% of copper. Those results correlated to a molar ratio for Cu:Ru of 11:1 instead of the targeted ratio of 4:1 and, therefore, the stoichiometric formula added up to $Cu_{2.75}Ru_{0.25}(BTC)_2*xH_2O$ presuming that exclusively a structure based on HKUST-1 was formed. That means that around 8 % of the Cu^{2+} centers in the framework structure would have been substituted by Ru^{3+} centers.

Table 19: Cu:Ru ratio in Cu-Ru-BTC according to ICP-OES measurements.

	wt%
ruthenium	3.2
copper	23.0

5.3. Characterization

In order to confirm the isoreticular structure and to exclude the formation of additional Ru-containing phases (*e.g.* clusters or nanoparticles), Cu-Ru-BTC was thoroughly characterized by X-ray diffraction (XRD), infrared (ATR-IR) and X-ray absorption spectroscopy (XAS). To further analyze the novel bimetallic framework, nitrogen physisorption measurements (BET) and thermogravimetric analysis (TG/DTA) were applied.

5.3.1. Structure

X-ray diffraction measurements were carried out to prove that the novel framework Cu-Ru-BTC was crystalline and isoreticular to pure Cu-BTC. The diffractograms (Figure 33) confirmed that the synthesis resulted in a metal-organic framework with the targeted HKUST-1 structure although the crystallinity of the bimetallic framework was slightly lower compared to that of the reference Cu-BTC. It is important to note that no additional phases were detected by XRD. This could either mean that a phase pure material was obtained, that the additional phases were amorphous or that the crystallites of other phases were too small to be detected by this method.

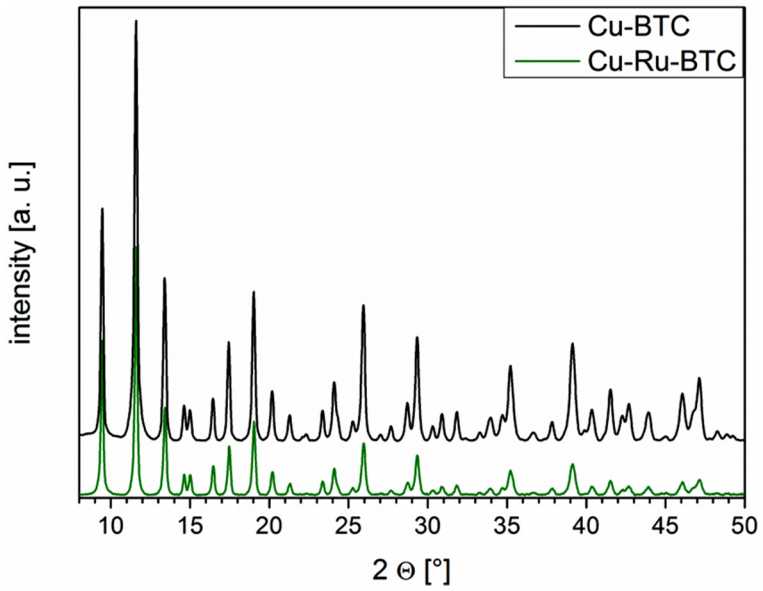

Figure 33: X-ray diffraction patterns of Cu-Ru-BTC (green) and Cu-BTC (black).

Infrared spectra (ATR-IR) were recorded to exclude the presence of residual precursor species (*e.g.* H_3BTC) in the pore system. The spectra of Cu-Ru-BTC and Cu-BTC (Figure 34) were almost identical and in both cases no additional band originating from free acid molecules (Figure 34, grey), which would be expected around $\nu = 1690\ cm^{-1}$, could be detected. This observation indicated that the pore system solely contained solvent molecules, which can be removed by thermal activation and, hence, that the metal centers in the framework structure should be accessible.

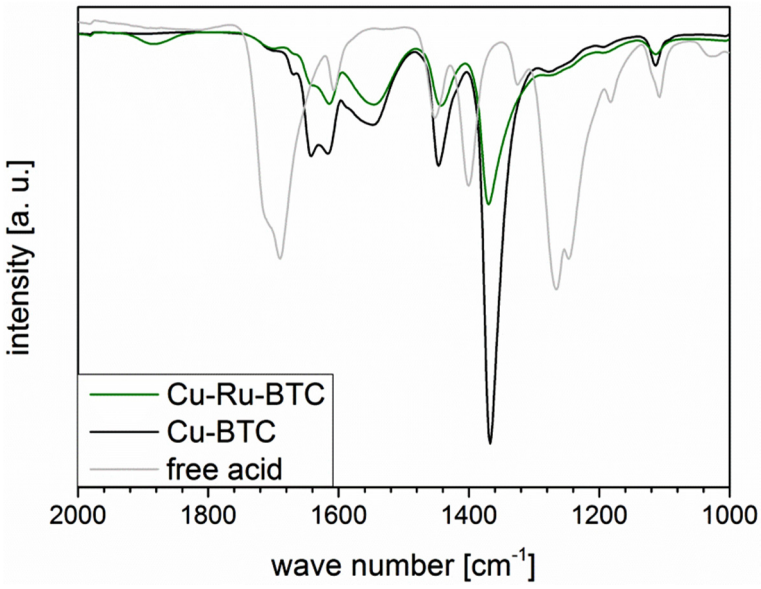

Figure 34: Infrared spectra of Cu-Ru-BTC (green), Cu-BTC (black) and H_3BTC (light grey).

X-ray absorption spectroscopy (XAS) was applied to determine the oxidation state of the metal centers as well as the geometry and composition of their coordination sphere. The spectra for Cu-Ru-BTC were recorded at the Cu and Ru K-edges (8979 eV and 22117 eV, respectively) and, as a reference, a spectrum of Cu-BTC was collected at the Cu K-edge. The evaluation of the spectra should reveal valuable information to confirm the incorporation of ruthenium ions into the HKUST-1 framework structure and to exclude the formation of additional phases such as Ru clusters or nanoparticles.

XANES spectroscopy provides information about the oxidation state and coordination geometry of metal centers. The two spectra of Cu-Ru-BTC and Cu-BTC at the Cu K-edge (Figure 35, left) did not show a significant difference, which proved that the local chemical environment at the Cu^{2+} centers was almost identical. The small pre-edge peak at 8977 eV is characteristic for a quadrupole transition which indicated a Cu^{2+} oxidation state with a d^9 configuration.[26, 253-255] This interpretation is also supported by the 1s→4p+ ligand-to-metal charge transfer shake-down transition, which is visible as a weak shoulder at 8985 eV.[26, 253, 256]

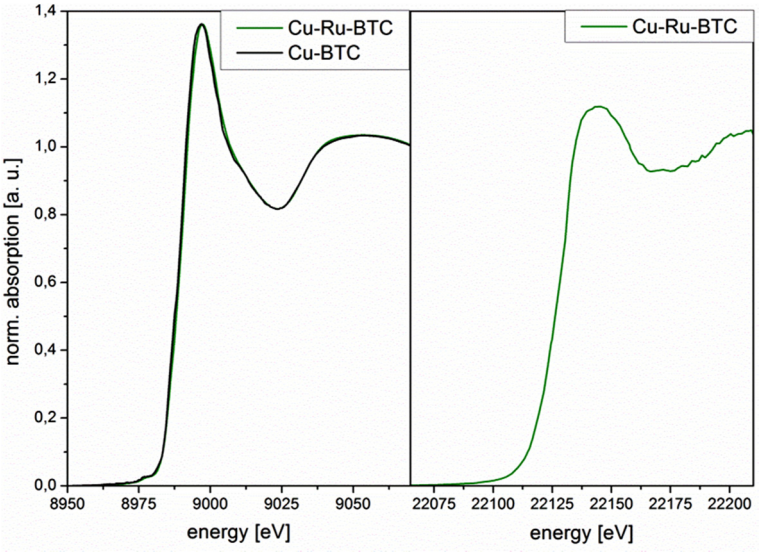

Figure 35: Normalized X-ray absorption spectra of Cu–Ru-BTC (green) and Cu-BTC (black) at the Cu K-edge (left) and spectrum of Cu–Ru-BTC at the Ru K-edge (right).

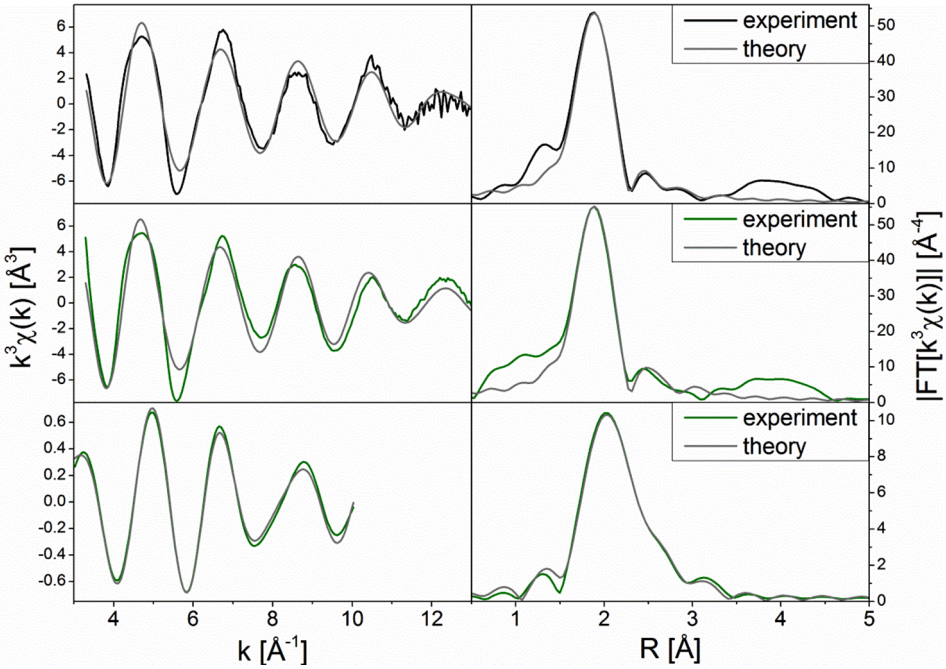

Figure 36: EXAFS spectra $k^3\chi(k)$ (left) and the corresponding Fourier transformed functions (right) of Cu-BTC (top) and Cu-Ru-BTC at the Cu K-edge (middle) and at the Ru K-edge (bottom); the theoretical fit is shown in grey.

EXAFS analysis of the spectra provides information about the local structure at the metal centers. The coordination parameters obtained by fitting of the EXAFS data (Table 20) also confirmed the resemblance of the bimetallic framework and pure Cu-BTC (Figure 36, middle and top). At a distance of 1.95 Å the Cu^{2+} centers in both materials were coordinated by five oxygen atoms, which could be attributed to four coordinated carboxylate groups of four

different BTC linker molecules and one solvent molecule, *e.g.* water. At a distance of approximately 2.64 Å the second copper ion of the paddlewheel structure was found for both Cu-Ru-BTC and Cu-BTC, which agreed very well with crystal structure analysis[53] reported in literature and data from previous EXAFS analysis of Cu-BTC[256].

For Cu-Ru-BTC an additional shell was found at 2.72 Å, which could be ascribed to a Cu-Ru shell containing approximately 0.1 ruthenium neighbors. Since ICP-OES revealed a Cu:Ru ratio of 11:1 (Table 19), that value matched the one derived from EXAFS analysis very well. Although the number of backscattering atoms was quite low, the shell is significant because the mismatch between experiment and theory (both the fit index R and the reduced error χ^2_{red}) increased significantly without the Ru shell. The four carbon atoms of the carboxylate groups of the linker molecules were detected at a distance of approximately 2.85 Å, which again was in good agreement with crystal structure analysis[53]. Further carbon shells could not be distinguished, which was probably due to the higher noise level and the intrinsic backscattering properties of carbon as a light element.

Table 20: Fitting parameters of the EXAFS analysis and results for the spectra of Cu-Ru-BTC at the Cu and Ru K-edges and Cu-BTC at the Cu K-edge.

sample	Abs-Bs[a]	N(Bs)[b]	R(Abs-Bs)[c] [Å]	σ[d] [Å]	R[e] [%] χ^2_{red}[f] E_f[g] [eV] Afac[h]
Cu-BTC Cu-Edge	Cu-O	4.7 ± 0.2	1.946 ± 0.019	0.077 ± 0.007	28.48 $4.5141*10^{-6}$ 7.189 0.7946
	Cu-Cu	1.1 ± 0.1	2.624 ± 0.026	0.102 ± 0.010	
	Cu-C	3.3 ± 0.3	2.835 ± 0.028	0.074 ± 0.007	
Cu-Ru-BTC Cu-Edge	Cu-O	4.9 ± 0.2	1.950 ± 0.019	0.077 ± 0.007	31.27 $6.0317*10^{-6}$ 8.350 0.7878
	Cu-Cu	1.3 ± 0.1	2.649 ± 0.026	0.112 ± 0.011	
	Cu-Ru	0.1 ± 0.01	2.720 ± 0.027	0.081 ± 0.008	
	Cu-C	5.6 ± 0.5	2.860 ± 0.028	0.112 ± 0.011	
Cu-Ru-BTC Ru-Edge	Ru–O	3.9 ± 0.3	2.071 ± 0.020	0.032 ± 0.003	9.564 $1.4013*10^{-6}$ −2.062 0.4294
	Ru–Cu	1.1 ± 0.1	2.672 ± 0.026	0.089 ± 0.008	
	Ru–C	4.1 ± 0.4	2.738 ± 0.027	0.112 ± 0.011	

[a] Abs = X-ray absorbing atom, BS = backscattering atom; [b] number of backscattering atoms; [c] distance between absorbing and backscattering atom; [d] Debye–Waller-like factor; [e] fit index; [f] reduced χ^2 error (considers the error to the experiment as well as the number of independent points and the number of varied parameters); [g] Fermi energy that accounts for the shift between theory and experiment; [h] amplitude reducing factor.

The edge energy of 22126 eV and the whiteline structure seen in the XANES spectrum of Cu-Ru-BTC at the Ru K-edge (Figure 35, right) are characteristic for an oxidation state of Ru^{3+}. The low ruthenium concentration and the resulting weak signal made Fourier filtering necessary for the spectrum taken at the Ru K-edge. The filtering was applied for distances between 1 Å and 3 Å. The untreated spectrum is shown in Figure 37, and the treated one is depicted in Figure 36, bottom left. Even after Fourier filtering, an EXAFS analysis (Figure 36, bottom) was only possible up to k = 10 $Å^{-1}$ in χ(k).

A shell with four oxygen atoms could be fitted at a distance of 2.07 Å, which was a slightly larger bond length than expected from the previous analysis for Cu at the Cu K-edge. The ionic radius of Ru^{3+} is smaller than that of Cu^{2+} (0.82 Å compared to 0.87 Å)[257], which should have resulted in a shorter Ru-O bond length. In addition, the Cu-Ru distance derived from the Ru K-edge spectrum was slightly shorter (2.67 Å) than the one resulting from the Cu K-edge spectrum (2.72 Å). Both effects can most probably be attributed to the loss of resolution due to the smaller *k*-range that could be used for the fit because of the low signal to noise ratio. When the copper neighbors were replaced by a ruthenium shell in the fit, the error values (both the fit index R and the reduced error χ^2_{red}) increased strongly. Thus, the additional formation of Ru-Ru paddlewheel structures or other Ru-containing phases, *e.g.* clusters or nanoparticles, could be excluded within the detection limit of the method. At a distance of 2.74 Å the four carbon atoms of the carboxylate groups of the linker molecules could be discerned, which matched the results at the Cu K-edge. Generally, the results of the EXAFS analyses of both the Cu and Ru K-edge matched very well.

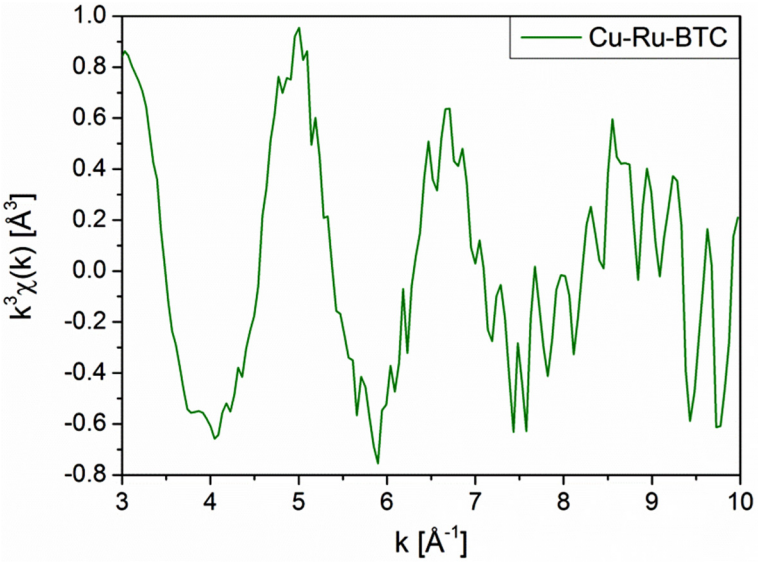

Figure 37: EXAFS spectrum of Cu-Ru-BTC before Fourier filtering recorded at the Ru-edge.

The results presented in this chapter all confirmed that Cu-Ru-BTC crystallized in a structure isoreticular to HKUST-1, in which the Cu^{2+} centers in the paddlewheel units were partially substituted by Ru^{3+} ions (Scheme 28).

5.3.2. Physical properties

Nitrogen physisorption measurements were applied to determine the specific surface area, the micropore volume and, thus, the accessibility of the metal centers in the porous framework structure. The specific surface area determined for Cu-BTC (S_{BET}: 1560 m²/g; Figure 38 and Table 21) matched the literature reports[53, 97, 100-101, 103] for HKUST-1 very well. However, the value established for Cu-Ru-BTC (570 m²/g; Figure 38 and Table 21) was significantly lower.

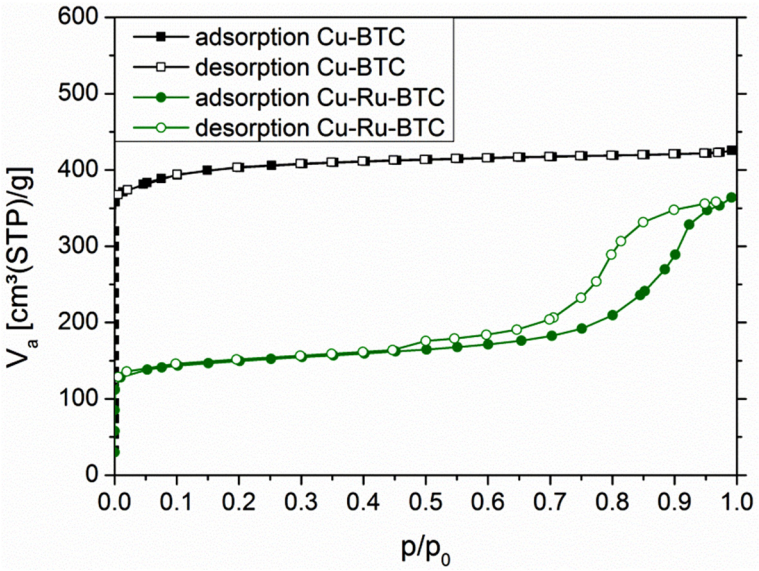

Figure 38: Adsorption (filled symbols) and desorption (open symbols) isotherms of Cu-Ru-BTC (green) and Cu-BTC (black) obtained by nitrogen physisorption measurements.

Table 21: S_{BET}, $S_{Langmuir}$ and micropore volume of Cu-Ru-BTC and Cu-BTC calculated from nitrogen physisorption measurements.

sample	S_{BET} [m²/g]	$S_{Langmuir}$ [m²/g]	micropore volume [cm³/g]
Cu-Ru-BTC	570	710	0.18
Cu-BTC	1560	1850	0.60

A similar trend has been observed for the bimetallic framework Cu-Zn-BTC[140], where the specific surface area dropped to S_{BET} = 830 m²/g, when a comparable amount of the second metal (Zn^{2+}) was incorporated. This was explained by coordination defects at the Zn^{2+} centers

and the resulting incomplete formation of 3D porosity. For Cu-Ru-BTC the larger size difference of the ionic radii between Cu^{2+} (0.87 Å[257]) and Ru^{3+} (0.82 Å[257]) compared to Zn^{2+} (0.88 Å[257]) and the counter ion, which is necessary to compensate the additional charge of Ru^{3+}, might have increased the disorder in the framework structure and caused the reduced porosity. The XRD pattern of Cu-Ru-BTC already indicated a lower crystallinity of the bimetallic framework and, therefore, confirmed the presence of an increased number of defect sites in the structure. Nevertheless, the framework metal centers should be accessible and employable for catalytic applications.

Thermogravimetric analysis (Figure 39) of Cu-Ru-BTC performed in air revealed a mass loss of approximately 15 wt% in the temperature range < 150 °C, which originated from water. In the same temperature range a mass loss of about 35 wt% of incorporated water was found for Cu-BTC. This observation also supported a reduced porosity of the bimetallic framework compared to pure Cu-BTC. Evaluation of the TG curves (Figure 39, solid line) revealed a slightly reduced thermal stability for Cu-Ru-BTC (265 °C compared to 290 °C for Cu-BTC). The shift of the minimum in the DTA curve (Figure 39, dotted line), which indicates the maximum rate of decomposition, from 310 °C for Cu-BTC to 290 °C for Cu-Ru-BTC also confirmed that the decomposition of the bimetallic framework started at slightly lower temperatures.

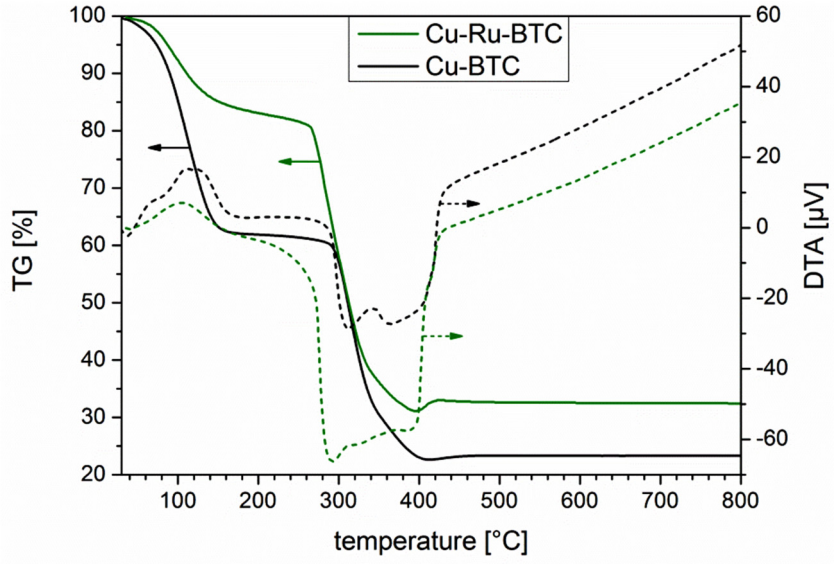

Figure 39: Thermogravimetric analysis (solid line) and differential thermal analysis (dotted line) of Cu-Ru-BTC (green) and Cu-BTC (black).

5.4. Conclusion

In summary, a novel bimetallic metal-organic framework Cu-Ru-BTC was successfully synthesized applying mild reaction conditions (ambient pressure, 60 °C). X-ray diffraction measurements revealed that the framework structure was isoreticular to HKUST-1 and X-ray absorption spectroscopy confirmed that the Ru^{3+} centers were exclusively incorporated in the framework lattice, partially replacing the Cu^{2+} centers in the paddlewheel structure. ATR-IR spectroscopy further proved that no residual precursor species (*e.g.* free carboxylic acid molecules) were present in the pore structure. X-ray absorption spectroscopy excluded the undesired formation of additional Ru-containing phases (neither Ru-Ru paddlewheels nor Ru nanoparticles or clusters). Thermogravimetric analysis and nitrogen physisorption measurements revealed that the bimetallic framework Cu-Ru-BTC was stable up to 265 °C in air and featured a high specific surface area of 570 m²/g. The Cu:Ru ratio determined by ICP-OES and corroborated by XAS was approximately 11:1, which corresponded to the stoichiometric formula $Cu_{2.75}Ru_{0.25}(BTC)_2*xH_2O$.

Due to its structure and physical properties Cu-Ru-BTC is considered an interesting metal-organic framework for future applications as bifunctional catalyst or for adsorption studies.

6. Final conclusion and outlook

In the present thesis, the design of novel catalyst systems based on metal-organic frameworks was accomplished applying different synthetic concepts.

The immobilization of defined Pd^{2+} complexes on amine groups in the metal-organic framework MIL-53-NH_2(Al) (Chapter 2) as well as in mixed-linker MIL-53-NH_2(x) (MIXMOF, Chapter 3) was achieved and the resulting materials were successfully probed for their activity in Heck-type C-C coupling reactions. A novel synthetic route at ambient pressure was developed and applied for the MOF preparation as an advancement of the established solvothermal synthesis. The new method has the benefit of enabling an easy scale-up, which is important for possible applications that require large amounts of the material. Moreover, X-ray diffraction patterns and IR spectra revealed that MIL-53-NH_2(x)_lt materials without residual acid molecules in the pores were obtained directly *via* this new route. Therefore, elaborate purification of the materials, which has been reported in literature for materials prepared under solvothermal conditions, could be avoided. ^{1}H NMR spectra of dissolved samples confirmed that the linker ratio employed in the synthesis of mixed-linker MIL-53-NH_2(Al) and the actual ratio in the resulting materials were identical confirming that both linker molecules were incorporated in the structure with the same preference. Although longer reaction times increased the crystallinity of the materials (XRD), the composition remained unchanged (^{1}H NMR), which proved the homogeneous distribution of the different linkers in the framework, while excluding the formation of core-shell particles.

A two-step post-synthetic modification (PSM) reaction using first maleic anhydride and then palladium acetate was designed to immobilize defined mononuclear Pd^{2+} complexes on the amine groups in the framework structure. While the specific surface area of MIL-53-NH_2(Al) drastically decreased throughout the modification process from S_{BET} = 980 m^2/g to S_{BET} = 90 m^2/g, this effect could be minimized for the mixed-linker frameworks (S_{BET} = 500 m^2/g for MIL-53-NH_2(40)-Mal-Pd). At the same time, a higher palladium loading was achieved for the mixed-linker frameworks (approximately 3.0 wt% compared to 2.1 wt% for MIL-53-NH_2(Al)-Mal-Pd). Obviously, the mixed-linker MOFs remained highly porous after the immobilization of the Pd^{2+} complexes due to the dilution of the amine groups in the material, thus, proving the benefits of combining the MIXMOF and PSM concepts. The incorporation of palladium was confirmed by atomic absorption spectroscopy (AAS) and the presence of defined complexes was proven by X-ray absorption spectroscopy (XAS). However, when high amounts of the palladium precursor were applied to test the maximally

achievable loading of defined Pd^{2+} complexes, the additional formation of undesired palladium nanoparticles was observed. This fact clearly illustrates the importance of parameter optimization during preparation and thorough characterization of the resulting materials.

The Pd-containing MOFs were applied in Heck-type C-C coupling reactions of bromo- or chlorobenzene and styrene. Due to the strong C-Br and especially C-Cl bonds, it is demanding to activate those substrates. However, at 140 °C, full conversion (TON ≈ 8490) and a high selectivity towards stilbene (> 92 %) were achieved after 3 h with the MOF-based catalysts in the coupling of bromobenzene and styrene with only 0.01 mol% palladium. The catalysts were also remarkably active in the coupling of chlorobenzene and styrene. After 6 h at 160 °C a turnover number of TON ≈ 1790 was accomplished. Although the increased specific surface area of the modified mixed-linker MOFs did not have a beneficial influence on the coupling reaction of bromobenzene and styrene, in the coupling reaction of chlorobenzene the selectivity towards stilbene did increase significantly in the presence of the MIXMOFs (84 % compared to 78 % for MIL-53-NH_2(Al)-Mal-Pd).

To further improve those MOF-based catalysts, functionalized single- and mixed-linker frameworks based on DUT-5 were synthesized (Chapter 4). DUT-5 is isoreticular to MIL-53(Al)_ht but is constructed from elongated linker molecules (biphenyl-4,4'-dicarboxylate) leading to larger pore dimensions. Employing MOFs with larger cavities most probably broadens the scope and complexity of substrates available for post-synthetic modification and, ultimately, also for catalysis. To enable the modification of DUT-5, functionalized linker molecules bearing an additional amine, alkyne, nitro or azide group were synthesized by the Bräse group (Institute of Organic Chemistry, KIT). Those linkers were then employed in the preparation of single- and mixed-linker frameworks at ambient pressure which again facilitates an easy scale-up. XRD patterns and IR spectra of the amine-, alkyne- and nitro-functionalized materials confirmed the successful incorporation of those groups into single- and mixed-linker DUT-5 frameworks. Although a DUT-5-like structure with low crystallinity was formed in presence of the azide-functionalized linker, the azide group was not stable under the applied reaction conditions and the transformation into the corresponding carbazole was observed instead. A crystalline material isoreticular to DUT-5 could not be obtained with the azide-functionalized linker, even at milder reaction conditions. The porosity of the MIXDUT-5-amine(x) frameworks could be tuned by variation of the amine content, and the specific surface area steadily increased with decreasing number of amine groups. Although the thermal stability of all materials decreased after the

incorporation of additional groups, all functionalized metal-organic frameworks were stable to at least 340 °C in air. For MIXDUT-5-amine(x) (x = 25, 50, 75) and MIXDUT-5-nitro(50) the perfect match between the initially applied linker ratio and the linker ratio in the resulting MOFs could be confirmed by thermogravimetric analysis coupled with IR spectroscopy and by ^{1}H NMR of dissolved samples, respectively.

The post-synthetic modification of MIXDUT-5-amine(50) was accomplished with maleic anhydride, 2-pyridinecarboxaldehyde and salicylaldehyde in a "proof-of-principle" study. Although the specific surface area of MIXDUT-5-amine(50)-Mal slightly decreased, MIXDUT-5-amine(50)-Sal and MIXDUT-5-amine(50)-Pyal retained all of their porosity. Therefore, the benefits of applying functionalized metal-organic frameworks with extended pore dimensions in post-synthetic modification reactions could be confirmed.

For future studies, the immobilization of a variety of different metal complexes in mixed-linker metal-organic frameworks based on MIL-53(Al) as well as on DUT-5 might be of interest. To give an example, manganese complexes could be utilized for a variety of aerobic oxidation reactions. In order to prevent the leaching of active species the chelating ligand needs to be tailored for each metal center individually. In addition, due to their defined pore structure the introduced MOFs might be attractive materials for size-selective catalysis, *e.g.* converting exclusively the smaller or linear substrates in a mixture of reagents.

In another approach, the unsaturated Cu^{2+} framework metal centers in HKUST-1 were partially substituted by Ru^{3+} ions in a direct synthesis at ambient pressure, thus, creating a bimetallic metal-organic framework (Chapter 5). The novel material Cu-Ru-BTC has the stoichiometric formula $Cu_{2.75}Ru_{0.25}(BTC)_2$*x$H_2O$, which was determined by ICP-OES, and a crystalline structure that is isoreticular to HKUST-1 (XRD). The successful incorporation of the Ru^{3+} centers into the paddlewheel SBUs was proven by X-ray absorption spectroscopy, which also excluded the formation of additional undesired ruthenium phases, *e.g.* clusters or nanoparticles. Obviously, the synthesis of a new bimetallic framework Cu-Ru-BTC that is porous (S_{BET} = 570 m^2/g) and thermally stable in air up to 265 °C was successfully accomplished under mild reaction conditions. Those characteristics in combination with the unsaturated metal centers render Cu-Ru-BTC an interesting material for future studies on gas adsorption applications and catalysis (*e.g.* selective oxidation reactions).

7. Experimental Details

7.1. Materials

7.1.1. Synthesis of MIL-53-NH_2(Al)

0.9660 g (5.33 mmol, 1 eq) 2-aminobenzene-1,4-dicarboxylic acid (aminoterephthalic acid, H_2ABDC) were dissolved in 25 mL H_2O and 20 mL *N,N*-dimethylformamide (DMF) at 90 °C under reflux. A solution of 2.0000 g (5.33 mmol, 1 eq) $Al(NO_3)_3$*$9H_2O$ in 5 mL H_2O was added and the reaction mixture was stirred at 90 °C under reflux for 24 h. After filtration the material was washed with 3 x 10 mL DMF and 1 x 30 mL H_2O. The sample was dried overnight at room temperature and then for 3 days at 130 °C in air atmosphere.

7.1.2. Post-synthetic modification of MIL-53-NH_2(Al)

The framework was modified in a two-step post-synthetic modification reaction.

1st step: modification with maleic anhydride: 4 mmol (4 eq) maleic anhydride were dissolved in 25 mL acetonitrile. 1 mmol (1 eq) MIL-53-NH_2(Al) was suspended in the solution and the reaction mixture was heated under reflux to 80 °C for 24 h. After filtration the resulting material was washed with 5 x 20 mL acetonitrile, 1 x 20 mL *N,N*-dimethylformamide (DMF) and 1 x 20 mL H_2O. The sample was dried overnight at room temperature and then for 3 days at 130 °C in air atmosphere.

2nd step: modification with palladium acetate: The amount of Pd precursor was calculated in regard to the literature value of 40 % of the amino functions being successfully modified with maleic anhydride.[163] 0.1 - 0.6 mmol (0.25 – 1.5 eq) Pd(II) acetate were dissolved in 12 mL *N,N*-dimethylformamide (DMF). 1.0 mmol (1.0 eq) MIL-53-NH_2(Al)-Mal was suspended in the solution and the reaction mixture was heated to 60 °C for 4 h. After filtration the resulting material was washed with 3 x 12 mL DMF and 1 x 12 mL H_2O. The sample was dried overnight at room temperature and then for 2 days at 130 °C in air atmosphere.

7.1.3. Synthesis of MIXMIL-53-NH_2(x) (x=40, 50, 60, 80)

Mixed-linker metal-organic frameworks based on MIL-53-NH_2(Al) containing 40 %, 50 %, 60 % and 80 % aminoterephthalate were synthesized. 5.33 mmol of the linker molecules 2-aminobenzene-1,4-dicarboxylic acid and benzene-1,4-dicarboxylic acid (terephthalic acid,

H_2BDC, ratios are listed in Table 22) were dissolved in 25 mL H_2O and 50 mL DMF at 90 °C under reflux. A solution of 2.0 g (5.33 mmol) $Al(NO_3)_3*9H_2O$ in 5 mL H_2O was added and the reaction mixtures were stirred under reflux for 24 h at 90 °C. After filtration the materials were washed with 3 x 25 mL DMF and 1 x 25 mL H_2O. The samples were dried overnight at room temperature and then for 3 days at 130 °C in air atmosphere.

Table 22: Ratios of aminoterephthalic acid and terephthalic acid applied in the synthesis of MIXMIL-53-NH_2(x).

	H_2ABDC [%]	H_2ABDC [g]	H_2BDC [%]	H_2BDC [g]
MIL-53-NH_2(40)	40	0.3860	60	0.5310
MIL-53-NH_2(50)	50	0.4830	50	0.4430
MIL-53-NH_2(60)	60	0.5790	40	0.3540
MIL-53-NH_2(80)	80	0.7720	20	0.1770

7.1.4. Post-synthetic modification of MIXMIL-53-NH_2(x) (x=40, 50, 60, 80)

The MIXMIL-53-NH_2(x) were modified in a two-step post-synthetic modification reaction.

1st step: modification with maleic anhydride: 4 eq maleic anhydride (based on the number of amine groups) were dissolved in 50 mL acetonitrile. 2 mmol of the MIXMIL-53-NH_2(x) were suspended in the solution and the reaction mixtures were heated to 80 °C under reflux for 24 h. After filtration the resulting materials were washed with 5 x 20 mL acetonitrile, 1 x 20 mL *N,N*-dimethylformamide (DMF) and 1 x 20 mL H_2O. The samples were dried overnight at room temperature and then for 3 days at 130 °C in air atmosphere.

2nd step: modification with palladium acetate: The amount of Pd precursor was calculated in regard to the literature value of 40 %[163] of all linkers being successfully modified with maleic anhydride. 0.15 mmol (0.25 eq per modified linker) palladium(II) acetate were dissolved in 20 mL DMF. 1.5 mmol (1 eq) of the modified MIXMIL-53-NH_2(x) was suspended in the solution and the reaction mixtures were heated to 60 °C for 4 h. After filtration the resulting materials were washed with 3 x 20 mL *N,N*-dimethylformamide (DMF) and 1 x 20 mL H_2O. The samples were dried overnight at room temperature and then for 3 days at 130 °C in air atmosphere.

7.1.5. Synthesis of functionalized DUT-5

0.54 mmol of the functionalized biphenyl-4,4'-dicarboxylic acid molecules (see Table 23) were dissolved in 20 mL *N,N*-dimethylformamide (DMF) at 120 °C. A solution of 0.2600 g (0.70 mmol) aluminum nitrate nonahydrate ($Al(NO_3)_3*9H_2O$) in 5 mL DMF was added. The reaction mixture was stirred for 24 h under reflux at 120 °C. After filtration the metal-organic frameworks were washed with 3 x 25 mL of DMF and 1 x 25 mL of H_2O. The solid was dried overnight at room temperature and then for 3 days at 130 °C.

Table 23: Mass of linker molecules applied in the synthesis of functionalized DUT-5.

linker molecule	acronym	mass [g]
2-amino-[1,1'-biphenyl]-4,4'-dicarboxylic acid	H_2amineBPDC	0.1377
2-ethynyl-[1,1'-biphenyl]-4,4'-dicarboxylic acid	H_2alkyneBPDC	0.1425
2-azido-[1,1'-biphenyl]-4,4'-dicarboxylic acid	H_2azideBPDC	0.1516
2-nitro-[1,1'-biphenyl]-4,4'-dicarboxylic acid	H_2nitroBPDC	0.1537

7.1.6. Synthesis of mixed-linker MIXDUT-5-functionality(x) (x=25, 50, 75)

0.54 mmol of the linker molecules (defined ratios of biphenyl-4,4'-dicarboxylic acid and functionalized biphenyl-4,4'-dicarboxylic acid, Table 24) were dissolved in 20 mL *N,N*-dimethylformamide (DMF) at 120 °C.

Table 24: Ratios and masses of linker molecules applied in the synthesis of MIXDUT-5 frameworks.

linker molecules	ratio	acronym	mass [g]
H_2BPDC : H_2amineBPDC	3 : 1	MIXDUT-5-amine(25)	0.0972 : 0.0344
H_2BPDC : H_2amineBPDC	1 : 1	MIXDUT-5-amine(50)	0.0648 : 0.0688
H_2BPDC : H_2amineBPDC	1 : 3	MIXDUT-5-amine(75)	0.0324 : 0.1032
H_2BPDC : H_2alkyneBPDC	3 : 1	MIXDUT-5-alkyne(25)	0.0972 : 0.0356
H_2BPDC : H_2alkyneBPDC	1 : 1	MIXDUT-5-alkyne(50)	0.0648 : 0.0712
H_2BPDC : H_2alkyneBPDC	1 : 3	MIXDUT-5-alkyne(75)	0.0324 : 0.1069
H_2BPDC : H_2nitroBPDC	1 : 1	MIXDUT-5-nitro(50)	0.0654 : 0.0776
H_2BPDC : H_2azideBPDC	1 : 1	MIXDUT-5-azide(50)	0.0648 : 0.0758
H_2BPDC : H_2amineBPDC : H_2alkyneBPDC	1 : 1 : 1	MIXDUT-5- amine(33)-alkyne(33)	0.0432 : 0.0459 : 0.0475

A solution of 0.2600 g (0.70 mmol) $Al(NO_3)_3*9H_2O$ in 5 mL DMF was added. The reaction mixture was stirred for 24 h under reflux at 120 °C. After filtration the metal-organic frameworks were washed with 3 x 25 mL of DMF and 1 x 25 mL of H_2O. The solid was dried overnight at room temperature and then for 3 days at 130 °C.

7.1.7. Post-synthetic modification of mixed-linker MIXDUT-5(50)

7.1.7.1. Synthesis of MIXDUT-5-amine(50)-Mal

0.3922 g maleic anhydride (4 mmol, 8 eq) were dissolved in 25 mL acetonitrile and 0.2917 g (1 mmol, 1 eq) of freshly dried MIXDUT-5-amine(50) were suspended in the solution. The reaction mixture was then heated under reflux to 80 °C for 24 h. After filtration the modified framework was washed with 4 x 20 mL acetonitrile, 1 x 20 mL DMF and 1 x 20 mL H_2O. The solid was dried overnight at room temperature and then for 3 days at 130 °C in air.

7.1.7.2. Synthesis of MIXDUT-5-amine(50)-Sal

1.2213 g salicylaldehyde (10 mmol, 20 eq) were dissolved in 25 mL toluene and 0.2917 g (1 mmol, 1 eq) of freshly dried MIXDUT-5-amine(50) were suspended in the solution. The reaction mixture was then heated under reflux to 100 °C for 72 h. After filtration the modified framework was washed with 5 x 25 mL toluene. The solid was dried overnight at room temperature and then for 3 days at 130 °C in air.

7.1.7.3. Synthesis of MIXDUT-5-amine(50)-Pyal

1.0711 g 2-pyridinecarboxaldehyde (10 mmol, 20 eq) were dissolved in 25 mL toluene and 0.2917 g (1 mmol, 1 eq) of freshly dried MIXDUT-5-amine(50) were suspended in the solution. The reaction mixture was then heated under reflux to 100 °C for 72 h. After filtration the modified framework was washed with 5 x 25 mL toluene. The solid was dried overnight at room temperature and then for 3 days at 130 °C in air.

7.1.7.4. Synthesis of MIXDUT-5-alkyne(50)-Pyaz

0.0505 g 2-pyridine azide (0.42 mmol), 0.0208 g $CuSO_4*5H_2O$ (0.08 mmol) and 0.0165 g sodium ascorbate (0.08 mmol) were dissolved in 20 mL DMF and 0.2962 g (1 mmol) of freshly dried MIXDUT-5-alkyne(50) were suspended in the solution. The reaction mixture was then kept at room temperature for 24 h. After filtration the modified framework was

washed with 1 x 10 mL DMF, 5 x 10 mL H_2O and 10 mL DCM. The solid was dried overnight at room temperature and then for 3 days at 130 °C in air.

7.1.8. Synthesis of CuBTC

1.1690 g $Cu(NO_3)_2*3H_2O$ (4.84 mmol) were dissolved in 25 mL H_2O at 100 °C. A solution of 0.4910 g benzene-1,3,5-tricarboxylic acid (H_3BTC, 2.34 mmol) in 25 mL *N,N*-dimethylformamide (DMF) was added and the reaction mixture was stirred under reflux for 24 h at 100 °C. After filtration the resulting material was washed with 5 x 25 mL DMF and 5 x 25 mL H_2O. The samples were dried overnight at room temperature and then for three days at 130 °C in air atmosphere.

7.1.9. Synthesis of CuRuBTC

0.9352 g $Cu(NO_3)_2*3H_2O$ (3.87 mmol) and 0.2580 g $RuCl_3*xH_2O$ (38 w% Ru, 0.97 mmol) were dissolved at 60 °C in 25 mL ethanol. A solution of 0.4910 g benzene-1,3,5-tricarboxylic acid (H_3BTC, 2.34 mmol) in 25 mL *N,N*-dimethylformamide (DMF) was added and the reaction mixture was stirred under reflux for 24 h at 60 °C. After filtration the resulting material was washed with 5 x 25 mL DMF and 5 x 25 mL ethanol. The samples were dried overnight at room temperature and then for three days at 130 °C in air atmosphere.

7.2. Methods

7.2.1. Powder X-ray diffraction (XRD)

Powder X-ray diffraction measurements were performed using a Bruker D8 Advance. The samples were analyzed in the range $2\Theta = 4 - 50°$ using Cu Kα radiation (1.54 Å). The step width was $2\Theta = 0.0164°$ with a dwell time of 2 s.

7.2.2. Nitrogen physisorption measurements

Prior to the nitrogen physisorption the samples were activated for 20 h at 130 °C in vacuum. Measurements were carried out using a Belsorp mini II from BEL Japan and a multi point method. The specific surface area was determined using the BET method (Brunauer, Emmett, Teller) and the BEL Master software. The micropore volume was determined using the t-plot method.

7.2.3. Attenuated total reflection infrared spectroscopy (ATR-IR)

IR data were acquired using a FT-IR spectrometer Vertex 70 from Bruker Optics equipped with a Golden Gate Single Reflection ATR sample cell from Specac and a liquid nitrogen cooled MCT detector. The data were collected from 4500 cm^{-1} to 600 cm^{-1} and the arithmetic average of 400 measurements was taken for each spectrum.

7.2.4. Thermogravimetric analysis (TG)

Differential thermal analysis/thermogravimetry (DTA/TG) was performed with a NETZSCH STA 409C applying α-Al_2O_3 as crucible material and reference sample. The samples were heated under air flow from room temperature to 1000 °C with a heating rate of 5 K/min.

7.2.5. Thermogravimetric analysis coupled with infrared spectroscopy (TG-IR)

Thermogravimetric analysis (TGA) coupled with FT-IR online gas analysis was performed using a NETZSCH STA 449 F3 connected to a BRUKER TensorII. The samples were heated in 10 % O_2/He (total gas flow: 50 mL/min) with 5 K/min from 50 °C to 1000 °C. FT-IR spectra were recorded during the temperature treatment using a BRUKER gas cell (TGA-IR) and a liquid nitrogen cooled MCT detector. Transfer line and gas cell were heated to 230 °C.

7.2.6. Nuclear magnetic resonance spectroscopy (NMR)

10 mg of the samples were digested in 0.5 mL NaOH/D_2O. Spectra were recorded on a Bruker Ascend 400 MHz NMR spectrometer. Chemical shifts were referenced to internal solvent resonances and are reported relative to tetramethylsilane.

7.2.7. Atomic absorption spectroscopy (AAS)

For AAS measurements a Z-6100 Polarized Zeeman atomic absorption spectrometer from Hitachi was used. The Pd-containing solid frameworks were digested in 7 mL aqua regia and diluted with 93 mL distilled water. The catalyst materials as well as the solutions of the hot filtration test were analyzed.

7.2.8. Inductively coupled plasma optical emission spectrometry (ICP-OES)

ICP-OES was carried out using an Agilent 725 and argon was used as carrier gas and to create the plasma. The sample was dissolved in 5 mL nitric acid, 3 mL hydrochloric acid and 0.5 mL hydrogen peroxide using a 600 W microwave oven from Anton Parr.

7.2.9. X-ray absorption spectroscopy (XAS)

7.2.9.1. MIL-53-NH_2(Al)-Mal-Pd

The XAS experiments were performed at HASYLAB (Hamburger Synchrotronstrahlungs-labor) using beamline X1 (energy range: 7 – 100 keV) at DORIS III (4.45 GeV, 120 mA current) at DESY (Deutsches Elektronen-Synchrotron) in Hamburg (Germany). For the measurement at the Pd K-edge (24350 eV) a Si(311) double-crystal monochromator was used. All spectra were recorded in transmission mode using boron nitride pellets at ambient temperature.

7.2.9.2. MIL-53-NH_2(x)-Mal-Pd (x=40, 60, 80)

XAS experiments were performed at the "Spline" beamline BM25A at ESRF (European Synchrotron Radiation Facility) in Grenoble (France). The measurements at the palladium K-edge (24350 eV) were carried out with a Si(311) double-crystal monochromator and a maximum synchrotron beam current of 200 mA and a ring energy of 6.0 GeV. Spectra of the undiluted powders placed between two Kapton® windows were recorded in fluorescence mode at ambient temperature.

7.2.9.3. Cu-Ru-BTC and Cu-BTC

XAS experiments were performed at the "Spline" beamline BM25A at the ESRF (European Synchrotron Radiation Facility) in Grenoble (France) and at the XAS beamline at ANKA (Angströmquelle Karlsruhe) in Karlsruhe (Germany). Two different double-crystal monochromators were used for the measurements at the copper K-edge (8979 eV) and at the Ru K-edge (22117 eV) (Si(111) and Si(311), respectively). The maximum beam current at both synchrotrons was 200 mA with a ring energy of 6.0 GeV at ESRF and 2.5 GeV at ANKA. The spectra at the copper K-edge were measured in fluorescence mode at ambient temperature using pellets with cellulose as a binder to avoid self-absorption effects. Due to the

low ruthenium concentration the spectrum at the Ru K-edge was recorded using an undiluted sample.

7.2.10. Gas chromatography (GC)

For GC measurements a GC-2010 Plus from Shimadzu with a non-polar column (Rxi®-5Sil MS, length: 30 m, diameter: 0.25 mm, film thickness: 0.25 µm) and a FID detector was used. 1 µL of the sample was injected and vaporized at 250 °C. The column was heated from 50 °C to 280 °C at a rate of 10 K/min.

7.3. Catalytic tests

7.3.1. Heck reaction of bromobenzene and styrene

In a typical experiment 10 mmol bromobenzene, 15 mmol styrene, 12 mmol sodium acetate and 2.3 mmol diethylen-glycol-dibutyl-ether as internal GC standard were dissolved in 10 mL *N*-methyl-2-pyrrolidone (NMP) in a sealed glass tube. 0.01 mol% of the catalyst (based on Pd in regard to bromobenzene) were suspended in the reaction mixture and the mixture was then heated to 140 °C for 3 h.
For the hot filtration test the catalyst was filled into a paper filter, which was removed from the reaction mixture after 0.5 h. The reaction was then resumed for another 2.5 h. Samples for GC analysis were taken after 0.5 h and (0.5 + 2.5) h.

7.3.2. Heck reaction of chlorobenzene and styrene

In a typical experiment 10 mmol chlorobenzene, 15 mmol styrene, 12 mmol potassium hydroxide, 6 mmol tetrabutylammonium bromide (TBAB) and 2.3 mmol diethylen-glycol-dibutyl-ether as internal GC standard were dissolved in 10 mL *N*-methyl-2-pyrrolidone (NMP) in a sealed glass tube. 0.01 mol% of the catalyst (based on Pd in regard to chlorobenzene) were suspended in the reaction mixture and the mixture was then heated to 160 °C for 6 h.

8. References

[1] G. Férey, *Chem. Mater.* **2001**, *13*, 3084-3098.

[2] C. Serre, F. Millange, C. Thouvenot, M. Noguès, G. Marsolier, D. Louër and G. Férey, *J. Am. Chem. Soc.* **2002**, *124*, 13519-13526.

[3] G. Ferey, *Chem. Soc. Rev.* **2008**, *37*, 191-214.

[4] G. Ferey and C. Serre, *Chem. Soc. Rev.* **2009**, *38*, 1380-1399.

[5] S. Kitagawa and M. Kondo, *Bull. Chem. Soc. Jpn.* **1998**, *71*, 1739-1753.

[6] S. Kitagawa, R. Kitaura and S.-i. Noro, *Angew. Chem. Int. Ed.* **2004**, *43*, 2334-2375.

[7] S. Bureekaew, S. Shimomura and S. Kitagawa, *Sci. Technol. Adv. Mater.* **2008**, *9*, 014108.

[8] H.-C. J. Zhou and S. Kitagawa, *Chem. Soc. Rev.* **2014**, *43*, 5415-5418.

[9] H. Li, C. E. Davis, T. L. Groy, D. G. Kelley and O. M. Yaghi, *J. Am. Chem. Soc.* **1998**, *120*, 2186-2187.

[10] H. Li, M. Eddaoudi, M. O'Keeffe and O. M. Yaghi, *Nature* **1999**, *402*, 276-279.

[11] J. L. C. Rowsell and O. M. Yaghi, *Microporous Mesoporous Mater.* **2004**, *73*, 3-14.

[12] H. Furukawa, K. E. Cordova, M. O'Keeffe and O. M. Yaghi, *Science* **2013**, *341*.

[13] G. Ferey, C. Mellot-Draznieks, C. Serre, F. Millange, J. Dutour, S. Surble and I. Margiolaki, *Science* **2005**, *309*, 2040-2042.

[14] H. Furukawa, N. Ko, Y. B. Go, N. Aratani, S. B. Choi, E. Choi, A. Ö. Yazaydin, R. Q. Snurr, M. O'Keeffe, J. Kim and O. M. Yaghi, *Science* **2010**, *329*, 424-428.

[15] O. K. Farha, I. Eryazici, N. C. Jeong, B. G. Hauser, C. E. Wilmer, A. A. Sarjeant, R. Q. Snurr, S. T. Nguyen, A. Ö. Yazaydın and J. T. Hupp, *J. Am. Chem. Soc.* **2012**, *134*, 15016-15021.

[16] U. Müller, M. Schubert, F. Teich, H. Puetter, K. Schierle-Arndt and J. Pastre, *J. Mater. Chem.* **2006**, *16*, 626-636.

[17] A. U. Czaja, N. Trukhan and U. Müller, *Chem. Soc. Rev.* **2009**, *38*, 1284-1293.

[18] C. Janiak and J. K. Vieth, *New J. Chem.* **2010**, *34*, 2366-2388.

[19] M. Eddaoudi, J. Kim, N. Rosi, D. Vodak, J. Wachter, M. O'Keeffe and O. M. Yaghi, *Science* **2002**, *295*, 469-472.

[20] J. L. C. Rowsell, A. R. Millward, K. S. Park and O. M. Yaghi, *J. Am. Chem. Soc.* **2004**, *126*, 5666-5667.

[21] S. Bourrelly, P. L. Llewellyn, C. Serre, F. Millange, T. Loiseau and G. Férey, *J. Am. Chem. Soc.* **2005**, *127*, 13519-13521.

[22] J. L. C. Rowsell and O. M. Yaghi, *Angew. Chem. Int. Ed.* **2005**, *44*, 4670-4679.

[23] L. J. Murray, M. Dinca and J. R. Long, *Chem. Soc. Rev.* **2009**, *38*, 1294-1314.

[24] S. Couck, T. Remy, G. V. Baron, J. Gascon, F. Kapteijn and J. F. M. Denayer, *Phys. Chem. Chem. Phys.* **2010**, *12*, 9413-9418.

[25] S. Couck, E. Gobechiya, C. E. A. Kirschhock, P. Serra-Crespo, J. Juan-Alcañiz, A. Martinez Joaristi, E. Stavitski, J. Gascon, F. Kapteijn, G. V. Baron and J. F. M. Denayer, *ChemSusChem* **2012**, *5*, 740-750.

[26] E. Borfecchia, S. Maurelli, D. Gianolio, E. Groppo, M. Chiesa, F. Bonino and C. Lamberti, *J. Phys. Chem. C* **2012**, *116*, 19839-19850.

[27] L. Alaerts, C. E. A. Kirschhock, M. Maes, M. A. van der Veen, V. Finsy, A. Depla, J. A. Martens, G. V. Baron, P. A. Jacobs, J. F. M. Denayer and D. E. De Vos, *Angew. Chem. Int. Ed.* **2007**, *46*, 4293-4297.

[28] D. Britt, D. Tranchemontagne and O. M. Yaghi, *Proc. Natl. Acad. Sci. USA* **2008**, *105*, 11623-11627.

[29] J.-R. Li, R. J. Kuppler and H.-C. Zhou, *Chem. Soc. Rev.* **2009**, *38*, 1477-1504.

[30] M. G. Plaza, A. F. P. Ferreira, J. C. Santos, A. M. Ribeiro, U. Müller, N. Trukhan, J. M. Loureiro and A. E. Rodrigues, *Microporous Mesoporous Mater.* **2012**, *157*, 101-111.

[31] T. Borjigin, F. Sun, J. Zhang, K. Cai, H. Ren and G. Zhu, *Chem. Commun.* **2012**, *48*, 7613-7615.

[32] Z. R. Herm, E. D. Bloch and J. R. Long, *Chem. Mater.* **2013**, *26*, 323-338.

[33] L. E. Kreno, K. Leong, O. K. Farha, M. Allendorf, R. P. Van Duyne and J. T. Hupp, *Catal. Rev.* **2012**, *112*, 1105-1125.

[34] D. Liu, K. Lu, C. Poon and W. Lin, *Inorg. Chem.* **2014**, *53*, 1916-1924.

[35] L. Heinke, M. Tu, S. Wannapaiboon, R. A. Fischer and C. Wöll, *Microporous Mesoporous Mater.* **2015**, *216*, 200-215.

[36] K. Müller-Buschbaum, F. Beuerle and C. Feldmann, *Microporous Mesoporous Mater.* **2015**, *216*, 171-199.

[37] P. Serra-Crespo, M. A. van der Veen, E. Gobechiya, K. Houthoofd, Y. Filinchuk, C. E. A. Kirschhock, J. A. Martens, B. F. Sels, D. E. De Vos, F. Kapteijn and J. Gascon, *J. Am. Chem. Soc.* **2012**, *134*, 8314-8317.

[38] K. M. L. Taylor-Pashow, J. D. Rocca, Z. Xie, S. Tran and W. Lin, *J. Am. Chem. Soc.* **2009**, *131*, 14261-14263.

[39] M. C. Bernini, D. Fairen-Jimenez, M. Pasinetti, A. J. Ramirez-Pastor and R. Q. Snurr, *J. Mater. Chem. B* **2014**, *2*, 766-774.

[40] S. Nagata, K. Kokado and K. Sada, *Chem. Commun.* **2015**, *51*, 8614-8617.

[41] S. Bauer and N. Stock, *Chem. Unserer Zeit* **2007**, *41*, 390-398.

[42] S. Bauer, C. Serre, T. Devic, P. Horcajada, J. Marrot, G. Férey and N. Stock, *Inorg. Chem.* **2008**, *47*, 7568-7576.

[43] M. Lammert, S. Bernt, F. Vermoortele, D. E. De Vos and N. Stock, *Inorg. Chem.* **2013**, *52*, 8521-8528.

[44] Z. Ni and R. I. Masel, *J. Am. Chem. Soc.* **2006**, *128*, 12394-12395.

[45] N. A. Khan, E. Haque and S. H. Jhung, *Phys. Chem. Chem. Phys.* **2010**, *11*, 2625-2631.

[46] O. Kozachuk, K. Yusenko, H. Noei, Y. Wang, S. Walleck, T. Glaser and R. A. Fischer, *Chem. Commun.* **2011**, *47*, 8509-8511.

[47] Z. Wang, J. Liu, H. K. Arslan, S. Grosjean, T. Hagendorn, H. Gliemann, S. Bräse and C. Wöll, *Langmuir* **2013**, *29*, 15958-15964.

[48] C.-T. Chen and K. S. Suslick, *Coord. Chem. Rev.* **1993**, *128*, 293-322.

[49] N. R. Champness and M. Schröder, *Curr. Opin. Solid State Mater. Sci.* **1998**, *3*, 419-424.

[50] R. Robson, *J. Chem. Soc., Dalton Trans.: Inorg. Chem.* **2000**, 3735-3744.

[51] T. Loiseau, C. Serre, C. Huguenard, G. Fink, F. Taulelle, M. Henry, T. Bataille and G. Ferey, *Chem. Eur. J.* **2004**, *10*, 1373-1382.

[52] I. Senkovska, F. Hoffmann, M. Fröba, J. Getzschmann, W. Böhlmann and S. Kaskel, *Microporous Mesoporous Mater.* **2009**, *122*, 93-98.
[53] S. S. Y. Chui, S. M. F. Lo, J. P. H. Charmant, A. G. Orpen and I. D. Williams, *Science* **1999**, *283*, 1148-1150.
[54] J. R. Long and O. M. Yaghi, *Chem. Soc. Rev.* **2009**, *38*, 1213-1214.
[55] D. J. Tranchmontagne, Z. Ni, M. O'Keeffe and O. M. Yaghi, *Angew. Chem. Int. Ed.* **2008**, *47*.
[56] T. Ahnfeldt, D. Gunzelmann, T. Loiseau, D. Hirsemann, J. Senker, G. Ferey and N. Stock, *Inorg. Chem.* **2009**, *48*, 3057-3064.
[57] S. Biswas, T. Ahnfeldt and N. Stock, *Inorg. Chem.* **2010**, *50*, 9518-9526.
[58] V. Guillerm, F. Ragon, M. Dan-Hardi, T. Devic, M. Vishnuvarthan, B. Campo, A. Vimont, G. Clet, Q. Yang, G. Maurin, G. Férey, A. Vittadini, S. Gross and C. Serre, *Angew. Chem. Int. Ed.* **2012**, *51*, 9267-9271.
[59] J. A. Groves, S. R. Miller, S. J. Warrender, C. Mellot-Draznieks, P. Lightfoot and P. A. Wright, *Chem. Commun.* **2006**, 3305-3307.
[60] M. T. Wharmby, J. P. S. Mowat, S. P. Thompson and P. A. Wright, *J. Am. Chem. Soc.* **2011**, *133*, 1266-1269.
[61] M. Kim, J. A. Boissonnault, C. A. Allen, P. V. Dau and S. M. Cohen, *Dalton Trans.* **2012**, *41*, 6277-6282.
[62] S. E. Wenzel, M. Fischer, F. Hoffmann and M. Fröba, *J. Mater. Chem.* **2012**, *22*, 10294-10302.
[63] K. Peikert, F. Hoffmann and M. Fröba, *Chem. Commun.* **2012**, *48*, 11196-11198.
[64] Y. Cai, A. R. Kulkarni, Y.-G. Huang, D. S. Sholl and K. S. Walton, *Cryst. Growth Des.* **2014**, *14*, 6122-6128.
[65] K. Peikert, F. Hoffmann and M. Froba, *CrystEngComm* **2015**, *17*, 353-360.
[66] F. Millange, C. Serre and G. Ferey, *Chem. Commun.* **2002**, 822-823.
[67] C. Serre, S. Bourrelly, A. Vimont, N. A. Ramsahye, G. Maurin, P. L. Llewellyn, M. Daturi, Y. Filinchuk, O. Leynaud, P. Barnes and G. Férey, *Adv. Mater.* **2007**, *19*, 2246-2251.
[68] A. Boutin, M.-A. Springuel-Huet, A. Nossov, A. Gédéon, T. Loiseau, C. Volkringer, G. Férey, F.-X. Coudert and A. H. Fuchs, *Angew. Chem. Int. Ed.* **2009**, *48*, 8314-8317.
[69] A. Boutin, S. Couck, F.-X. Coudert, P. Serra-Crespo, J. Gascon, F. Kapteijn, A. H. Fuchs and J. F. M. Denayer, *Microporous Mesoporous Mater.* **2011**, *140*, 108-113.
[70] M. Pera-Titus, T. Lescouet, S. Aguado and D. Farrusseng, *J. Phys. Chem. C* **2012**, *116*, 9507-9516.
[71] N. Reimer, B. Gil, B. Marszalek and N. Stock, *CrystEngComm* **2012**, *14*, 4119-4125.
[72] T. Lescouet, E. Kockrick, G. Bergeret, M. Pera-Titus and D. Farrusseng, *Dalton Trans.* **2011**, *40*, 11359-11361.
[73] J. P. S. Mowat, V. R. Seymour, J. M. Griffin, S. P. Thompson, A. M. Z. Slawin, D. Fairen-Jimenez, T. Duren, S. E. Ashbrook and P. A. Wright, *Dalton Trans.* **2012**, *41*, 3937-3941.
[74] T. R. Whitfield, X. Wang, L. Liu and A. J. Jacobson, *Solid State Sci.* **2005**, *7*, 1096-1103.
[75] C. Volkringer, T. Loiseau, N. Guillou, G. Ferey, E. Elkaim and A. Vimont, *Dalton Trans.* **2009**, 2241-2249.

[76] E. Stavitski, E. A. Pidko, S. Couck, T. Remy, E. J. M. Hensen, B. M. Weckhuysen, J. Denayer, J. Gascon and F. Kapteijn, *Langmuir* **2011**, *27*, 3970-3976.
[77] M. Maes, F. Vermoortele, M. Boulhout, T. Boudewijns, C. Kirschhock, R. Ameloot, I. Beurroies, R. Denoyel and D. E. De Vos, *Microporous Mesoporous Mater.* **2012**, *157*, 82-88.
[78] L. Alaerts, M. Maes, L. Giebeler, P. A. Jacobs, J. A. Martens, J. F. M. Denayer, C. E. A. Kirschhock and D. E. De Vos, *J. Am. Chem. Soc.* **2008**, *130*, 14170-14178.
[79] S. Couck, J. F. M. Denayer, G. V. Baron, T. Rémy, J. Gascon and F. Kapteijn, *J. Am. Chem. Soc.* **2009**, *131*, 6326-6327.
[80] M. G. Goesten, J. Juan-Alcañiz, E. V. Ramos-Fernandez, K. B. Sai Sankar Gupta, E. Stavitski, H. van Bekkum, J. Gascon and F. Kapteijn, *J. Catal.* **2011**, *281*, 177-187.
[81] M. G. Goesten, K. B. Sai Sankar Gupta, E. V. Ramos-Fernandez, H. Khajavi, J. Gascon and F. Kapteijn, *CrystEngComm* **2012**, *14*, 4109-4111.
[82] J. Gascon, U. Akray, M. D. Hernandez-Alonso, G. P. M. van Klink and F. Kapteijn, *J. Catal.* **2009**, *261*, 75-87.
[83] S. Couck, Y.-Y. Liu, K. Leus, G. V. Baron, P. Van der Voort and J. F. M. Denayer, *Microporous Mesoporous Mater.* **2015**, *206*, 217-225.
[84] S. Halis, N. Reimer, A. Klinkebiel, U. Lüning and N. Stock, *Microporous Mesoporous Mater.* **2015**, *216*, 13-19.
[85] J. H. Cavka, S. Jakobsen, U. Olsbye, N. Guillou, C. Lamberti, S. Bordiga and K. P. Lillerud, *J. Am. Chem. Soc.* **2008**, *130*, 13850-13851.
[86] S. Chavan, J. G. Vitillo, D. Gianolio, O. Zavorotynska, B. Civalleri, S. Jakobsen, M. H. Nilsen, L. Valenzano, C. Lamberti, K. P. Lillerud and S. Bordiga, *Phys. Chem. Chem. Phys.* **2012**, *14*, 1614-1626.
[87] L. Chen, S. Rangan, J. Li, H. Jiang and Y. Li, *Green Chem.* **2014**, *16*, 3978-3985.
[88] H. Fei and S. M. Cohen, *Chem. Commun.* **2014**, *50*, 4810-4812.
[89] S. J. Garibay and S. M. Cohen, *Chem. Commun.* **2010**, *46*, 7700-7702.
[90] J. Kim, S.-N. Kim, H.-G. Jang, G. Seo and W.-S. Ahn, *Appl. Catal. A* **2013**, *453*, 175-180.
[91] X.-C. Yi, F.-G. Xi, Y. Qi and E.-Q. Gao, *RSC Adv.* **2015**, *5*, 893-900.
[92] N. Ko, J. Hong, S. Sung, K. E. Cordova, H. J. Park, J. K. Yang and J. Kim, *Dalton Trans.* **2015**.
[93] D. J. Tranchemontagne, J. R. Hunt and O. M. Yaghi, *Tetrahedron* **2008**, *64*, 8553-8557.
[94] J. Song, Z. Luo, D. K. Britt, H. Furukawa, O. M. Yaghi, K. I. Hardcastle and C. L. Hill, *J. Am. Chem. Soc.* **2011**, *133*, 16839-16846.
[95] L. T. L. Nguyen, T. T. Nguyen, K. D. Nguyen and N. T. S. Phan, *Appl. Catal. A* **2012**, *425–426*, 44-52.
[96] A. F. P. Ferreira, J. C. Santos, M. G. Plaza, N. Lamia, J. M. Loureiro and A. E. Rodrigues, *Chem. Eng. J.* **2011**, *167*, 1-12.
[97] S. Marx, W. Kleist and A. Baiker, *J. Catal.* **2011**, *281*, 76-87.
[98] K.-J. Kim, Y. J. Li, P. B. Kreider, C.-H. Chang, N. Wannenmacher, P. K. Thallapally and H.-G. Ahn, *Chem. Commun.* **2013**, *49*, 11518-11520.
[99] S. Khoshhal, A. A. Ghoreyshi, M. Jahanshahi and M. Mohammadi, *RSC Adv.* **2015**, *5*, 24758-24768.

[100] K. Schlichte, T. Kratzke and S. Kaskel, *Microporous Mesoporous Mater.* **2004**, *73*, 81-88.
[101] L. Alaerts, E. Séguin, H. Poelman, F. Thibault-Starzyk, P. A. Jacobs and D. E. De Vos, *Chem. Eur. J.* **2006**, *12*, 7353-7363.
[102] E. Pérez-Mayoral and J. Čejka, *ChemCatChem* **2011**, *3*, 157-159.
[103] L. H. Wee, M. R. Lohe, N. Janssens, S. Kaskel and J. A. Martens, *J. Mater. Chem.* **2012**, *22*, 13742-13746.
[104] P. Chowdhury, C. Bikkina, D. Meister, F. Dreisbach and S. Gumma, *Microporous Mesoporous Mater.* **2009**, *117*, 406-413.
[105] G. Majano and J. Pérez-Ramírez, *Helv. Chim. Acta* **2012**, *95*, 2278-2286.
[106] E. S. Sanil, K.-H. Cho, S.-K. Lee, U. H. Lee, S. Ryu, H. Lee, J.-S. Chang and Y. Hwang, *J. Porous Mater.* **2015**, *22*, 171-178.
[107] C. R. Wade and M. Dinca, *Dalton Trans.* **2012**, *41*, 7931-7938.
[108] X. Yan, S. Komarneni, Z. Zhang and Z. Yan, *Microporous Mesoporous Mater.* **2014**, *183*, 69-73.
[109] L. Mitchell, B. Gonzalez-Santiago, J. P. S. Mowat, M. E. Gunn, P. Williamson, N. Acerbi, M. L. Clarke and P. A. Wright, *Catal. Sci. Technol.* **2013**, *3*, 606-617.
[110] A. Arnanz, M. Pintado-Sierra, A. Corma, M. Iglesias and F. Sánchez, *Adv. Synth. Catal.* **2012**, *354*, 1347-1355.
[111] S. Abednatanzi, A. Abbasi and M. Masteri-Farahani, *J. Mol. Catal. A: Chem.* **2015**, *399*, 10-17.
[112] L. J. Murray, M. Dinca, J. Yano, S. Chavan, S. Bordiga, C. M. Brown and J. R. Long, *J. Am. Chem. Soc.* **2010**, *132*, 7856-7857.
[113] L. Xie, S. Liu, C. Gao, R. Cao, J. Cao, C. Sun and Z. Su, *Inorg. Chem.* **2007**, *46*, 7782-7788.
[114] P. Maniam and N. Stock, *Inorg. Chem.* **2011**, *50*, 5085-5097.
[115] L.-G. Qiu, Z.-Q. Li, Y. Wu, W. Wang, T. Xu and X. Jiang, *Chem. Commun.* **2008**, 3642-3644.
[116] J. I. Feldblyum, M. Liu, D. W. Gidley and A. J. Matzger, *J. Am. Chem. Soc.* **2011**, *133*, 18257-18263.
[117] M. Kramer, U. Schwarz and S. Kaskel, *J. Mater. Chem.* **2006**, *16*, 2245-2248.
[118] A. D. Burrows, *CrystEngComm* **2011**, *13*, 3623-3642.
[119] H. Furukawa, U. Müller and O. M. Yaghi, *Angew. Chem. Int. Ed.* **2015**, *54*, 3417-3430.
[120] S. Furukawa, K. Hirai, Y. Takashima, K. Nakagawa, M. Kondo, T. Tsuruoka, O. Sakata and S. Kitagawa, *Chem. Commun.* **2009**, 5097-5099.
[121] S. Furukawa, K. Hirai, K. Nakagawa, Y. Takashima, R. Matsuda, T. Tsuruoka, M. Kondo, R. Haruki, D. Tanaka, H. Sakamoto, S. Shimomura, O. Sakata and S. Kitagawa, *Angew. Chem. Int. Ed.* **2009**, *48*, 1766-1770.
[122] K. Koh, A. G. Wong-Foy and A. J. Matzger, *Chem. Commun.* **2009**, 6162-6164.
[123] Y. Yoo and H.-K. Jeong, *Cryst. Growth Des.* **2010**, *10*, 1283-1288.
[124] Y. Wei, S. Han, D. A. Walker, P. E. Fuller and B. A. Grzybowski, *Angew. Chem. Int. Ed.* **2012**, *51*, 7435-7439.
[125] L. Wang, W. Yang, Y. Li, Z. Xie, W. Zhu and Z.-M. Sun, *Chem. Commun.* **2014**, *50*, 11653-11656.

[126] H. Deng, C. J. Doonan, H. Furukawa, R. B. Ferreira, J. Towne, C. B. Knobler, B. Wang and O. M. Yaghi, *Science* **2010**, *327*, 846-850.
[127] A. D. Burrows, C. G. Frost, M. F. Mahon and C. Richardson, *Angew. Chem. Int. Ed.* **2008**, *47*, 8482-8486.
[128] W. Kleist, F. Jutz, M. Maciejewski and A. Baiker, *Eur. J. Inorg. Chem.* **2009**, 3552-3561.
[129] D. N. Bunck and W. R. Dichtel, *Chem. Eur. J.* **2013**, *19*, 818-827.
[130] W. Kleist, M. Maciejewski and A. Baiker, *Thermochim. Acta* **2010**, *499*, 71-78.
[131] M. Ranocchiari, C. Lothschütz, D. Grolimund and J. A. van Bokhoven, *Proc. R. Soc. A* **2012**, *468*, 1985-1999.
[132] S. Marx, W. Kleist, J. Huang, M. Maciejewski and A. Baiker, *Dalton Trans.* **2010**, *39*, 3795-3798.
[133] Y. Jiang, J. Huang, S. Marx, W. Kleist, M. Hunger and A. Baiker, *J. Phys. Chem. Lett.* **2010**, *1*, 2886-2890.
[134] Y. Jiang, J. Huang, S. Marx, W. Kleist, M. Hunger and A. Baiker, *J. Phys. Chem. Lett.* **2010**, *1*, 2886-2890.
[135] T. Lescouet, E. Kockrick, G. Bergeret, M. Pera-Titus, S. Aguado and D. Farrusseng, *J. Mater. Chem.* **2012**, *22*, 10287-10293.
[136] M. Kim, J. F. Cahill, K. A. Prather and S. M. Cohen, *Chem. Commun.* **2011**, *47*, 7629-7631.
[137] O. Kozachuk, I. Luz, F. X. Llabres i Xamena, H. Noei, M. Kauer, H. B. Albada, E. D. Bloch, B. Marler, Y. Wang, M. Muhler and R. A. Fischer, *Angew. Chem. Int. Ed.* **2014**, *53*, 7058-7062.
[138] J. A. Botas, G. Calleja, M. Sánchez-Sánchez and M. G. Orcajo, *Langmuir* **2010**, *26*, 5300-5303.
[139] C. Serre, F. Millange, C. Thouvenot, N. Gardant, F. Pelle and G. Ferey, *J. Mater. Chem.* **2004**, *14*, 1540-1543.
[140] F. Gul-E-Noor, B. Jee, M. Mendt, D. Himsl, A. Pöppl, M. Hartmann, J. Haase, H. Krautscheid and M. Bertmer, *J. Phys. Chem. C* **2012**, *116*, 20866-20873.
[141] B. Jee, M. Hartmann and A. Poeppl, *Mol. Phys.* **2013**, *111*, 2950-2966.
[142] B. Jee, P. S. Petkov, G. N. Vayssilov, T. Heine, M. Hartmann and A. Poeppl, *J. Phys. Chem. C* **2013**, *117*, 8231-8240.
[143] D. F. Sava Gallis, M. V. Parkes, J. A. Greathouse, X. Zhang and T. M. Nenoff, *Chem. Mater.* **2015**, *27*, 2018-2025.
[144] Z. Wang and S. M. Cohen, *J. Am. Chem. Soc.* **2007**, *129*, 12368-12369.
[145] K. K. Tanabe, Z. Wang and S. M. Cohen, *J. Am. Chem. Soc.* **2008**, *130*, 8508-8517.
[146] S. J. Garibay, Z. Wang, K. K. Tanabe and S. M. Cohen, *Inorg. Chem.* **2009**, *48*, 7341-7349.
[147] K. K. Tanabe and S. M. Cohen, *Chem. Soc. Rev.* **2011**, *40*, 498-519.
[148] Z. Wang and S. M. Cohen, *Chem. Soc. Rev.* **2009**, *38*, 1315-1329.
[149] S. M. Cohen, *Nature* **2009**, *461*, 602-603.
[150] A. D. Burrows and S. M. Cohen, *CrystEngComm* **2012**, *14*, 4095-4095.
[151] S. M. Cohen, *Catal. Rev.* **2012**, *112*, 970-1000.
[152] C. J. Doonan, W. Morris, H. Furukawa and O. M. Yaghi, *J. Am. Chem. Soc.* **2009**, *131*, 9492-9493.

[153] J. S. Costa, P. Gamez, C. A. Black, O. Roubeau, S. J. Teat and J. Reedijk, *Eur. J. Inorg. Chem.* **2008**, *2008*, 1551-1554.
[154] Y.-F. Song and L. Cronin, *Angew. Chem. Int. Ed.* **2008**, *47*, 4635-4637.
[155] M. Savonnet, D. Bazer-Bachi, N. Bats, J. Perez-Pellitero, E. Jeanneau, V. Lecocq, C. Pinel and D. Farrusseng, *J. Am. Chem. Soc.* **2010**, *132*, 4518-4519.
[156] S. Bhattacharjee, D.-A. Yang and W.-S. Ahn, *Chem. Commun.* **2011**, *47*, 3637-3639.
[157] T. Ahnfeldt, D. Gunzelmann, J. Wack, J. Senker and N. Stock, *CrystEngComm* **2012**, *14*, 4126-4136.
[158] A. D. Burrows and L. L. Keenan, *CrystEngComm* **2012**, *14*, 4112-4114.
[159] T. Lescouet, J. G. Vitillo, S. Bordiga, J. Canivet and D. Farrusseng, *Dalton Trans.* **2013**, *42*, 8249-8258.
[160] Z. Wang and S. M. Cohen, *Angew. Chem. Int. Ed.* **2008**, *47*, 4699-4702.
[161] Z. Wang, K. K. Tanabe and S. M. Cohen, *Inorg. Chem.* **2009**, *48*, 296-306.
[162] K. K. Tanabe and S. M. Cohen, *Angew. Chem. Int. Ed.* **2009**, *48*, 7424-7427.
[163] S. J. Garibay, Z. Wang and S. M. Cohen, *Inorg. Chem.* **2010**, *49*, 8086-8091.
[164] E. Dugan, Z. Wang, M. Okamura, A. Medina and S. M. Cohen, *Chem. Commun.* **2008**, *29*, 3366-3368.
[165] C. Volkringer and S. M. Cohen, *Angew. Chem. Int. Ed.* **2010**, *49*, 4644-4648.
[166] W. Zhu, C. He, P. Wu, X. Wu and C. Duan, *Dalton Trans.* **2012**, *41*, 3072-3077.
[167] M. Savonnet, A. Camarata, J. Canivet, D. Bazer-Bachi, N. Bats, V. Lecocq, C. Pinel and D. Farrusseng, *Dalton Trans.* **2012**, *41*, 3945-3948.
[168] C. Liu, T. Li and N. L. Rosi, *J. Am. Chem. Soc.* **2012**, *134*, 18886-18888.
[169] J. D. Evans, C. J. Sumby and C. J. Doonan, *Chem. Soc. Rev.* **2014**, *43*, 5933-5951.
[170] B. Liu, S. Jie, Z. Bu and B.-G. Li, *J. Mol. Catal. A: Chem.* **2014**, *387*, 63-68.
[171] K. Leus, G. Vanhaelewyn, T. Bogaerts, Y.-Y. Liu, D. Esquivel, F. Callens, G. B. Marin, V. Van Speybroeck, H. Vrielinck and P. Van Der Voort, *Catal. Today* **2013**, *208*, 97-105.
[172] E. D. Bloch, D. Britt, C. Lee, C. J. Doonan, F. J. Uribe-Romo, H. Furukawa, J. R. Long and O. M. Yaghi, *J. Am. Chem. Soc.* **2010**, *132*, 14382-14384.
[173] F. Carson, S. Agrawal, M. Gustafsson, A. Bartoszewicz, F. Moraga, X. Zou and B. Martín-Matute, *Chem. Eur. J.* **2012**, *18*, 15337-15344.
[174] K. Leus, Y.-Y. Liu, M. Meledina, S. Turner, G. Van Tendeloo and P. Van Der Voort, *J. Catal.* **2014**, *316*, 201-209.
[175] S.-N. Kim, S.-T. Yang, J. Kim, J.-E. Park and W.-S. Ahn, *CrystEngComm* **2012**, *14*, 4142-4147.
[176] D. Farrusseng, S. Aguado and C. Pinel, *Angew. Chem. Int. Ed.* **2009**, *48*, 7502-7513.
[177] A. Corma, H. Garcia and F. X. Llabres i Xamena, *Chem. Rev.* **2010**, *110*, 4606-4655.
[178] M. Yoon, R. Srirambalaji and K. Kim, *Catal. Rev.* **2011**, *112*, 1196-1231.
[179] M. Ranocchiari and J. A. van Bokhoven, *Phys. Chem. Chem. Phys.* **2011**, *13*, 6388-6396.
[180] A. Dhakshinamoorthy, M. Alvaro and H. Garcia, *Chem. Commun.* **2012**, *48*, 11275-11288.
[181] J. Gascon, A. Corma, F. Kapteijn and F. X. Llabrés i Xamena, *ACS Catal.* **2013**, *4*, 361-378.

[182] A. Dhakshinamoorthy, M. Opanasenko, J. Čejka and H. Garcia, *Adv. Synth. Catal.* **2013**, *355*, 247-268.
[183] A. Dhakshinamoorthy, M. Opanasenko, J. Cejka and H. Garcia, *Catal. Sci. Technol.* **2013**, *3*, 2509-2540.
[184] K. Leus, Y.-Y. Liu and P. Van Der Voort, *Catal. Rev.* **2014**, *56*, 1-56.
[185] J. Liu, L. Chen, H. Cui, J. Zhang, L. Zhang and C.-Y. Su, *Chem. Soc. Rev.* **2014**, *43*, 6011-6061.
[186] A. Dhakshinamoorthy, A. M. Asiri and H. Garcia, *Chem. Commun.* **2014**.
[187] S. Proch, J. Herrmannsdörfer, R. Kempe, C. Kern, A. Jess, L. Seyfarth and J. Senker, *Chem. Eur. J.* **2008**, *14*, 8204-8212.
[188] M. Meilikhov, K. Yusenko, D. Esken, S. Turner, G. Van Tendeloo and R. A. Fischer, *Eur. J. Inorg. Chem.* **2010**, *2010*, 3701-3714.
[189] S. Gao, N. Zhao, M. Shu and S. Che, *Appl. Catal. A* **2010**, *388*, 196-201.
[190] M. Müller, S. Turner, O. I. Lebedev, Y. Wang, G. van Tendeloo and R. A. Fischer, *Eur. J. Inorg. Chem.* **2011**, *2011*, 1876-1887.
[191] Y. Huang, Z. Zheng, T. Liu, J. Lü, Z. Lin, H. Li and R. Cao, *Catal. Commun.* **2011**, *14*, 27-31.
[192] J. Hermannsdörfer and R. Kempe, *Chem. Eur. J.* **2011**, *17*, 8071-8077.
[193] Y. Huang, S. Gao, T. Liu, J. Lü, X. Lin, H. Li and R. Cao, *ChemPlusChem* **2012**, *77*, 106-112.
[194] A. Dhakshinamoorthy and H. Garcia, *Chem. Soc. Rev.* **2012**, *41*, 5262-5284.
[195] F. G. Cirujano, F. X. Llabres i Xamena and A. Corma, *Dalton Trans.* **2012**, *41*, 4249-4254.
[196] V. I. Isaeva, O. P. Tkachenko, E. V. Afonina, L. M. Kozlova, G. I. Kapustin, W. Grünert, S. E. Solov'eva, I. S. Antipin and L. M. Kustov, *Microporous Mesoporous Mater.* **2013**, *166*, 167-175.
[197] H. R. Moon, D.-W. Lim and M. P. Suh, *Chem. Soc. Rev.* **2013**, *42*, 1807-1824.
[198] Z. Fang, J. P. Durholt, M. Kauer, W. Zhang, C. Lochenie, B. Jee, B. Albada, N. Metzler-Nolte, A. Poppl, B. Weber, M. Muhler, Y. Wang, R. Schmid and R. A. Fischer, *J. Am. Chem. Soc.* **2014**, *136*, 9627-9636.
[199] S.-H. Cho, B. Ma, S. T. Nguyen, J. T. Hupp and T. E. Albrecht-Schmitt, *Chem. Commun.* **2006**, 2563-2565.
[200] S.-H. Cho, T. Gadzikwa, M. Afshari, S. T. Nguyen and J. T. Hupp, *Eur. J. Inorg. Chem.* **2007**, *2007*, 4863-4867.
[201] F. Song, C. Wang, J. M. Falkowski, L. Ma and W. Lin, *J. Am. Chem. Soc.* **2010**, *132*, 15390-15398.
[202] G. A. E. Oxford, D. Dubbeldam, L. J. Broadbelt and R. Q. Snurr, *J. Mol. Catal. A: Chem.* **2011**, *334*, 89-97.
[203] A. Bhunia, M. A. Gotthardt, M. Yadav, M. T. Gamer, A. Eichhöfer, W. Kleist and P. W. Roesky, *Chem. Eur. J.* **2013**, *19*, 1986-1995.
[204] K. S. Suslick, P. Bhyrappa, J.-H. Chou, M. E. Kosal, S. Nakagaki, D. W. Smithenry and S. R. Wilson, *Acc. Chem. Res.* **2005**, *38*, 283-291.
[205] A. Fateeva, P. A. Chater, C. P. Ireland, A. A. Tahir, Y. Z. Khimyak, P. V. Wiper, J. R. Darwent and M. J. Rosseinsky, *Angew. Chem. Int. Ed.* **2012**, *51*, 7440-7444.

[206] C. Zou, T. Zhang, M.-H. Xie, L. Yan, G.-Q. Kong, X.-L. Yang, A. Ma and C.-D. Wu, *Inorg. Chem.* **2013**, *52*, 3620-3626.
[207] X.-L. Yang, C. Zou, Y. He, M. Zhao, B. Chen, S. Xiang, M. O'Keeffe and C.-D. Wu, *Chem. Eur. J.* **2014**, *20*, 1447-1452.
[208] E. N. Jacobsen, W. Zhang and M. L. Guler, *J. Am. Chem. Soc.* **1991**, *113*, 6703-6704.
[209] E. N. Jacobsen, W. Zhang, A. R. Muci, J. R. Ecker and L. Deng, *J. Am. Chem. Soc.* **1991**, *113*, 7063-7064.
[210] J. Gascon, U. Aktay, M. D. Hernandez-Alonso, G. P. M. van Klink and F. Kapteijn, *J. Catal.* **2009**, *261*, 75-87.
[211] M. Hartmann and M. Fischer, *Microporous Mesoporous Mater.* **2012**, *164*, 38-43.
[212] F. X. Llabrés i Xamena, F. G. Cirujano and A. Corma, *Microporous Mesoporous Mater.* **2012**, *157*, 112-117.
[213] A. R. Burgoyne and R. Meijboom, *Catal. Lett.* **2013**.
[214] M. Opanasenko, A. Dhakshinamoorthy, M. Shamzhy, P. Nachtigall, M. Horacek, H. Garcia and J. Cejka, *Catal. Sci. Technol.* **2013**, *3*, 500-507.
[215] P. Serra-Crespo, E. V. Ramos-Fernandez, J. Gascon and F. Kapteijn, *Chem. Mater.* **2011**, *23*, 2565-2572.
[216] J. Long, S. Wang, Z. Ding, S. Wang, Y. Zhou, L. Huang and X. Wang, *Chem. Commun.* **2012**, *48*, 11656-11658.
[217] E. Perez-Mayoral, Z. Musilova, B. Gil, B. Marszalek, M. Polozij, P. Nachtigall and J. Cejka, *Dalton Trans.* **2012**, *41*, 4036-4044.
[218] I. Luz, F. X. Llabrés i Xamena and A. Corma, *J. Catal.* **2010**, *276*, 134-140.
[219] A. Dhakshinamoorthy, M. Alvaro and H. Garcia, *ACS Catal.* **2010**, *1*, 48-53.
[220] A. Dhakshinamoorthy, M. Alvaro and H. Garcia, *Adv. Synth. Catal.* **2009**, *351*, 2271-2276.
[221] A. Dhakshinamoorthy, M. Alvaro and H. Garcia, *ChemCatChem* **2010**, *2*, 1438-1443.
[222] A. Dhakshinamoorthy, M. Alvaro and H. Garcia, *Chem. Eur. J.* **2011**, *17*, 6256-6262.
[223] A. Henschel, K. Gedrich, R. Kraehnert and S. Kaskel, *Chem. Commun.* **2008**, 4192-4194.
[224] N. V. Maksimchuk, O. V. Zalomaeva, I. Y. Skobelev, K. A. Kovalenko, V. P. Fedin and O. A. Kholdeeva, *Proc. R. Soc. A* **2012**, *468*, 2017-2034.
[225] O. V. Zalomaeva, A. M. Chibiryaev, K. A. Kovalenko, O. A. Kholdeeva, B. S. Balzhinimaev and V. P. Fedin, *J. Catal.* **2013**, *298*, 179-185.
[226] N. V. Maksimchuk, K. A. Kovalenko, V. P. Fedin and O. A. Kholdeeva, *Chem. Commun.* **2012**, *48*, 6812-6814.
[227] O. A. Kholdeeva, I. Y. Skobelev, I. D. Ivanchikova, K. A. Kovalenko, V. P. Fedin and A. B. Sorokin, *Catal. Today* **2014**, *238*, 54-61.
[228] N. V. Maksimchuk, K. A. Kovalenko, V. P. Fedin and O. A. Kholdeeva, *Adv. Synth. Catal.* **2010**, *352*, 2943-2948.
[229] M. J. Beier, W. Kleist, M. T. Wharmby, R. Kissner, B. Kimmerle, P. A. Wright, J.-D. Grunwaldt and A. Baiker, *Chem. Eur. J.* **2012**, *18*, 887-898.
[230] J. A. R. Navarro, E. Barea, J. M. Salas, N. Masciocchi, S. Galli, A. Sironi, C. O. Ania and J. B. Parra, *Inorg. Chem.* **2006**, *45*, 2397-2399.
[231] F. X. Llabrés i Xamena, A. Abad, A. Corma and H. Garcia, *J. Catal.* **2007**, *250*, 294-298.

[232] S. Schuster, E. Klemm and M. Bauer, *Chem. Eur. J.* **2012**, *18*, 15831-15837.
[233] S. Opelt, V. Krug, J. Sonntag, M. Hunger and E. Klemm, *Microporous Mesoporous Mater.* **2012**, *147*, 327-333.
[234] P. V. Dau and S. M. Cohen, *Chem. Commun.* **2013**, *49*, 6128-6130.
[235] F. Zhao, M. Shirai, Y. Ikushima and M. Arai, *J. Mol. Catal. A: Chem.* **2002**, *180*, 211-219.
[236] N. T. S. Phan, M. Van Der Sluys and C. W. Jones, *Adv. Synth. Catal.* **2006**, *348*, 609-679.
[237] K. Köhler, W. Kleist and S. S. Pröckl, *Inorg. Chem.* **2007**, *46*, 1876-1883.
[238] S. Reimann, J. Stötzel, R. Frahm, W. Kleist, J.-D. Grunwaldt and A. Baiker, *J. Am. Chem. Soc.* **2011**, *133*, 3921-3930.
[239] A. F. Schmidt and A. A. Kurokhtina, *Kinet Catal* **2012**, *53*, 714-730.
[240] W. Kleist, J.-K. Lee and K. Köhler, *Eur. J. Inorg. Chem.* **2009**, *2009*, 261-266.
[241] W. Kleist, S. S. Pröckl and K. Köhler, *Catal. Lett.* **2008**, *125*, 197-200.
[242] M. A. Gotthardt, A. Beilmann, R. Schoch, J. Engelke and W. Kleist, *RSC Adv.* **2013**, *3*, 10676-10679.
[243] N. Toshima, M. Harada, T. Yonezawa, K. Kushihashi and K. Asakura, *J. Phys. Chem.* **1991**, *95*, 7448-7453.
[244] S. S. Pröckl, W. Kleist, M. A. Gruber and K. Köhler, *Angew. Chem. Int. Ed.* **2004**, *43*, 1881-1882.
[245] M. A. Gotthardt, R. Schoch, T. S. Brunner, M. Bauer and W. Kleist, *ChemPlusChem* **2015**, *80*, 188-195.
[246] M. A. Gotthardt, S. Grosjean, T. S. Brunner, J. Kotzel, A. M. Gänzler, S. Wolf, S. Bräse and W. Kleist, *Dalton Trans.* **2015**, *10.1039/c5dt02276b*.
[247] T. Gadzikwa, G. Lu, C. L. Stern, S. R. Wilson, J. T. Hupp and S. T. Nguyen, *Chem. Commun.* **2008**, 5493-5495.
[248] M. A. Gotthardt, R. Schoch, S. Wolf, M. Bauer and W. Kleist, *Dalton Trans.* **2015**, *44*, 2052-2056.
[249] M. Opanasenko, M. Shamzhy and J. Čejka, *ChemCatChem* **2013**, *5*, 1024-1031.
[250] M. Pagliaro, S. Campestrini and R. Ciriminna, *Chem. Soc. Rev.* **2005**, *34*, 837-845.
[251] C. Deraedt, M. d'Halluin and D. Astruc, *Eur. J. Inorg. Chem.* **2013**, *2013*, 4881-4908.
[252] D. J. Nelson, S. Manzini, C. A. Urbina-Blanco and S. P. Nolan, *Chem. Commun.* **2014**, *50*, 10355-10375.
[253] L. S. Kau, D. J. Spirasolomon, J. E. Pennerhahn, K. O. Hodgson and E. I. Solomon, *J. Am. Chem. Soc.* **1987**, *109*, 6433-6442.
[254] K. C. C. Kharas, D. J. Liu and H. J. Robota, *Catal. Today* **1995**, *26*, 129-145.
[255] A. B. Ene, M. Bauer, T. Archipov and E. Roduner, *Phys. Chem. Chem. Phys.* **2010**, *12*, 6520-6531.
[256] C. Prestipino, L. Regli, J. G. Vitillo, F. Bonino, A. Damin, C. Lamberti, A. Zecchina, P. L. Solari, K. O. Kongshaug and S. Bordiga, *Chem. Mater.* **2006**, *18*, 1337-1346.
[257] A. F. Holleman and E. Wiberg, *Lehrbuch der Anorganischen Chemie*, Walter de Gruyter & Co., Berlin, **1995**, p. 1838-1841.

9. Appendix

Abbreviations and symbols

AAS	atomic absorption spectroscopy
ABDC	2-aminobenzene-1,4-dicarboxylate
ATR-IR	attenuated total reflection infrared
BDC	benzene-1,4-dicarboxylate
BET	Brunauer-Emmett-Teller method
BPDC	biphenyl-4,4'-dicarboxylate
BPyDC	2,2'-bipyridine-5,5'-dicarboxylate
BrBz	bromobenzene
BTC	benzene-1,3,5-tricarboxylate
ClBz	chlorobenzene
COMOC	Centre for Ordered Materials, Organometallics and Catalysis
DMF	*N,N*-dimethylformamide
DTA	differential thermal analysis
DUT	Dresden University of Technology
e.g.	exempli gratia (for example)
eq	equivalent(s)
EXAFS	extended X-ray absorption fine structure
FID	flame ionization detector
g	gram
GC	gas chromatography
h	hour
HKUST	Hong Kong University of Science and Technology
ICP-OES	inductively coupled plasma optical emission spectrometry
i.e.	id est (that is)
IRMOF	isoreticular metal-organic framework
KIT	Karlsruhe Institute of Technology
Mal	maleic anhydride
MIL	Matériaux de l'Institut Lavoisier

min	minute
MIXMOF	mixed-linker metal-organic framework
mL	milliliter
mmol	millimole
MOF	metal-organic framework
mol%	mole percent
NMP	*N*-methyl-2-pyrrolidone
NMR	nuclear magnetic resonance
NU	Northwestern University
PSM	post-synthetic modification
Pyal	2-pyridinecarboxaldehyde
Pyaz	2-pyridine azide
PyDC	pyridin-3,5-dicarboxylat
Sal	salicylaldehyde
S_{BET}	specific surface area determined by the BET method
$S_{Langmuir}$	specific surface area determined by the Langmuir method
SBU	secondary building unit
STA	University of St. Andrews
TBAB	tetrabutylammonium bromide
TBHP	*tert*-butyl hydroperoxide
TG	thermogravimetric analysis
TG-IR	thermogravimetric analysis coupled with infrared
TOF	turnover frequency
TON	turnover number
UHM	University of Hamburg Material
UMCM	University of Michigan Crystalline Material
XANES	X-ray absorption near edge structure
XAS	X-ray absorption spectroscopy
XPS	X-ray photoelectron spectroscopy
XRD	X-ray diffraction

Acknowledgements

I am very grateful to many people who supported me during my PhD work – not only scientifically but also personally.

Foremost, I am much obliged to Priv.-Doz. Dr. Wolfgang Kleist, who took me on as his first PhD student in Karlsruhe and provided a very interesting and versatile topic for this thesis. I am extremely grateful for the fruitful discussions and the scientific support he offered.

Furthermore, I would also like to thank Prof. Dr. Jan-Dierk Grunwaldt for giving me the possibility to complete this thesis at the Institute for Chemical Technology and Polymer Chemistry, "Chemical Technology and Catalysis". I am also very grateful for the infrastructure (*e.g.* labs, instruments) he provided.

Prof. Dr. Matthias Bauer and Roland Schoch are gratefully acknowledged for analyzing the XAS data and performing some of the experiments during their beamtimes. DESY and ESRF are acknowledged for providing beamtime and infrastructure.

I would like to thank Prof. Dr. Stefan Bräse and Dr. Sylvain Grosjean for providing the functionalized biphenyl-4,4'-dicarboxylic acid molecules and for scientific discussions.

Prof. Dr. Peter W. Roesky is gratefully acknowledged for providing the NMR spectrometer. I would also like to thank Tobias S. Brunner for performing the measurements and for scientific support.

Prof. Dr. Claus Feldmann is acknowledged for supplying the instrument for TG analysis. Thanks to Dr. Silke Wolf for performing the measurements.

I am very grateful to Angela Beilmann, who performed AAS and TG-IR measurements and Andreas M. Gänzler, who evaluated the TG-IR data. I would also like to thank Benjamin Mutz, Karin Walter, Konstantin Hengst and Hermann Köhler for performing XRD and ICP-OES measurements at Campus North. Thanks to Hans Weickenmeier, who always lent a helping hand in case of technical problems.

There have been a number of diploma and bachelor students who contributed to the work presented in this thesis. Thanks to Julia Engelke, Yesim Murat and Voicu Muntean (diploma students) as well as Johannes Kotzel, Manuel Heinzelmann, Tobias Hofmann and Lukas Warmuth (bachelor students).

Additionally, I am grateful to the colleagues of the Grunwaldt group and the Deutschmann group for the good working atmosphere and the great times I had with them. Thanks for helping me out scientifically and for the fun we had during barbecues, group events or the Skiseminar. I would like to thank especially all those people I shared an office with – you know who you are.

I am very grateful to Benjamin Mutz and Susanne Gotthardt, who sacrificed their spare time to revise this thesis scientifically and linguistically.

Thanks to my family, who always supported me throughout my studies. I am especially obliged to my parents for their financial support, which made life so much easier.

Finally, I would like to thank my friends, who never doubted me and supported my decisions. Thanks for making life fun and always making me laugh.

Teaching

Laboratory course

03/2013 – present Management of the laboratory course "Chemical Technology" for Bachelor students (Applied Chemistry) and Master students (Specialization subject) and supervision of experiments

Supervised diploma theses

[1] 03/2012 – 05/2012

„Synthese und postsynthetische Modifizierung von Metal-Organic Frameworks auf Basis von MIL-53-NH_2(Al) für Anwendungen in der Katalyse", Julia Engelke

[2] 05/2012 – 10/2012

„Anwendung der Metal-Organic Frameworks STA-12 und STA-16 als Katalysatoren in der Oxidation von Alkoholen", Yesim Murat

[3] 10/2012 – 04/2013

„Synthese und Charakterisierung der Metal-Organic Frameworks Cu-BTC und Cu-BTC-PyDC sowie deren Anwendung als Katalysatoren in der Synthese von *N*-Benzylidenbenzylamin", Voicu Muntean

Supervised bachelor theses

[1] 04/2014 – 07/2014

„Synthese, Charakterisierung und postsynthetische Modifizierung von funktionalisierten Metal-Organic Frameworks auf Basis von DUT-5", Johannes Kotzel

[2] 07/2014 – 10/2014

„Metallorganische Netzwerke mit immobilisierten Mangankomplexen als Katalysatoren für die aerobe Epoxidierung von *trans*-Stilben", Manuel Heinzelmann

[3] 02/2015 – 05/2015

„Bimetallische MOF mit CuBTC-Struktur für Anwendungen in der Katalyse", Lukas Warmuth

[4] 02/2015 – 05/2015

„Synthese und Charakterisierung metallorganischer Gerüstverbindungen auf Basis von MIL-101", Tobias Hofmann

Publications

Parts of the results presented in this thesis have previously been published in the following journal articles and were adapted or reproduced by permission of The Royal Society of Chemistry and Wiley-VCH, respectively.

[1] **Synthesis and post-synthetic modification of amine-, alkyne-, azide- and nitro-functionalized metal-organic frameworks based on DUT-5**
M. A. Gotthardt, S. Grosjean, T. S. Brunner, J. Kotzel, A. M. Gänzler, S. Wolf, S. Bräse and W. Kleist, *Dalton Trans.* **2015**, *44*, 16802-16809.

[2] **Synthesis and characterization of bimetallic metal–organic framework Cu–Ru-BTC with HKUST-1 structure**
M. A. Gotthardt, R. Schoch, S. Wolf, M. Bauer and W. Kleist, *Dalton Trans.* **2015**, *44*, 2052-2056.

[3] **Design of Highly Porous Single-Site Catalysts through Two-Step Postsynthetic Modification of Mixed-Linker MIL-53(Al)**
M. A. Gotthardt, R. Schoch, T. S. Brunner, M. Bauer and W. Kleist, *ChemPlusChem* **2015**, *80*, 188-195.

[4] **Immobilization of Pd complexes onto metal-organic frameworks *via* post-synthetic modification – A new concept for the design of heterogeneous catalysts for Heck-type coupling reactions**
M. A. Gotthardt, A. Beilmann, R. Schoch, J. Engelke and W. Kleist, *RSC Adv.* **2013***, 3,* 10676-10679.

[5] **Salen-Based Coordination Polymers of Manganese and the Rare-Earth Elements: Synthesis and Catalytic Aerobic Epoxidation of Olefins**
A. Bhunia, M. A. Gotthardt, M. Yadav, M. T. Gamer, A. Eichhöfer, W. Kleist and P. W. Roesky, *Chem. Eur. J.* **2013**, *19*, 1986-1995.

Oral presentations

[1] **"Design of Heterogeneous Catalysts *via* Post-Synthetic Modification of Mixed-Linker Metal-Organic Frameworks"**
M. A. Gotthardt, W. Kleist
25. Deutsche Zeolith-Tagung, March 6th to March 8th, 2013, Hamburg, Germany

Poster presentations

[1] **"Design of Metal-Organic Framework Catalysts Using Mixed Linkers and Post-Synthetic Modification"**
W. Kleist, M. A. Gotthardt
ICC 2012, July 1st to July 6th, 2012, Munich, Germany

[2] **"Post-Synthetic Modification of Mixed-Linker Metal-Organic Frameworks for Applications in Heterogeneous Catalysis"**
M. A. Gotthardt, J. Engelke, W. Kleist
MOF 2012, September 16th to September 19th, 2012, Edinburgh, Scotland

[3] "**Post-synthetic immobilization of metal complexes on metal-organic frameworks – A new concept for the design of Pd catalysts for Heck reactions"**
M. A. Gotthardt, W. Kleist
Europacat XI, September 1st to September 6th, 2013, Lyon, France

[4] **"Aerobic Oxidation of Alcohols using the Metal-Organic Frameworks STA-12 and STA-16 as Catalysts"**
M. A. Gotthardt, Y. Murat, W. Kleist
26. Deutsche Zeolith-Tagung, February 26th to February 28th, 2014, Paderborn, Germany

[5] **"Single-Site Catalysts *via* Two-Step Post-Synthetic Modification of Mixed-Linker MIL-53(Al)"**
M. A. Gotthardt, W. Kleist
6th International FEZA Conference, September 8th to September 11th, 2014, Leipzig, Germany

[6] **"Synthesis and characterization of a bimetallic metal-organic framework Cu-Ru-BTC with HKUST-1 structure"**
M. A. Gotthardt, R. Schoch, S. Wolf, M. Bauer, W. Kleist
27. Deutsche Zeolith-Tagung, February 25th to February 27th, 2015, Oldenburg, Germany

[7] **"Aerobic epoxidation of olefins by salen-based coordination polymers of Mn and rare-earth elements"**
M. A. Gotthardt, A. Bhunia, M. Yadav, P. W. Roesky, W. Kleist
48. Jahrestreffen Deutscher Katalytiker, March 11th to March 13th, 2015, Weimar